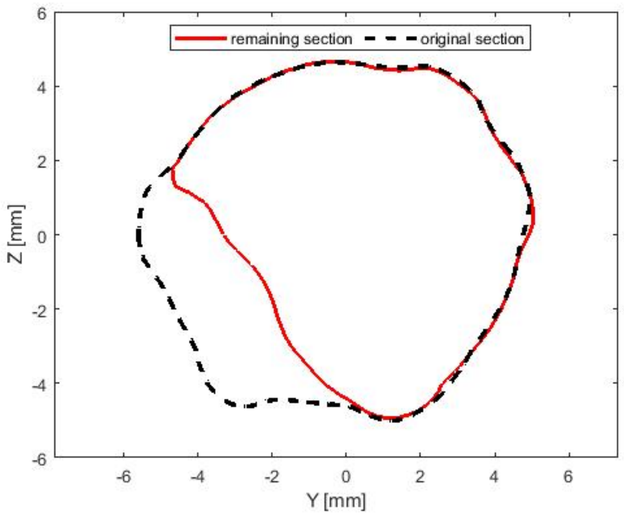

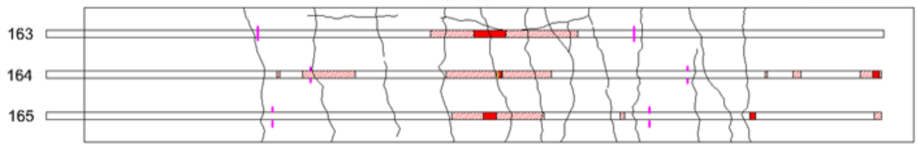

Effect of Cracks and Fibres on Reinforcement Corrosion

Edge beam applications

Master's thesis in Master Program Structural Engineering and Building Technology

REBECCA HENRIKSSON
MARIE ÅHS

Department of Architecture and Civil Engineering
CHALMERS UNIVERSITY OF TECHNOLOGY
Master's thesis ACEX30-19-25
Gothenburg, Sweden 2019

Master's thesis ACEX30-19-25

Effect of Cracks and Fibres on Reinforcement Corrosion

Edge beam applications

Master's thesis in the Master's program Structural Engineering and Building Technology

REBECCA HENRIKSSON
MARIE ÅHS

Department of Architecture and Civil Engineering
Division of Structural Engineering
Concrete Structures Group
Chalmers University of Technology
Gothenburg, Sweden 2019

Effect of Cracks and Fibres on Reinforcement Corrosion
Edge beam applications

REBECCA HENRIKSSON, MARIE ÅHS

Supervisors:
Björn Thomasson, Sweco Civil AB
Magnus Bäckström, Sweco Civil AB
Teresa E Chen, Postdoc, Department of Architecture and Civil Engineering

Examiner: Karin Lundgren, Department of Architecture and Civil Engineering

Master's Thesis ACEX30-19-25
Department of Architecture and Civil Engineering
Division of Structural Engineering
Concrete Structures
Chalmers University of Technology
SE-412 96 Gothenburg
Telephone +46 31 772 1000

Cover: Cross-section with the minimum area in the corrosion pit of a reinforcement bar, and cracks and corrosion along the beam.

Department of Architecture and Civil Engineering
Gothenburg, Sweden 2019

Effect of Cracks and Fibres on Reinforcement Corrosion
Edge beam applications

REBECCA HENRIKSSON, MARIE ÅHS
Department of Architecture and Civil Engineering
Chalmers University of Technology

Abstract

Concrete structures, such as edge beams on road bridges, are often located in salty environments, where the reinforcement often corrode due to cracks and de-icing salt. That can result in decreased service life and high maintenance costs of these structures. Concrete has many advantages but has low tensile strength which often leads to cracks. Earlier studies have shown that fibres can limit the crack width but the relation between cracks and corrosion is rather unknown.

The aim of this thesis was to examine the correlation between the corrosion level and pre-induced transverse cracks by investigating concrete beams containing various fibres. Further, another aim was to perform an initial structural design for a future case study, which will examine the influence of fibres, regarding the durability and life time, when fibre reinforced concrete is used instead of ordinary plain concrete in edge beams.

The specimens studied in this thesis included reinforced concrete with plain concrete and fibre reinforcement containing different kinds of fibres; steel fibres, synthetic PVA fibres and hybridized steel fibres and PVA fibres. A part of the beams had been subjected to three-point bending and loaded until a pre-defined target crack width was reached. All beams were cyclically exposed to chloride solution for three years and naturally corroded for two more years in the laboratory. Measurements of the final crack widths were taken before the rebars were extracted. The crack pattern was drawn in AutoCAD and the critical corrosion level was obtained by 3D scanning.

The study showed that corrosion generally took place close to cracks but that it was difficult to see a dependency of the critical corrosion level on the maximum flexural crack width. Most bars in fibre reinforced concrete had a lower critical corrosion level than in plain concrete under the same conditions, but a few rebars had larger critical corrosion level in fibre reinforced concrete, which may be due to uneven fibre distribution. It was found that the longitudinal cracks, induced by corrosion expansion, influenced the degree of corrosion when they were present. However, some severe pitting corrosion did not induce any longitudinal cracks. Finally, the design procedure on an edge beam following the standard was presented. The suggested design load and dimensions will be used in a future case study to compare the life time of reinforced concrete edge beam with and without fibre reinforcement.

Keywords: FRC, PVA fibre, steel fibre, pit corrosion, edge beams, 3D scanning.

Effekter av sprickor och fibrer på armeringskorrosion
Applikation på kantbalkar

REBECCA HENRIKSSON, MARIE ÅHS
Institutionen för arkitektur och samhällsbyggnadsteknik
Chalmers tekniska högskola

Sammanfattning

Betongkonstruktioner, såsom kantbalkar på vägbroar, är ofta belägna i salta miljöer där armeringen ofta korroderar på grund av sprickor och tösalter. Det kan leda till en förkortad livslängd och höga underhållskostnader för dessa konstruktioner. Betong har många fördelar men den har en låg draghållfasthet vilket ofta leder till sprickor. Tidigare studier har visat att fibrer kan begränsa sprickbredden men förhållandet mellan sprickor och korrosion är relativt okänt.

Syftet med detta examensarbete var att hitta en korrelation mellan korrosion och påtvingade tvärgående sprickor genom att undersöka betongbalkar innehållande olika typer av fibrer. Vidare var ett annat syfte att förbereda en design för en framtida fallstudie, som kommer att undersöka fibrernas inverkan på hållbarhet och livstid när fiberarmerad betong används i kantbalkar istället för traditionell betong.

Provkropparna som studerades i detta examensarbete innefattade armerad betong med vanlig betong och fiberarmerad betong innehållande olika typer av fibrer: stålfibrer, syntetiska PVA-fibrer och en hybrid med stålfibrer och PVA-fibrer. En del av balkarna hade belastats i trepunktsböjning tills en fördefinierad sprickbredd uppnåddes. Alla balkarna utsattes cykliskt för en kloridlösning i tre år och därefter tilläts de att korrodera naturligt i ytterligare två år i laboratoriet. Mätningar av de slutliga sprickbredderna gjordes innan armeringsjärnen plockades ur betongen. Sprickmönstret ritades i AutoCAD och den kritiska korrosionsnivån erhölls genom 3D-skanning.

Studien visade att korrosion generellt ägde rum nära sprickor men att det är svårt att se samband mellan den kritiska korrosionsnivån och den maximala bredden på böjsprickan. De flesta stänger i den fiberarmerade betongen hade en lägre kritisk korrosionsnivå jämfört med de i den vanliga betongen som utsattes för samma förhållanden, men några stänger hade större kritisk korrosionsnivå i den fiberarmerade betongen. Det kan bero på ojämn fördelning av fibrer i betongen. Slutligen kunde det ses att det fanns längsgående sprickor, som uppkommit av den expanderande rosten och att dessa påverkade korrosionsgraden. Dock, för en del balkar, uppstod det inga längsgående sprickor, trots allvarlig gropkorrosion. Slutligen presenterades en designprocedur av en kantbalk enligt gällande normer. Den föreslagna lasten och dimensionerna kan användas i en kommande fallstudie för att jämföra livslängder för en armerad betongkantbalk med och utan fiberförstärkning.

Nyckelord: Fiberarmerad betong, PVA fibrer, stålfibrer, gropkorrosion, kantbalkar, 3D scanning.

Acknowledgements

Along this work, we had the opportunity to get guidance from experienced persons that we would like to thank. First of all, we would like to thank our supervisors at Sweco, Björn Thomasson and Magnus Bäckström, for all your thoughts and inputs. You have helped us with connecting our work to the industry.

We would also like to thank postdoc Teresa Chen and postdoc Carlos Gil Berrocal, at Chalmers, for all your experience and help. You always had time for us when we needed it at most.

We are also very thankful to our opponents, Stina Lundin and Viktoria Bodén, for their thoughts and exchange of ideas. It has been fun to cooperate with you and also take part of your work.

At last, we would like to thank our examiner Karin Lundgren for this opportunity to do this master thesis. You gave us great support and inspired us through this master thesis.

Rebecca Henriksson, Marie Åhs, Gothenburg, June 2019

Contents

Nomenclature

Greek Symbols

α_i Constants due to condition of reinforcement, cover thickness and acting load
α_{ef} Effective modular ratio
η_1, η_2 Constants during good adhesion condition and diameter < 32 mm (=1.0)
γ_s Safety factor
$\gamma_{c.acc}$ Partial coefficient for concrete in case of accidental load
γ_{M0} Partial coefficient for load bearing capacity (=1.0)
$\gamma_{s.acc}$ Partial coefficient for steel in case of accidental load
ϕ Diameter of the rebar
ϕ_s Transverse reinforcement from the bridge deck
ρ Ratio of reinforcement
σ_c The concrete stress
σ_s The steel stress
τ_{bm} Average bond stress
φ Final creep coefficient

Roman upper case letters

$\boldsymbol{C_{sec}}$ Vector with coordinates for the corroded section
$\boldsymbol{R_{sec}}$ Vector with coordinates for the reference section
A_c Cross-sectional area of the concrete
A_k Torsion Area ($Z_v \cdot Z_h$)
A_s Total cross-sectional area of the reinforcement
A_v Cross-sectional area of the baluster
$A_{c.ef}$ Effective concrete area in tensile zone
A_{corr} Area corroded section
A_{ref} Area reference section
A_{si} Cross-sectional area of one rebar
A_{sw} Total area of shear reinforcement
$Corr$ Corrosion rate
E_s Young's modulus of B500B
$E_{c,ef}$ Effective elastic modulus
F Horizontal accidental load
G_{TOT} Total self-weight of the designed edge beam (concrete + railing)
L_{cut} Considered contributing width in the cut
M_o Initial weight of rebar
$M_{Ed.1}$ Moment in the attachment of the baluster caused by the force F

$M_{Ed.2}$ Moment acting in the cut of the edge beam
$M_{Ed.k}$ Acting bending moment
M_{final} Final weight after sandblasting
M_{loss} Mass loss
$M_{pl.Rd}$ Plastic moment capacity of the baluster
$M_{Rd.k}$ Bending moment capacity
M_{Rd2} Moment capacity in the cut
$M_{u.Rd}$ Ultimate plastic moment capacity
$N(\sigma_s)$ Axial force acting on the uncracked parts of the element $(A_s \cdot \sigma_s)$
T_{Ed} Applied design torsion
$V_{Ed.h.1}$ Sub-part of horizontal shear force
$V_{Ed.h.2}$ Sub-part of horizontal shear force
$V_{Ed.v}$ Vertical shear force
V_{Ed} Global design shear force
$V_{pl.Rd}$ Plastic shear load capacity of the baluster
$V_{Rds.h}$ Horizontal shear resistance
$V_{Rds.v}$ Vertical shear resistance
$W_{y.pl}$ Plastic section modulus
Z_h The horizontal distance between the center points of the efficient width
Z_v The vertical distance between the center points of the efficient width
PD Maximum pit depth of the corroded section

Roman lower case letters

$b_{baluster}$ Width of the baluster
b_{beam} Width of the edge beam
b_{cut} Height of the cut
c_d Cover thickness
d_h Efficient height in the cross-section
d_v Efficient width in the cross-section
d_{cut} Efficient height in the cut
e_2 Distance between centre of the cut and attachment of the baluster
e_F Eccentricity between the location of F to the attachment of the baluster
f_{bd} Adhesive strength
f_{cm} Average compressive strength
f_{ctk} Tensile strength of the concrete
f_{ctm} Tensile strength
$f_{ft,res}$ Residual tensile strength
f_{uk} Ultimate tensile strength
f_{yd} Design yield strength
$f_{yk.baluster}$ Characteristic yield strength of the baluster
$f_{yk.s}$ Yield strength of the reinforcement in the case study
f_{yk} Characteristic yield stress of steel reinforcement in the experiment
k Correction factor due to removal of mill-scale
$l_t(\sigma_s)$ Transmission length
$l_{b.rqd}$ Required anchoring length
$l_{bd.1}$ Comparison length for the design anchorage length

$l_{bd.min}$	Minimum anchorage length
l_{bd}	Design anchorage length
$l_{t,max}$	Maximum transmission length
$q_{Ed.k}$	Line load ($\frac{V_{Ed}}{L_{cut}}$)
s_b	Spacing shear reinforcement
s_s	Spacing transverse reinforcement
$w(\sigma_s)$	Mean crack width with added fibres
w_{net}	The net crack width

Glossary

3D scanner A digital tool which scan and collect data of a real-world object. The collected data can be used to create 3D models. 3

AutoCAD AutoCAD is a commercial computer-aided design and drafting software application. 3

FRC Fibre Reinforced Concrete. 1

GOM Inspect Evaluation software for 3D measurement data. 3

HY Hybrid. 27
Hydrophilic Molecule or a protein that is readily soluble in water. 11

MATLAB Mathematical and technical calculation software. 3

PL Plain. 27
PVA Polyvinyl alcohol. 11

RC Reinforced Concrete. 1

ST Steel. 27
SY Synthetic. 27

W/C water-cement ratio. 10

1
Introduction

Concrete structures that are located near the coastal region or exposed to de-icing salt have problem with chloride-induced corrosion. The salty environment can result in decreased service life and high maintenance costs of these structures. The edge beams, in bridges, are especially exposed when the weather conditions require use of de-icing salts on roads. Bridges have a long service life, but the edge beams need to be repaired or exchanged more than once during this period (Mattsson & Sundquist 2007). However, it may be possible to design edge beams in another way compared to what is done today and thereby increase their service life.

1.1 Background

Corrosion of reinforcement is one of the most important degradation mechanisms affecting the durability of reinforced concrete structures. Corrosion of steel in concrete is mainly caused by either carbonation of the concrete cover or local breakdown of the passive layer due to the presence of chlorides. The main sources of chloride to induce corrosion in reinforced concrete structures are either de-icing salt, that is used during the winter to remove ice and snow on the roads, or chlorides that exist in marine environment. Edge beams are one a vulnerable structure and it is therefore interesting to study if it would be feasible to use fibre reinforced concrete instead of plain concrete to reduce corrosion problems in edge beams.

There are two different types of corrosion: general corrosion and pitting corrosion. When chlorides are present, a local type of corrosion occurs, termed "pitting corrosion". This can lead to a significant reduction of the bar's cross-sectional area, thereby severely affecting the integrity of the structure.

Furthermore, in Reinforced Concrete (RC) elements with cracks originating from mechanical loading or restraint forces, the cracks are known to act as a low resistance path for the ingress of external agents, thus becoming preferential locations for corrosion initiation. The crack widths can be reduced by adding fibres into the concrete mixture and recent doctoral thesis, written by Berrocal (2017), investigated how corrosion of the steel bars in Fibre Reinforced Concrete (FRC) will be influenced by the fibres. Berrocal (2017) includes experiments on concrete specimens that consist of different fibre mixtures and have been subjected to various loading conditions, and long-term exposure to chlorides. Part of the beams that were prepared by Berrocal in 2013, were used for investigation during this thesis.

1.2 Aim and objectives

The aim of this thesis is to examine the influence of pre-existing cracks and different fibres on the corrosion level. A subgoal is to provide the design process for an edge beam for a future case study that will investigate how cracks and corrosion change in edge beams when fibre reinforced concrete is used instead of traditionally reinforced concrete.

The master thesis will answer three main questions:

- Is the corrosion degree dependent on the transverse crack width?
- Is it sufficient to focus only on the transverse cracks when the relationship between cracks and corrosion is examined?
- Would it be possible to design an edge beam according to today's standard and design load, by comparing a traditionally reinforced edge beam with a reinforced edge beam where fibres are included in the mixture?

1.3 Limitation

Only chloride-induced corrosion, that can result in pitting corrosion, has been investigated. The solution, which the beams were exposed to, was chosen to imitate environments similar to structures exposed to de-icing salt, such as bridges and their edge beams. Marine structures are also subjected to similar environment. However, the concentration of ions present in sea water is less than the concentration in the experiments. As a result, the reaction process will accelerate in the experiment.

The thesis only investigates the cracks that were developed mechanically by three-point bending. Cracks that may impact differently on the corrosion, such as cracks from the tensile loads acting in normal direction and restraint cracking, are not covered in this study.

The critical corrosion level in fibre reinforced concrete were compared with that in plain concrete. However, the crack widths were not available in plain reinforced concrete beams which was analyzed in prior to the master project. As a result, the corrosion.induced crack widths in them cannot be compared with those measured in fibre reinforced concrete beams.

1.4 Method

In order to investigate the correlation between concrete cracks and steel corrosion, the crack pattern and corrosion pattern were examined with the following methods.

The crack widths on the reinforced concrete beams, with different concrete mixtures and subjected to different loading, were measured by a microscope with a 20x magnification and 0.02 mm resolution. Digital photos of the beams, with cracks marked, were taken and imported to AutoCAD where the documented results are visualized.

When all information regarding the outer layer of the beams were collected, the reinforcement bars were extracted from the beams by use of a jackhammer. The corrosion locations on the rebars were visually observed and measured. To be able to analyze the corrosion pits, the rebars were sand-blasted to clean the bars from rust and remaining concrete. The rebars were weighted after the sandblasting and by comparing with the initial weight, the weight loss was determined. The clean rebars were scanned with a 3D scanner and resulted in a 3D point-cloud and mesh. The software GOM Inspect was used to repair the 3D triangular mesh of the point-cloud generated in the scanner software, and MATLAB were used to determine the geometrical features of the corrosion pits by analyzing the point-cloud generated from the repaired mesh. The correlation between the crack pattern and the corrosion location was investigated through drawing the corrosion pattern and the documented crack patterns in AutoCAD.

2

Background knowledge on cracking, fibres and corrosion

Concrete has been used in structures for a long time because of its beneficial properties. Concrete has many advantages because of its high compressive strength, formability and its long service life. Regarding the aesthetic possibilities, it is basically just your fantasy that sets the limits. However, there are some disadvantages and one of those is that concrete has a low tensile strength. The low tensile strength often leads to cracks in the concrete and that may affect the degradation of the reinforcement. To understand the behavior of reinforced concrete, the following chapter describes the appearance of cracks, properties of fibre reinforced concrete and the corrosion process.

2.1 Appearance of cracks

When the tensile stress generated in concrete reaches its tensile strength under external loading or restraint forces, cracks appears in the concrete. Different types of loading condition will cause different types of cracks and therefore influence the structure differently. The cracks can be seen as transverse, shear and longitudinal cracks.

2.1.1 Transverse cracks

One common cause of transverse cracks is due to bending loads and normally, transverse cracks are often mentioned as bending cracks. Bending can be described by three stages; State I, State II and State III, visualized in Figure 2.1. They represent uncracked, cracked and plastic state. In the uncracked state, the structure has no crack at all, and the concrete carries almost all acting loads. In cracked state, the load is taken both by the concrete and the reinforcement. With increased load and more developed cracks, an increased part of the load is taken by the reinforcement. In the plastic state, either the steel or the concrete has a plastic material response (Al-emrani et al. 2013). For a simply supported reinforced concrete beam, loaded with a point load in the middle, the first bending cracks occur in the middle of the span and then more and more cracks appear towards the supports.

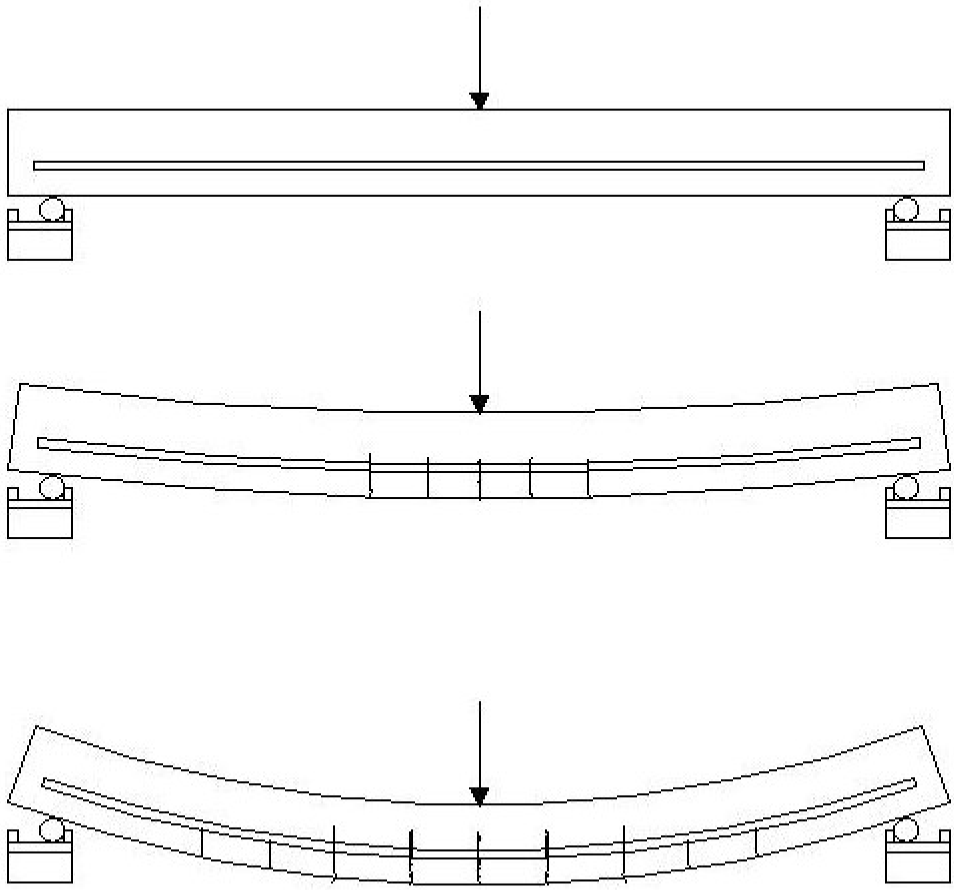

Figure 2.1: State I, II and III for bending cracks.

Almost all concrete structures are designed to be in state II for normal conditions, also called service state. This means that these structures need to handle the cracks and how the cracks influence the load-carrying capacity as well as the extra environmental exposure. The maximum crack width, which is allowed in a structure, is regulated by the structures' exposure class. There are ten different classes and the requirements in each class varies depending on the surrounding environment (EN 1992-1-1 2008).

2.1.2 Longitudinal cracks

The longitudinal cracks can arise when the tensile stress generated in concrete by the corrosion products accumulation exceeds the tensile strength of concrete. But also, for instance, plastic settlement and shrinkage can cause longitudinal cracks (Shaikh 2018).

Longitudinal cracks have often a larger area that is in contact with the rebar than transverse cracks. They result in easier access for chlorides, moisture and oxygen, which increase the corrosion of the reinforcement. The acceleration of the corrosion results in that longitudinal cracks are more dangerous than the transverse cracks. The service life for concrete structures with longitudinal cracks can be shortened (Shaikh 2018).

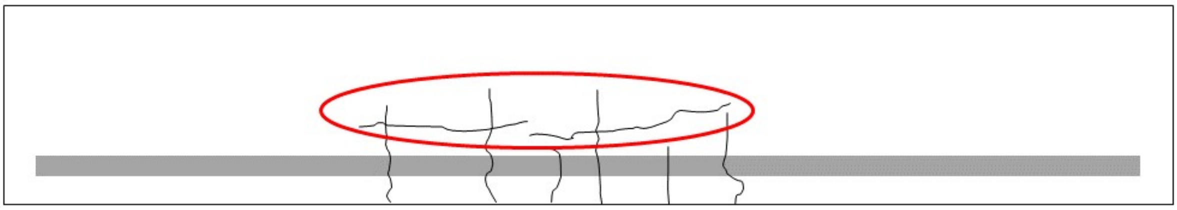

Figure 2.2: Longitudinal cracks induced by steel corrosion in a reinforced concrete beam.

2.1.3 Healing of cracks

Healed cracks can be seen as cracks filled with a white material. They can be healed completely or partially and according to Shaikh (2018) there are often cracks with small crack widths that are healed. The concrete heals the crack itself, which is called autogenous healing. This means that it heals without human intervention. The healing reduces the possibility for the reinforcement to corrode, since the chloride ingress is affected. Healing of cracks may occur when the CO_2 in the air reacts with $Ca(OH)_2$ (calcium hydroxide), CaO (calcium oxide) and moisture that is present in the concrete. This results in $CaCO_3$ (calcium carbonate), which is the white material in the filled cracks (Shaikh 2018).

The self-healing can reproduce stiffness and strength of the concrete. If the initial tensile stress is increased, it results in an accelerating healing process. One reason for this is, with increased tensile stress, it results in a larger area with surface cracks with small crack widths and by that can the healing process for the cracks start at the same time (Suryanto et al. 2015). In the report, written by Suryanto et al. (2015), a study has showed that the average recovery is 9.8% and 15.9% for specimens that are damaged to 30% and 60% respectively of their tensile strain capacity.

2.2 Fibre reinforced concrete

Plain concrete is commonly used for its compressive strength, but it has low tensile strength and toughness. Therefore, the concrete will crack and the cracks that are arising before failure will most likely have different crack widths (Zhang et al. 2018). For concrete structures such as ports, bridges and tunnels, the exposed condition is often salty, which decreases the durability of structures. These structures are often designed for a lifetime of 80-120 years and in order to achieve this service life, both Eurocode EN 1992-1-1 (2008) and Vägverket (2008) require limited crack widths and thick concrete covers for the reinforcement. The requirements can cause major problems during production, as they often require large amounts of reinforcement, which can lead to dense reinforcement layouts. To avoid this, it may be advantageous to use fibre reinforced concrete instead (Berrocal et al. 2017). When discontinuous discrete fibres are added into the concrete mix it is called fibre reinforced concrete.

According to Zhang et al. (2018), a lot of investigations by researchers have shown that the durability and mechanical properties of concrete can be improved by adding fibres into the concrete mix. The fibres limit the crack formation and also reduce the development of cracks due to shrinkage. The toughness is improved since there is a bridging affect, which means that even if the concrete is cracked, the fibres can transfer the forces over the cracks (Zhang et al. 2018). With a high amount of fibres, the strength in the material is higher after cracking than before cracking and as a result more scattered cracks will occur (Park & Yun 2011).

Today's regulations for the use of fibre reinforced concrete are limited. Fibres are mainly used in industrial floors, prefabricated tunnel segments, slabs on the ground, sprayed concrete and thin shell structures (Berrocal et al. 2017).

Previous attempts, made by Berrocal et al. (2017), have demonstrated that bars that are cast in fibre reinforced concrete have more scattered corrosion but less pitting corrosion. The study showed that fibre reinforcement is advantageous for use in structures exposed to chlorides in order to extend the service life. In the case of rebar corrosion, the fibres help to maintain the load-bearing and deformation capacity. The fibres also contribute to a delayed corrosion initiation, according to Berrocal et al. (2017), since the fibres limit the crack width.

2.2.1 Fibres

To be able to reach functional fibre reinforced concrete, it is necessary that the fibres have a high modulus of elasticity and a high tensile strength (Noushini et al. 2013). The purpose, by adding fibres into the mixture, is that they help to control the cracking process and allow the force to be transferred across the cracks. This behavior results in an increased ductility behavior and fracture energy.
The fibres can consist of steel, glass, natural materials and synthetic materials. Generally, steel fibres are the most common when using fibre reinforced concrete, but there are various types of fibres and also sizes. When the fibre has a length that is longer than the size of the maximum aggregate and the cement grains is smaller than the diameter of the cross-section of the fibre, it is called macro fibres. If the fibre is shorter than the aggregate, and the cross-section and cement grains is of the same order, is it instead a micro fibre (Löfgren 2005).

2.2.2 Steel fibres

As mentioned, steel fibres are used more frequently than other fibres. According to Svensk Standard SS-EN 14889-1:2006 (2006), steel fibres can be defined into groups based on the production method. The fibres can be pieces of cold-drawn steel wire, cut sheet fibres, fibres milled from steel blocks, melt extracted fibres or shaved cold-drawn fibres. Regardless of type, the fibres can be either straight or deformed and in common, all types of steel fibres should be able to be mixed homogeneous into the concrete. One type of fibre is shown in Figure 2.3

In an article by Zhang et al. (2018), a comparison on how the mechanical properties of steel reinforced concrete changed depending on traditional mixing and vibratory mixing, was mentioned. This comparison was made by Zhang et al. and the investigation showed that steel fibres can improve the properties with vibratory mixing due to the resulting distribution of the fibres.

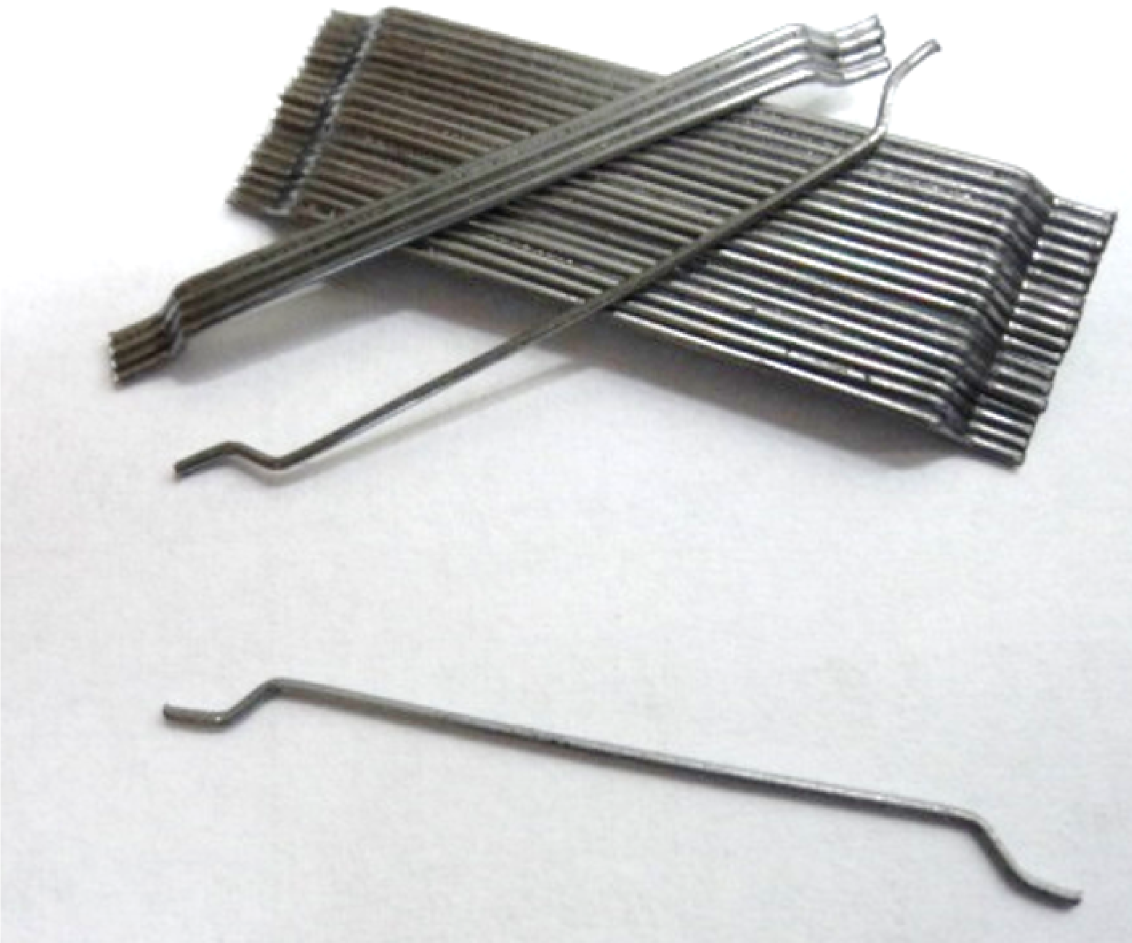

Figure 2.3: The steel fibres that where mixed into the concrete.

2.2.3 Corrosion of steel fibres

Steel fibre reinforced concrete differs from ordinary reinforced concrete. The ordinary reinforced concrete has reinforcement bars which are perfectly positioned with a protective covering layer. The steel fibres are scattered in the fibre reinforced concrete and the fibres could be placed close to the surface.

Corrosion of steel fibres in concrete usually occurs when the concrete is located in an unfavorable environment. This corrosion is considered to be less important for the durability, but it does exist. On the surface, corrosion of steel fibres is often seen as spots of corrosion and although it is only aesthetic, it is usually not desirable in structures (Balouch et al. 2010).

The presence of corrosion, can affect the strength since the fibres no longer contribute to the bridging effect above the cracks. But according to Balouch et al. (2010), the effect of surface corrosion can be reduced by decreasing the water-cement ratio (W/C) below 0.5 and design the mixture so that the fibres have a covering layer of 0.2 mm.

2.2.4 PVA fibres

Polyvinyl alcohol (PVA) is a water-soluble polymer produced by hydrolysis of polyvinyl acetate. Hydrolysis is a chemical reaction which means that a chemical compound is cleaved and create new structures, when a molecule of water is added. If the degree of hydrolysis is over 95%, polymers can crystallize (Nationalencyklopedin 2019). The chemical compound is visualized in Figure 2.4 where the right end is a chemical chain. PVA in its clean form is a white powder and from the powder, fibres can be formed (Noushini et al. 2013).

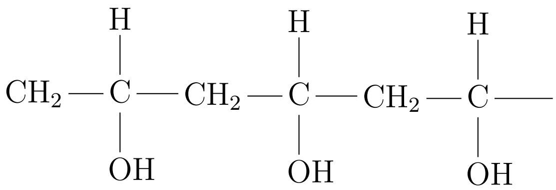

Figure 2.4: Chemical compound polyvinyl alcohol

PVA has many application areas. In addition to fibre reinforcement in concrete it can also be used as ropes, fishing nets, filters, paper and geo-textiles. PVA has good resistance, since Young's modulus is high and has high resistance to chemicals and UV-light. In addition, PVA has small strains and is not sensitive to creep (Polymer Properties Database 2017).

A report, written by Zhu et al. (2018), strengthens that PVA has good durability. It is mentioned that PVA has great mechanical and physical properties. Furthermore, PVA is resistant against corrosion, it is non-toxic and has a high bond strength. In previous studies it has been shown that the hydrophilic nature results in that PVA can increase the adhesive strength between cement and fibre (Zhu et al. 2018). Different sizes of PVA fibres are visualized in Figure 2.5.

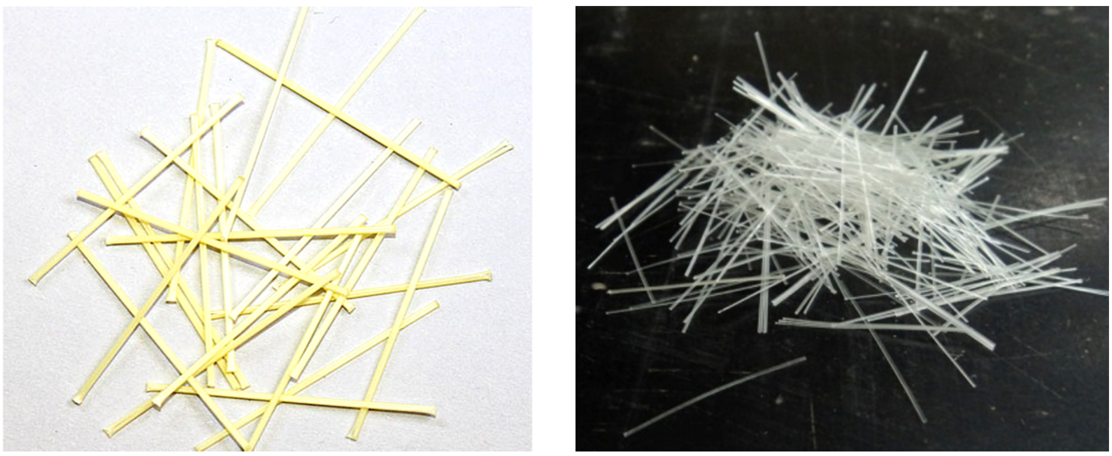

(a) PVA macro fibres. **(b)** PVA micro fibres.

Figure 2.5: Different types of PVA fibres.

2.3 Corrosion mechanisms

Corrosion cannot occur without water and oxygen. Thus water and oxygen need to be transported through the concrete to make corrosion possible. Transportation of molecules through concrete can occur in three different ways. When there is a movement of a fluid under a pressure differential, it is called permeation. The second mechanism is called diffusion and it means that ions, atoms or molecules move from regions with higher concentrations to regions with lower concentrations. The last mechanism is sorption. Sorption is the capillary attraction of a liquid, that transports in porous solids due to tension in the surface (Domone & Illston 2010).

A metal starts to corrode when it is included in a galvanic cell, according to Domone & Illston (2010). In a galvanic cell there is an anode, a cathode and an electrolyte, see Figure 2.6. The anode is where the oxidation reaction occurs and the cathode is where the reduction reaction takes place. Between the two components, there is an electrolyte, which is a liquid containing free ions, and is therefore an electric conductor. The reinforcement act as the anode and the oxygen acts as the cathode. The electrolyte is the capillary water, located inside the pores in the concrete. The oxidation process in the anode and the reduction in the cathode are needed for corrosion to occur. They appear at the same time, which can be described by Equation 2.1.

$$\begin{gathered} H_2O + \frac{1}{2}O_2 + 2e^- \rightarrow 2OH^- \\ Fe \rightarrow Fe^{2+} + 2e^- \end{gathered} \tag{2.1}$$

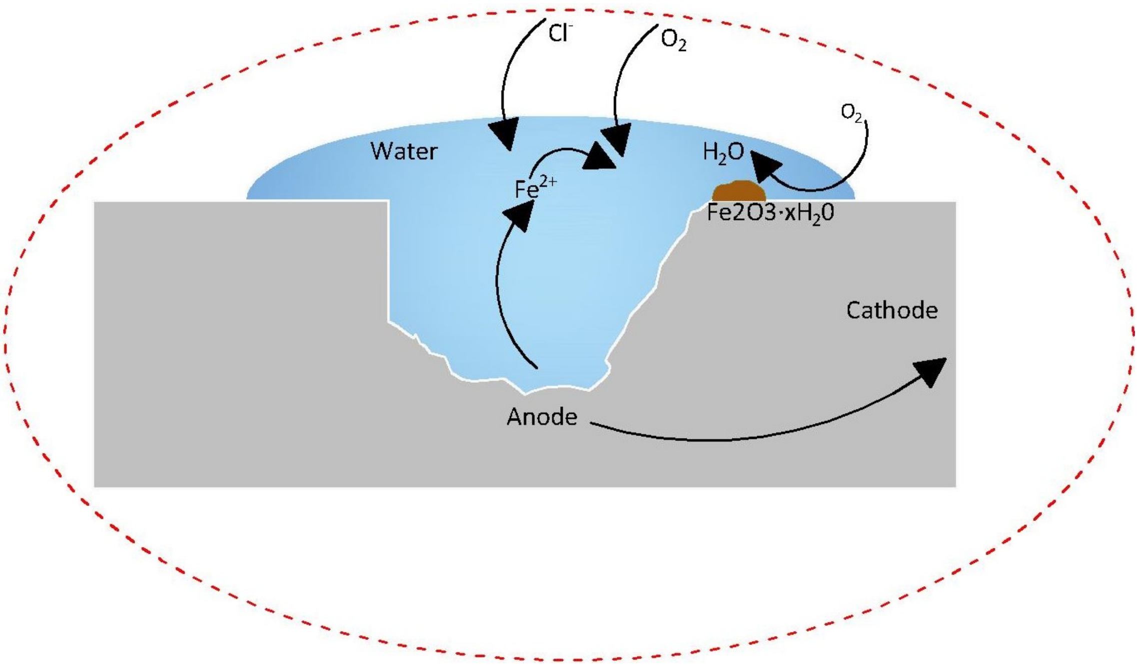

Figure 2.6: Chemical reactions when pitting corrosion in a reinforcement bar occurs.

The reinforcement is often already corroded before it is placed in the concrete. The humid air around the steel reacts with the steel and an oxidation product is created. The oxidation product can be described as a very thin layer of ferrous ferric oxide, Fe_3O_4. As a result, the thin layer protects the steel against further corrosion and thus the steel is mentioned as passive (Domone & Illston 2010).

In a new concrete structure, the reinforcement is well protected by a passive layer formed due to high alkalinity in the concrete pore solution. Degradation of this layer is caused by penetration of chloride ion Cl^- and carbon dioxide CO_2 from the structure's surrounding environment. By that, the protective layer of the steel is destroyed and corrosion of the steel can initiate (Fernandez et al. 2018).

Rust is a product of the corrosion process. Rust can result in spalling and cracking since the rust has two to six times bigger volume than the steel. The volume depends on the environmental conditions. The cracks and spalling can influence the characteristics of the structure (Zhu et al. 2013). After cracking, the reinforcement is more exposed and the corrosion rate may increase. As a result, the deterioration processes can proceed easier (Fernandez et al. 2018).

2.3.1 Carbonation induced corrosion

A concrete structure is almost always exposed to air and all the gases which the air exists of. These gases are for example CO_2 and oxygen. The CO_2 is dissolved in the water which penetrate into the concrete. A reaction between the CO_2 and the calcium hydroxide $Ca(OH)_2$ in the cement will occur and this will lower the pH in the concrete. A lower pH value contributes to a higher corrosion rate and increase the general corrosion of the steel according to Domone & Illston (2010). How fast the dissolved CO_2 and the water flow into the concrete, varies with lots of factors and according to Domone & Illston (2010) the three main factors are the saturation rate of the concrete, the porosity and the CO_2 content in the surrounding area.

In Figure 2.7 the carbonation process is shown in four steps. The first two steps show how the CO_2 starts to penetrate and lower the pH in the concrete. When the pH-value is lower than nine around the reinforcement bar, which is described in step three, the steel can start to corrode. In the last and fourth step, the rust has expanded and created stresses so that the concrete has developed a crack.

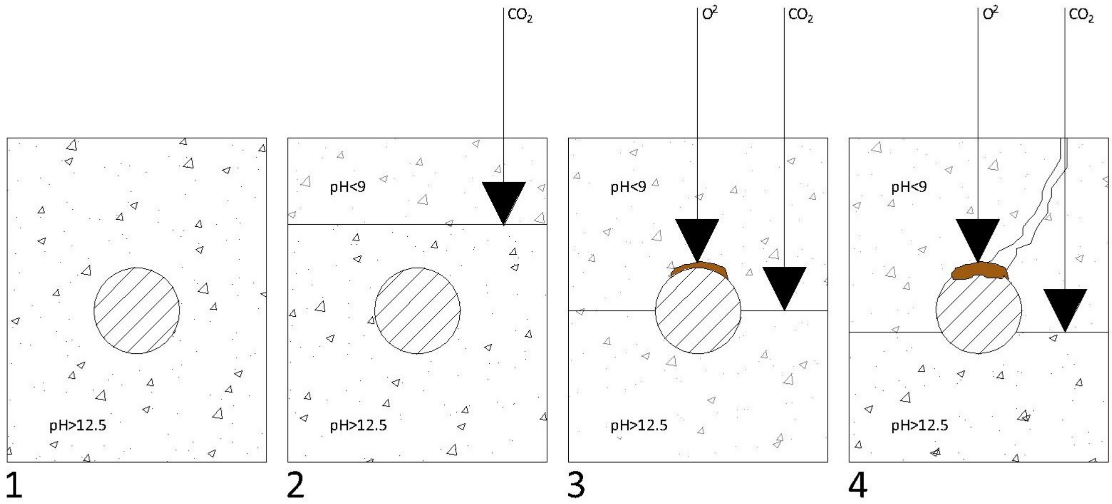

Figure 2.7: A carbonation process in concrete described in four steps.

2.3.2 Chloride induced corrosion

One of the most important degradation processes of reinforced concrete is corrosion due to chlorides. In an environment with high chloride levels, the chlorides penetrate into the concrete and when the chloride content is high enough, the reinforcement starts to corrode (Domone & Illston 2010). The exact threshold of chloride content is very hard to define according to Ahlström (2011). It varies depending on the manufacturing process, concrete mixture and possible additives. The period where the chloride penetrates through the concrete is called 'the safe time'/initiation period according to *Tuutti's service life model* (Tuutti 1982). During this time, the reinforcement is safe from corrosion. When the threshold is reached and the corrosion starts, the 'residual life'/propagation starts according to the same model, see Figure 2.8a. Tuttis' service life model is just one of many other models that describe the service-life. One other model is the *DuraCrete service-life model*, which also describes the initiating and propagation phase in a similar way as Tuuttis' model.

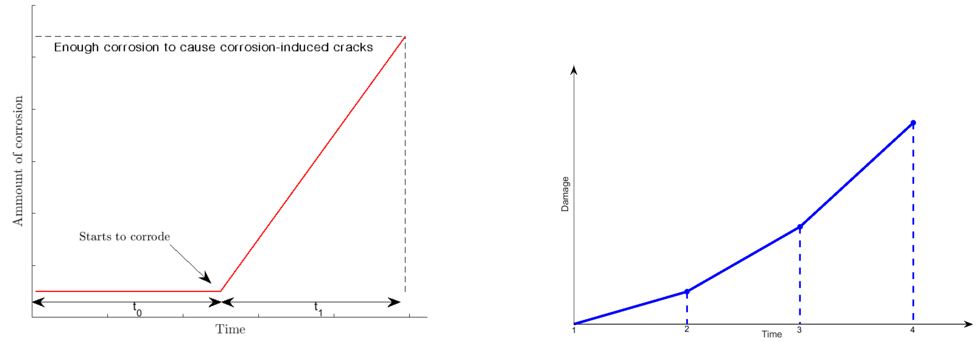

(a) *Tutti's service-life model.* Most of a concrete structure's service life is located in the part 'The safe time', t_0. Only a small part can be found in the 'Residual life', t_1, where the corrosion has initiated (Tuutti,1982).

(b) *Duracrete's service-life model* 1 = Depassivation, 2 = Cracking, 3 = Spalling, 4 = Collapse (Duracrete,2000)

Figure 2.8: Two different service-life models for reinforced concrete structures.

Corrosion of the steel in concrete can appear since there is a chloride transportation in the porosity of the concrete. The concrete porosity can arise both from cracks and hydration induced porosity (Wang et al. 2018).

2.3.3 Pit corrosion

Local pits in the reinforcement mainly develop due to chloride induced corrosion. When the concrete is in a wet environment, water and chloride penetrate into the concrete. When the water reaches the reinforcement, the steel reacts with it and oxidation occurs, at the so-called anode. In pitting corrosion, the cathode, i.e. where the electrons move to, is very close to the anode and the galvanic cell is very local, see Figure 2.6 in section 2.3. A local galvanic cell will not affect the reinforcement at the cathodic site, since it will be protected from oxidation, i.e. corrosion. This means that the already corroded part, anode, will continue to corrode, and the other part will not have problems with pitting corrosion (Domone & Illston 2010).

The pitting corrosion affects the properties of the reinforcement since there is loss of cross-sectional area. In a report by Andisheh et al. (2016), the result showed that the pit depth is increased over time. Since corrosion is an electro-chemical reaction, which means that there is an interplay between chemical compounds and electricity, there are steel losses that lead to corrosion products. The loss can affect the performance of the reinforcement in the concrete structure (Andisheh et al. 2016). Furthermore, it should be noted that loss of the total area in the cross section is more critical than the depth of the pit. Figure 2.9 shows a photo of a local pit on a rebar.

Figure 2.9: Example of a real pitting corrosion of a reinforcement bar

It is not just the cross-sectional area that is affected. Also, the moment of inertia and gravity center will be changed compared to a non-corroded rebar. If an axial tensile force is applied in the centre of the rebar, an eccentricity occurs when the rebar is subjected to pitting corrosion. The eccentricity results in compression forces at the opposite side of the pit and tensile forces at the face side of the pit. This also results in that the elastic strain increases at the face side of the pit and will decrease on the opposite side of the pit. As a result, bending of the rebar can be seen (Andisheh et al. 2016).

2.3.4 Corrosion influenced by cracks

Many studies have investigated how cracks influence the corrosion rate and its characteristics varies over time. Parameters as crack type, crack frequency, crack width and crack depth have been shown to influence the corrosion, according to Shaikh (2018). One of the most basic aspects of a crack and how it influences the concrete structure is that it opens an easy path for other substances to penetrate into the concrete. The substance will affect the steel and depassivate it so that a corrosion process starts (Shaikh 2018). Examples of those substances are carbon dioxide, oxygen, water and different types of chlorides.

All these substances affect the concrete and the reinforcement in different ways. Carbon dioxide starts a carbonation process, chloride increases the corrosion rate and water and oxygen are essential for corrosion to even occur. Several studies regarding the influence of cracks on corrosion have been performed and summarized in the article written by Shaikh (2018), but the results of the studies contradict each other. As a consequence, it is difficult to see whether the cracks affect the corrosion.

2.3.5 Steel fibres influence on chloride-induced corrosion

As mentioned, chloride induced corrosion contributes to a lot of damage on concrete structures. A bulk diffusion test has shown that the chloride transport properties of steel fibre reinforced concrete differs from plain concrete (Wang et al. 2018). The experiment was based on Fick's second law, which describes diffusion in dynamic systems where concentration can decrease or increase. From Fick's second law, a prediction model is established for the chloride ingress. Diffusion can in short terms be described as all kinds of chloride transport mechanisms in concrete and Fick's law is a suitable model to describe non-steady state diffusion. To calculate Fick's second law analytically, a constant chloride diffusion coefficient is assumed. But earlier studies have shown that the chloride diffusion constant is time dependent.

In a report, written by Wang et al. (2018), was the chloride diffusion coefficient 30-38% lower for steel fibre reinforced concrete compared to plain concrete when the specimens are subjected to tension. The initiation of corrosion for steel fibre reinforced concrete, when it's exposed to bending load, was 2.2-3.6 times longer than for plain concrete. And the time was also 6-40% longer for concrete that was unstressed (Wang et al. 2018). The variation is caused by the cover thickness and the fibre dosage in the concrete.

It can from that be assumed that steel fibre reinforced concrete has better resistance against chloride transport, compared with ordinary reinforced concrete, and the difference was clearer when the specimen was subjected to bending. On the other hand, steel fibres have a higher probability to corrode on the surface, since they are exposed to an aggressive environment, according to Hwang et al. (2015).

3
Literature review on edge beams

The edge beams have an important role in bridges. They should stiffen up and distribute the load on the bridge deck slab. They can also be included in other load-bearing elements, for example in the main beam, to ensure that water does not run over the edge and make it possible to fasten the railings.

3.1 Traditional types of edge beams

There are many different types of edge beams, and two of them are shown in Figure 3.1. The most common type in Sweden is the integrated edge beam (Pettersson & Sundquist 2014), visualized to the left in the figure. The integrated edge beam contributes with stiffness compared to the non-integrated edge beam. Both types of edge beams add a line load on the console part at the bridge deck, due to the self-weight.

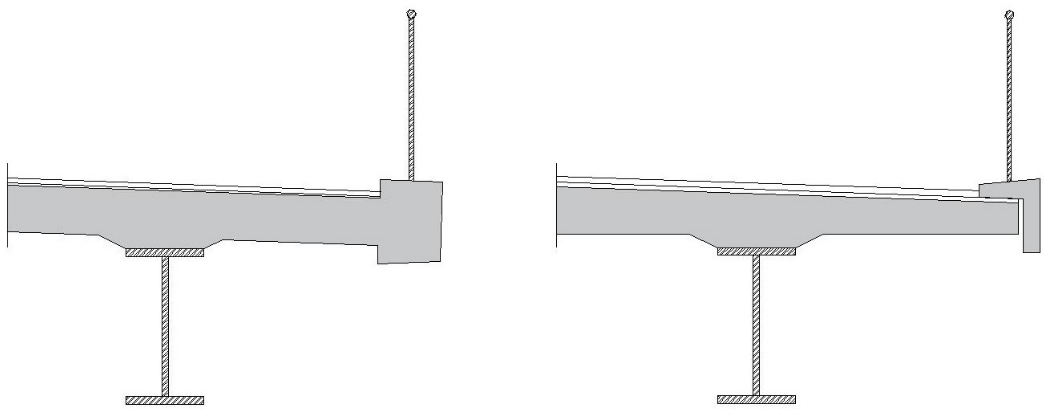

Figure 3.1: A principal sketch of two kinds of edge beams. The left sketch is showing an integrated, elevated edge beam. The right sketch is showing a non-integrated edge beam.

3.2 Common problems with edge beams

Since the edge beams are placed at the edge of the bridge, they are very unprotected. As a consequence of that, the edge beams often need to be repaired or exchanged more than once during the service life of the bridges (Mattsson & Sundquist 2007).

Edge beams are exposed to road salt, frost, moisture and sometimes collisions. These problems affect the performance of the edge beam and cause damage on the beam. One damage that can result in area loss of reinforcement and concrete cracking, is corrosion. If there are large crack widths, caused by mechanical loading and/or restraint forces, the concrete permeability increases. When the permeability is increased, it also enables to increase the corrosion in the reinforcement. The damage can also be mouldering and chemical decomposition which leads to a reduction of adhesion.

3.3 Design of edge beams

The edge beams can be found in different shapes depending on the bridge type. For pedestrian and road bridges, the design of the edge beam depends on the design of the railings. The attachment of the railing also affects the design of the reinforcement and the edge beam is designed so that the carrying capacity and dimensions are sufficient for the attachment of the railing. The edge beams on pedestrian bridges are mainly designed as elevated edge beams, recessed edge beams or in the same level as the coating layer. The edge beam shall be designed so that it provides a sufficient load distribution in the bridge console and it shall be designed to be able to take the section forces that arise due to point loads on the bridge console (Trafikverket 2018).

In Sweden, the steel in the edge beam on pedestrian or road bridges shall be designed according to corrosion class C5, according to SS-EN ISO 12944-2 (Trafikverket 2016), but other parts in steel are designed according to C4. The corrosion class is divided into five groups, depending on the environment around the structure, where C1 is where there is less risk of corrosion (indoor environment with low humidity) and C5 is where there is a high risk of corrosion (marine environment or areas with a lot of pollution) The concrete in the edge beam on road bridges should be designed according to exposure class XD3 or XF4, which on pedestrian bridges it should be designed according to class XD1 or XF4 (Trafikverket 2018). The exposure class XD is used for corrosion caused by chlorides other than sea water and exposure class XF is used for attacks by freezing/thawing with or without chlorides. For both classes, the number describes how wet the environment is. The corrosion class is used in design of concrete structures since different environments result in different corrosion speed. Cutouts on the edge beam, for instance for cable ducts, should be designed so that water does not remain in it.

In Sweden, edge beams shall have at least have seven reinforcing rebars with a diameter of 16 mm (Trafikverket 2018). But in an edge beam at the bridge deck console, it is often necessary with more reinforcement. Generally, a pedestrian or road bridge has a minimum reinforcement amount consisting of two rebars in the upper and inner edging corner, one rebar in the centre of the edge and two rebars in the bottom (Trafikverket 2018).

According to Trafikverket (2018), a road bridge or pedestrian bridge should have closed stirrups with a diameter of at least 10 mm and a centre distance not more than 300 mm in the edge beam. That can be compared with an edge beam on a railway bridge where the closed stirrups should have a diameter not less than 12 mm and the centre distance should not exceed 200 mm. In Figure 3.2, a principle sketch of the reinforcement in one of the most common edge beams, according to Pettersson & Sundquist (2014), in Sweden is visualized.

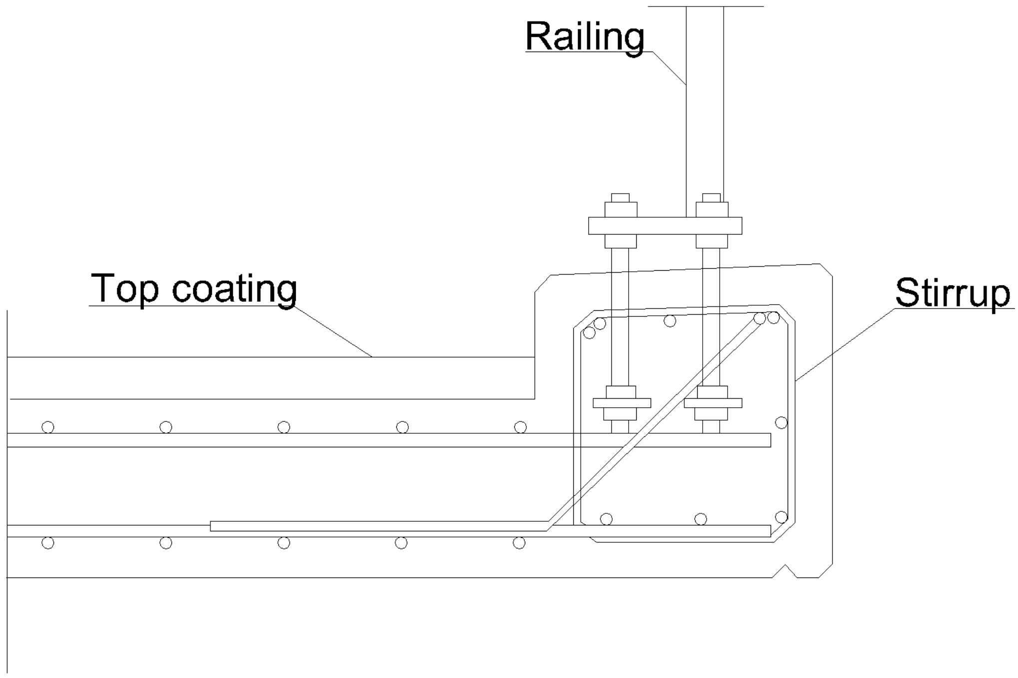

Figure 3.2: A principle sketch of how the reinforcement can be placed in an integrated edge beam.

3.4 Inspections of edge beams

In Sweden there are regulations requiring all bridges need to have a main inspection within every sixth year, which includes the edge beams. Depending on the condition of the bridge it can be inspected more frequently. The functional condition is judged depending on the functional requirements that the bridge were designed for. The separate elements' functional properties, expected degradation and also the relation between the actual and earlier measured values (Vägverket 2008) are parameters that are evaluated in the inspection.

All different elements in the bridge are described with four different condition classes that can be seen in Table 3.1. The classes are used as a help for the person that performs the inspection.

Table 3.1: The different condition classes that are used during an inspection.

Condition class	Definition
0	Inadequate function beyond 10 years
1	Inadequate function within 10 years
2	Inadequate function within 3 years
3	Inadequate function at inspection

To be able to choose the correct condition class to use, there are some limits for each structural element in the bridge. The limits are a benchmark for the inspector but it is always the inspector himself that judges based on experience. To evaluate the edge beam and to get the most critical condition, it is necessary to consider all assessment methods (Vägverket 2008). The limitations for edge beams are presented in Table 3.2 and they consider three main types of damages; corrosion, cracks and mouldering/chemical decomposition. Many of the limitations are also considering the loading conditions for the edge beam. A high load-bearing edge beam has tougher requirements than an edge beam which has less load-bearing.

Table 3.2: Limitations for different kinds of damages on edge beams.

Description	Type of damage	Limitation for class 3
Area loss for high and load-bearing edge beams	Corrosion	Element area loss >20%
Area loss for not high and load-bearing edge beams	Corrosion	Element area loss >40%
Maximum crack width	Bending-/tension crack	Crack width >0.6mm
Reduction of adhesion at the length L=1m for high and load-bearing edge beams	Mouldering/chemical decomposition	Reduction of adhesion >20%
Reduction of adhesion at the length L=1m for not high and load-bearing edge beams	Mouldering/chemical decomposition	Reduction of adhesion >40%
Reduction of element height in a cross-section (average)	Mouldering/chemical decomposition	Reduction of height >10 %

4
Test specimens and procedure

This chapter describes how the procedure of the experiment was performed. From Berrocal et al. (2018) research there were 22 beams which were available for this master thesis. The beams consist of four different mix proportions, with different types of reinforcement (plain reinforced concrete, reinforced concrete with steel fibres, reinforced concrete with PVA fibres and a reinforced concrete with hybrid fibres containing with both steel and PVA fibres) and have been exposed to sodium chloride (NaCl) solution for three years. The beams have also been exposed for different loading conditions: uncracked, cracked, cyclic loading and loaded during the whole time period.

4.1 Properties of beams

The beams had a length of 1100 mm, a height of 100 mm and a width of 180 mm. Since electrical equipment was used during the exposing time, the reinforcement bars needed to protrude 50 mm from the end of the beam. The cover thickness, between the edge and rebar, was 30 mm and the spacing between the reinforcement bars was 45 mm. In each beam, there were three ribbed reinforcing bars with $\phi 10$. The dimensions of the tested beams are shown in Figure 4.1.

Figure 4.1: The sketch shows dimensions of the tested beams [mm] (Berrocal et al. 2018).

The reinforcing steel was made of ribbed bars of B500B. The reinforcing steel, B500B, has a Young's modulus of $E_s = 200GPa$, according to Eurocode 2 (Al-emrani et al. 2013). The characteristic yield strength is $f_{yk} = 500MPa$. The design value is calculated as in Equation 4.1, where γ_s is a safety factor which normally is equal to 1.15 (at accidental load condition $\gamma_s = 1,0$).

$$f_{yd} = \frac{f_{yk}}{\gamma_s} \tag{4.1}$$

4.2 The concrete mixture

The concrete mixture was the same for all beams and they were consisting of a self compacting concrete mixture, with a water-cement ratio (w/c) of 0,47. C. Berrocal performed the casting of the beams and this following section present the properties and components from the casting. The components and the volume are presented in Table 4.1.

Table 4.1: The component content in the concrete mixture (Berrocal et al. 2018).

Component	**[kg/m^3]**
Cement (CEM I 42.5 N SR 3 MH/LA)	360
Limestone filler (Limus 40)	165
Fine aggregate (sand 0/4)	770
Coarse aggregate (crushed 5/16)	833
Effective water	169
Superplasticizer – Glenium 51/18	5.76
Air entrainer – MicroAir 105	0.72

There were three kinds of fibres present in the concrete mixture. One mixture consisted of steel fibres that had a length of 35 mm and was end-hooked, the second mixture was a hybrid between steel fibres and micro PVA fibres. The third mixture was called Synthetic and contained macro PVA fibres. The properties of the fibres can be seen in Table 4.2.

Table 4.2: Properties of the fibres used in the different mixtures (Berrocal et al. 2018).

Material	**Steel (low carbon steel)**	**Polyvinyl Alcohol (PVA)**	**Polyvinyl Alcohol (PVA)**
Property	Dramix* 65/35-BN	Kuralon TM RFS400	Kuralon TM RF4000
Length [mm]	35	18	30
Diameter [μm]	550	200	660
Shape	Hooked	Straight	Straight
Young's modulus, E [GPa]	210	30	29
Tensile Strength [MPa]	1100	1000	800

The fibre content in the four different mixtures are presented in Table 4.3. The fibre content was below 1% in all mixtures, which improves the toughness of the concrete but doesn't influence the strength of the concrete (Berrocal et al. 2018). A fibre content above 1.5% leads to pseudo strain-hardening which means that the material shows some tensile strain hardening behavior.

Table 4.3: Fibre content present in the different mixtures (Berrocal et al. 2018).

Fibre content [%]	Steel fibre	PVA [RFS400]	PVA [RF4000]
Plain (PL)/M1	-	-	-
Steel (ST)/M2	0.5	-	-
Hybrid (HY)/M3	0.35	0.15	-
Synthetic (SY)/M4	-	-	0.75

The beams were, as already mentioned, subjected to different loading conditions. Four beams, of those remaining, were never loaded and thus uncracked. Eight were loaded until target crack widths but after that unloaded. Six beams were loaded cyclic with five loading cycles and four beams were loaded permanently. All cracked beams have been subjected to a three-point bending pre-loading. The loaded beams were, after the pre-loading, also exposed to a sustained loading. All of those were loaded to an initial target crack width of either 0.1 mm or 0.4 mm, see Table 4.4. But, during the loading procedure one of the beams, with a supposed target crack width of 0.4 mm, was loaded up to a crack width of 0.8 mm by mistake, according to Berrocal et al. (2015).

Table 4.4: The beams and their properties that were used in this master thesis. The values in the parenthesis corresponds to the beam which became loaded to 0.8 mm, instead of 0.4 mm (Berrocal et al. 2018).

Load condition			Series	Target crack widths (mm)		Numbers of beams
uncracked			PL	-		1
			ST	-		1
			HY	-		1
			SY	-		1
cracked	**unloaded**	**1 cycle**	PL	0.1	0.4	2
			ST	0.1	0.4	2
			HY	0.1	0.4	2
			SY	0.1	0.4	2
		5 cycles	PL	0.1	0.4	2
			ST	0.1	0.4 (0.8)	2
			HY	0.1	0.4	2
	loaded		PL	0.1	0.4	2
			ST	0.1	0.4	2

Each beam has a name that consists of two parts. The first part describes the used concrete mixture and the beam nr. The second part, which is in the parenthesis, does also include the concrete mixture and beam nr but the loading condition and the obtained target crack width, are also included. Example of a beam name is shown in Figure 4.2.

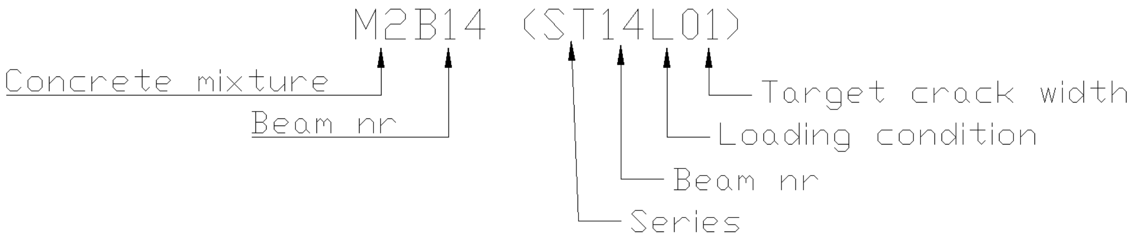

Figure 4.2: Each beam has a name which describe the used concrete mixture, fibre type, loading condition and target crack width (Berrocal et al. 2018).

4.3 Exposing environment

In three years the beams were partially exposed to a saltwater solution with 16.5% Sodium chloride, NaCl, which corresponds to a chloride extent of 10%. Before the beams were exposed to chlorides, they were subjected to potable water. This was done to ensure that the beams were saturated.

During the exposure of NaCl solution, the beams were allowed in cycles to dry in two weeks, followed by wet period of two weeks. During the drying periods, the beams were placed in a laboratory with a temperature between 16.9 °C and 24.1 °C. The relative humidity in the laboratory was between 30% and 60%.

4.4 Determination of crack widths and corrosion location

The evaluation of crack patterns of the reinforced concrete beams was done by analyzing them with naked eyes and optical microscope. Measurements along the cracks were performed at several locations. Although only transverse cracks were supposed to be handled in this thesis, measurements were taken longitudinal cracks as well. The reason for this was to create awareness of these, although the main goal was not to find any connections between longitudinal cracks and corrosion. As a final step of the crack documentation, a picture of the crack pattern, of each side of the beams, was taken. One example is shown in Figure 4.3.

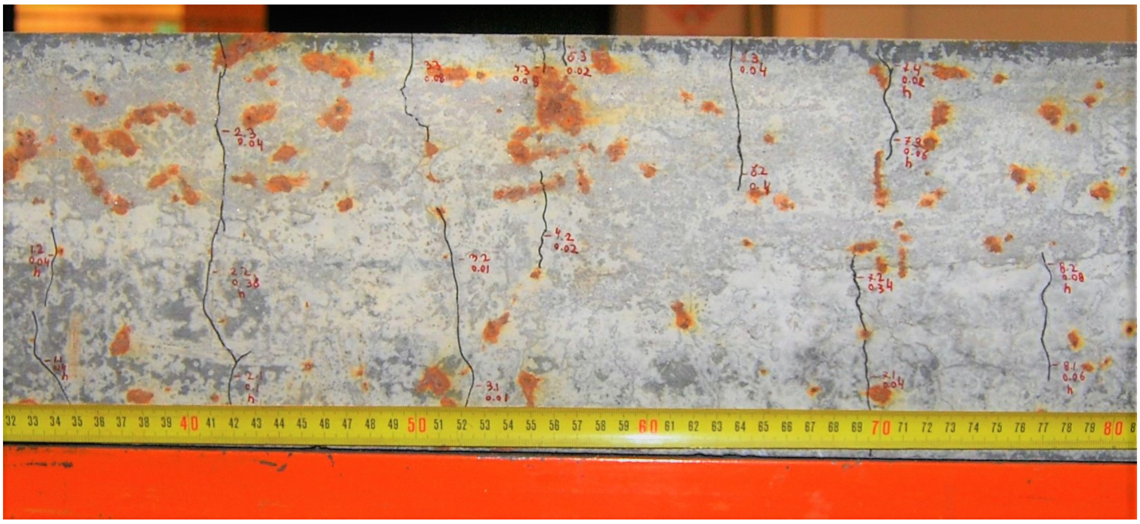

Figure 4.3: Picture of the crack pattern with measured crack widths.

Further, the reinforcement bars were extruded from the beams with help from a jackhammer. When the reinforcement was removed from the beams, it was possible to get a first view of corrosion regions, which was covered by corrosion products. From the first view, measurements of corrosion locations were taken before the reinforcement was sandblasted, as it may not be easy to discern the corrosion sites with very thin corrosion depth when rust is moved.

4.5 Mass loss of reinforcement

All rebars had been weighted before they were cast into the concrete beams. When they were extruded from the beams, there were residues of concrete, as well as rust on the bar's surface. Sandblasting was performed to clean the bars from rust and the remaining concrete.

The sandblasting was performed in several steps to ensure that the rebar was completely clean. It was ensured by performing at least two blasting sessions and if there was a mass loss higher than 0.2% between sandblasting session one and two, a third session was performed so that the requirement of a maximum mass loss of 0.2% between the blasting session was achieved.

By investigating the weight of each rebar before the concrete was cast and after the sandblasting, a weight loss was determined. To weight the rebars, a scale with a precision of 0.01 g was used. Since there is a weight loss due to the removal of corrosion that was arisen before casting, a factor k was decided by Berrocal et al. (2018). The factor k was decided to be 0.9978 by evaluating 15 non-corroded rebars which were cleaned mechanically with wire bristle brushes. Equation 4.2 gives the percentage of the weight-loss where k is the correction factor, M_o is the initial weight of the rebar and M_{final} is the final weight of the rebar after sand-blasting.

$$M_{loss} = \frac{k \cdot M_o - M_{final}}{k \cdot M_o} \tag{4.2}$$

Furthermore, measurements of the general corrosion and pit corrosion made it possible to compare the corrosion location with the crack location in AutoCAD.

4.6 Documentation of cracks

All photos of the crack pattern were imported into AutoCAD and scaled to fit the correct dimensions of the beams. Then, all cracks were drawn by following the existing cracks in the pictures, see Figure 4.4a.

New measurements of the location of corrosion were also performed and compared with the first view of corrosion location that was described in section 4.4. Pitting locations were identified as positions where the corrosion depth was obviously deeper than the surrounding region, while general corrosion regions refer to the location where corrosion products are deposited on the rebars surface but without obvious localized cavity. The location of general corrosion and pitting corrosion was implemented into the AutoCAD to be able to visualize the relation between crack location and corrosion location.

Since it was a 2D drawing, the direction of the pitting corrosion around the bars needed to be defined in some way. When they were placed in the beams, they were marked with a reference mark, at that side the cover thickness was the smallest, and this mark was used as a reference when the direction of the pit corrosion was documented. The definitions of the directions that are defined in Figure 4.4b are represented by different colours in the drawing. The final drawing for a beam, with cracks on the tension surface and location of corrosion, and its reinforcement is shown in Figure 4.5.

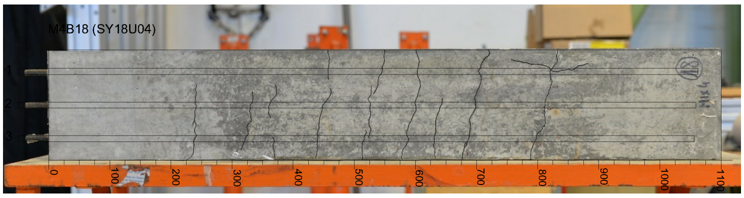

(a) Drawing cracks in AutoCAD by using a photo of a beam.

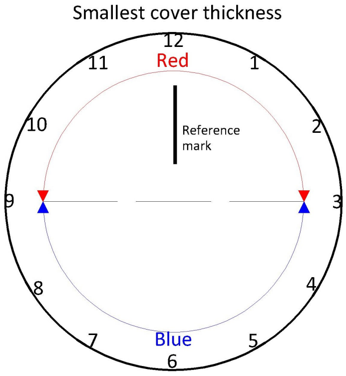

(b) Reference mark on a reinforcement bar and the definition of the drawing colours.

Figure 4.4: Drawing methods and definitions of pit location.

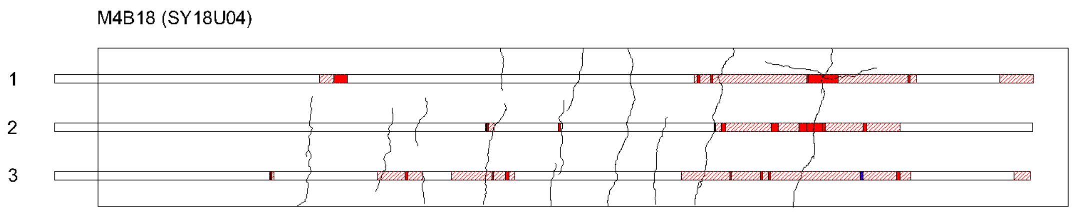

Figure 4.5: Final drawing of crack pattern and corrosion of reinforcement bars. The shaded pattern indicates general corrosion while the solid colour corresponds to pits.

4.7 Measurements of corrosion level

The level of corrosion was investigated in a few steps. First, the rebars were sand-blasted, weighted and the location of corrosion was examined. After that procedure, the rebars were 3D scanned. From the scanning it was possible to obatain the maximum cross-sectional area loss by analyzing each rebar in MATLAB.

4.7.1 3D scanning

The clean rebars were scanned with a 3D scanner to make it possible to determine the pit morphology in the reinforcing steel. The program requires a lot of memory of the computer and to circumvent this the rebars were cut to a maximum length of 500 mm. To ensure that the most crucial part of the rebars was included, which is where the pit is localized, it was not possible to cut all rebars at the same location. The 500 mm piece was placed in a stand for fixing the piece during the scanning. The stand that was used during the 3D scanning is seen in Figure 4.6.

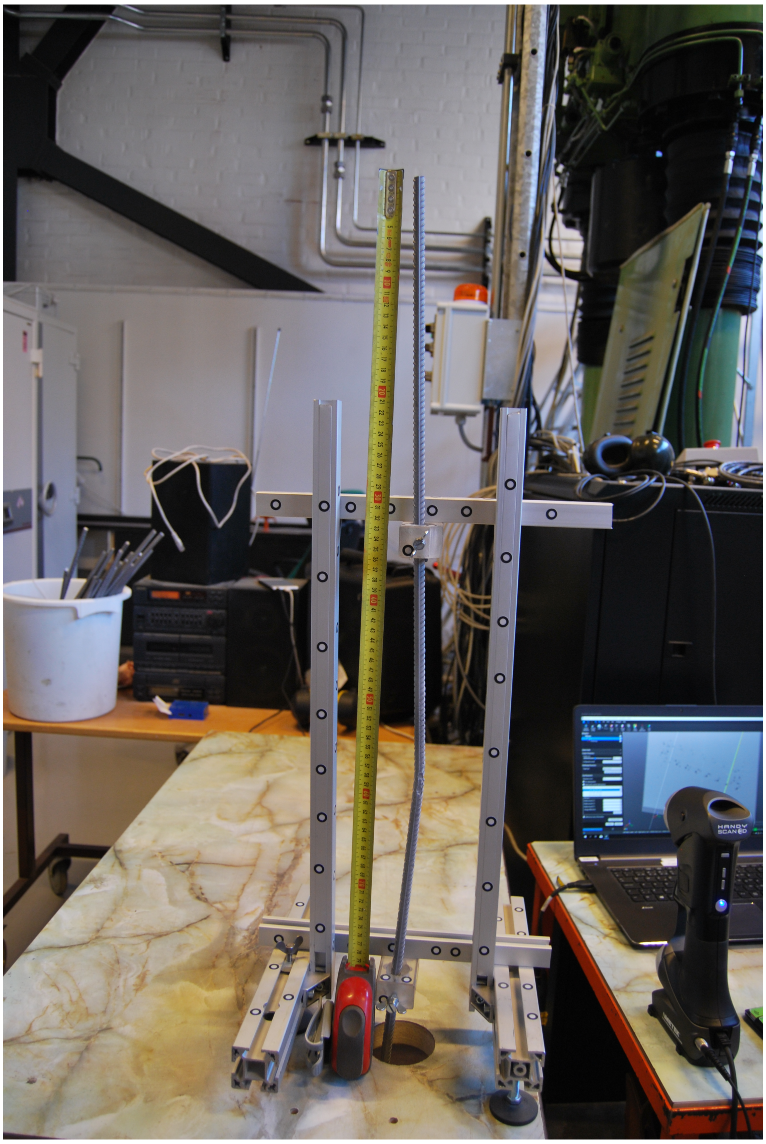

Figure 4.6: Arrangement of a reinforcement bar during the scanning process.

The 3D scanning was performed by Handy Scan 700™, which is a portable 3D scanner from Creaform. The scanner uses laser to create a 3D point-cloud and mesh, and according to Creaform (2019) has the 3D scanner a precision of 0.030 mm. Further, the software GOM Inspect was used to make a mesh, where it was possible to clean and fill the holes in the mesh from the 3D scanning. GOM Inspect is a free software for analyzing 3D data, that is generated from a 3D scanner or other measuring equipment, and analysis of 3D point clouds. The point-cloud that was given from GOM Inspect was imported to MATLAB R2018b where the result could be analyzed.

4.7.2 Evaluating the corrosion level in MATLAB

The point-cloud from GOM Inspect was imported into MATLAB 2018b. A coordinate system was aligned based on the imported point-cloud, were the X-coordinate was along the rebar. All scanned bars had some imperfections at their ends. To make sure they did not affect the result, 5-10mm of both their ends were excluded in the analysis. The matlab program, created and developed by Tahershamsi et al. (2017) and Berrocal et al. (2018), analyzed the point-cloud and converted it from 3D data to 2D and visualized it in two different types of plots. First, a diagram showing how the cross-sectional area varies along the length of the bar and secondly, a surface plot where the surface has been flattened out and visualized by colour variations in a surface plot, see Figure 4.7. The pitting location is identified by changes in the cross-sectional area, which is indicated by the colour-bar.

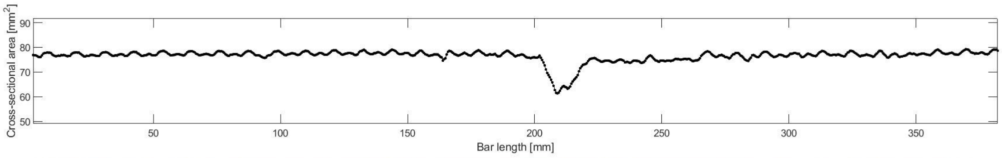

(a) Area variations along the bar

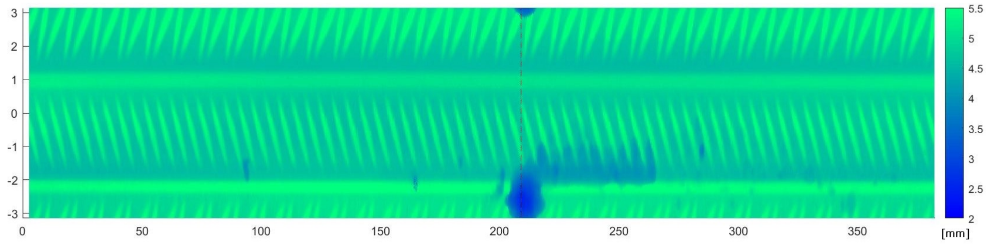

(b) Surface plot showing how the radius varies along the length of a bar. Blue areas in the surface plot correspond to a smaller radius and green a larger radius.

Figure 4.7: Area and radius variations along the bar

The critical cross-section is defined as the section with the minimum area. To find the depth of the pit and also the cross-sectional area loss, the program tries to find an uncorroded section which fit the corroded section as good as possible. This is done by an iteration process where the difference between the uncorroded reference section and the corroded section is calculated. An example of a matched cross-section is shown in Figure 4.8, where the part between the red line and dashed line indicates the loss of area due to corrosion. With a good match the pit depth, PD, and critical corrosion level, $Corr$, could be calculated as:

$$PD = max(\boldsymbol{R_{sec}} - \boldsymbol{C_{sec}}) \tag{4.3}$$

$$Corr = \frac{A_{ref} - A_{corr}}{A_{ref}} \tag{4.4}$$

Where $\boldsymbol{R_{sec}}$ is a vector with radius for the reference section and $\boldsymbol{C_{sec}}$ is a vector with radius for the corroded section. Further, A_{ref} and A_{corr} are the area of the reference section and corroded section respectively.

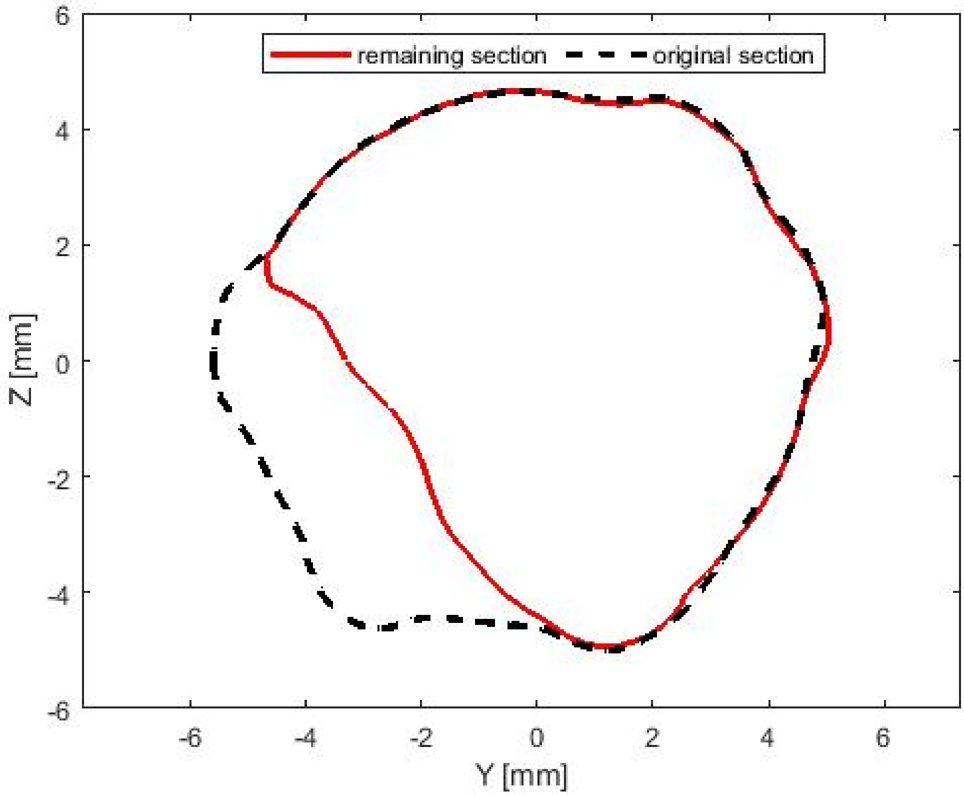

Figure 4.8: Example of an analyzed and matched section.

5 Experimental results

The following chapter presents the results that were obtained during this project. The results are presented in the same order as they were obtained. Firstly, an investigation of the surface of the concrete beams was made and the result is shown in section 5.1. After examining cracks in the beams and corrosion in the reinforcement, these were put together in common AutoCAD drawings for each beam. The final drawings are shown in section 5.2.

Further, analysis in MATLAB was performed. The analysis in MATLAB resulted in critical corrosion level and the maximum pith depth, summarized in Appendix A. This data is discussed in Sections 5.3-5.8. More graphs can be seen Appendix B.

5.1 Observation on the beams surface

In Figure 5.1 and Figure 5.2, steel fibre corrosion can be observed on the surface. The steel fibre corrosion was observed near the cracks but not inside the cracks. No effects of the fibres, in the beams which had synthetic fibres, are detected, see Figure 5.3.

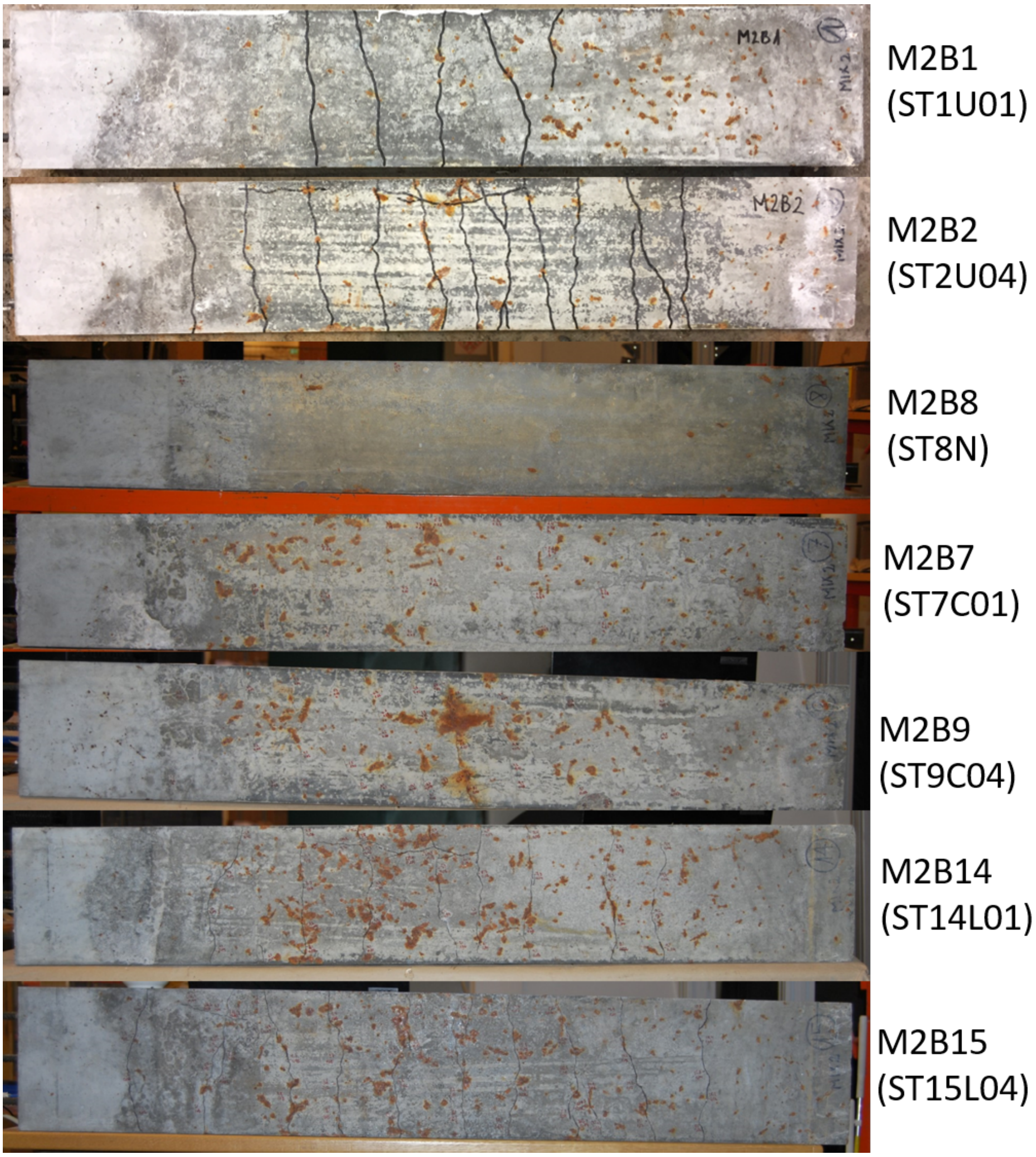

Figure 5.1: Surface of the steel fibre reinforced concrete beams.

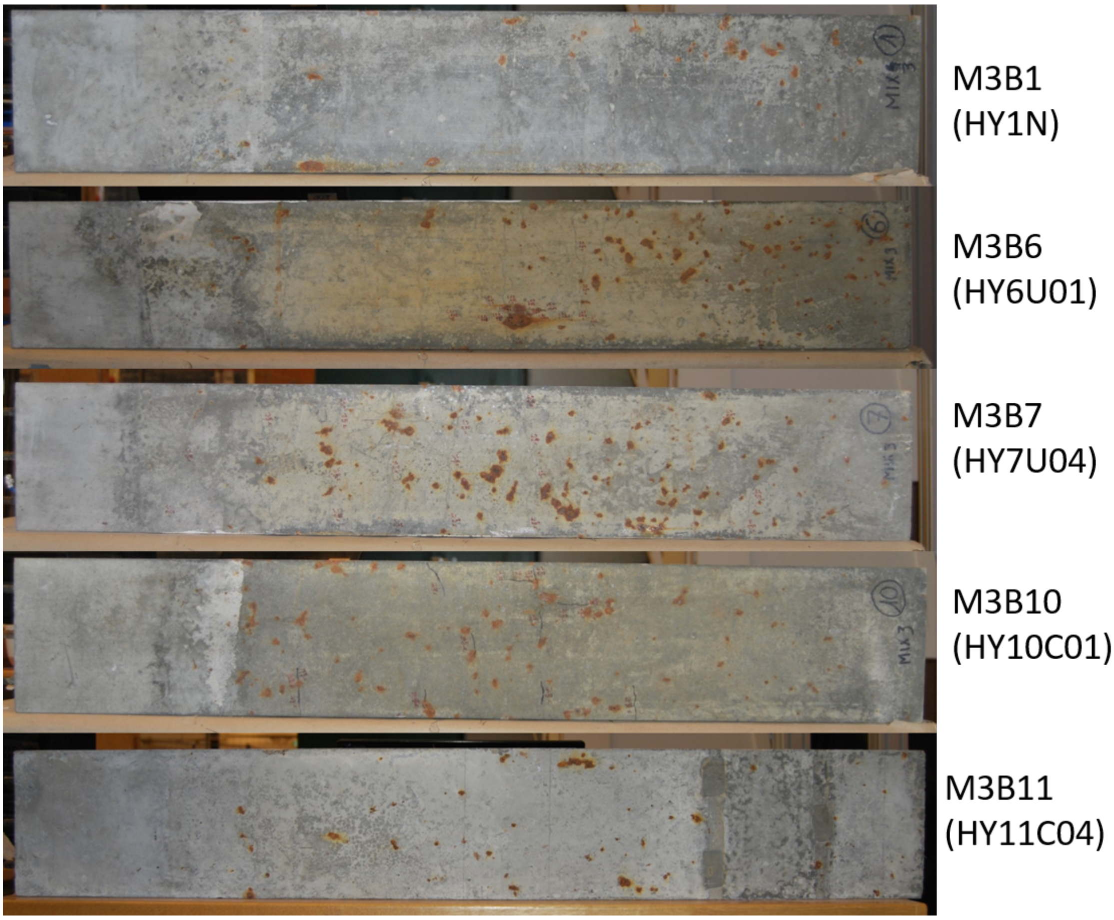

Figure 5.2: Surface of the hybrid fibre reinforced concrete beams.

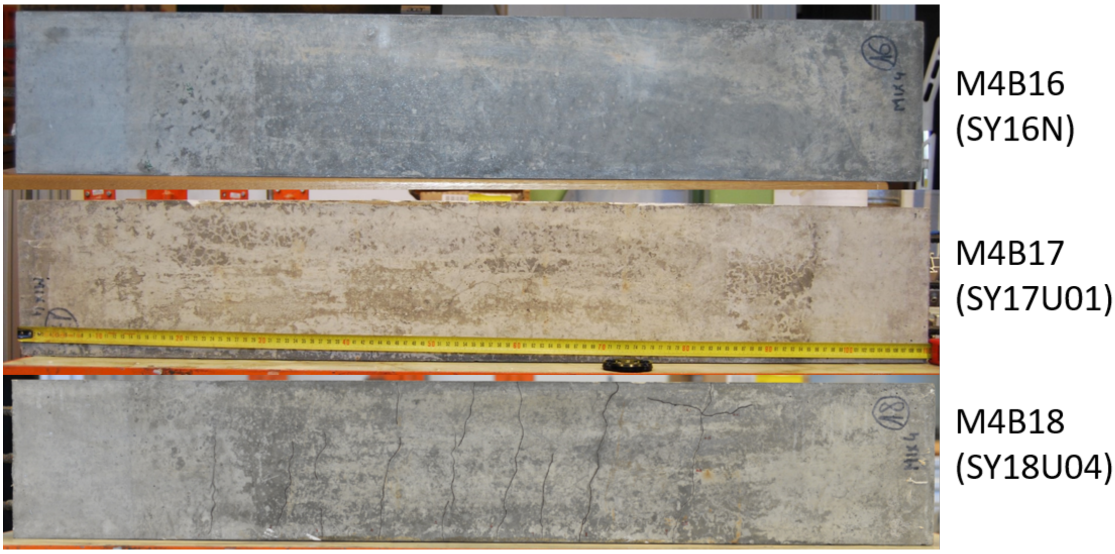

Figure 5.3: Surface of the synthetic fibre reinforced concrete beams.

5.2 Location of cracks and corrosion

The locations of the corrosion and the crack pattern, for the tension side of the beam, were investigated. Since corrosion can occur at different locations, and both as pitting corrosion and general corrosion, it is necessary to indicate them separately. The legend, shown in Figure 5.4, describes what is shown in the documenting AutoCAD drawings.

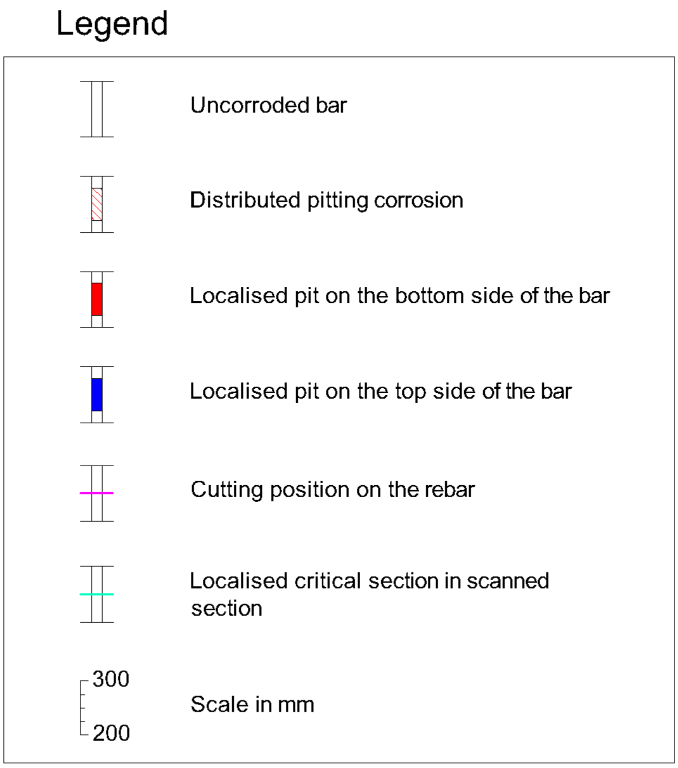

Figure 5.4: The legend that describes what is shown in the AutoCAD drawings.

The drawings show that the critical corrosion section often occur close to a crack, see 5.6-5.9. The observations can be seen for all types of concrete mixtures in the experiment.

Each rebar is given a specific number. The rebar numbers are defined as in Figure 5.5. Where the bottom is the tension side.

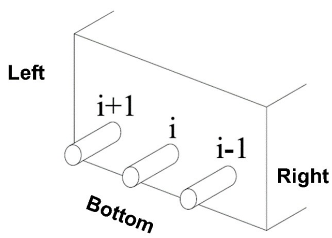

Figure 5.5: The definition of rebar numbers. The bottom is the tension side.

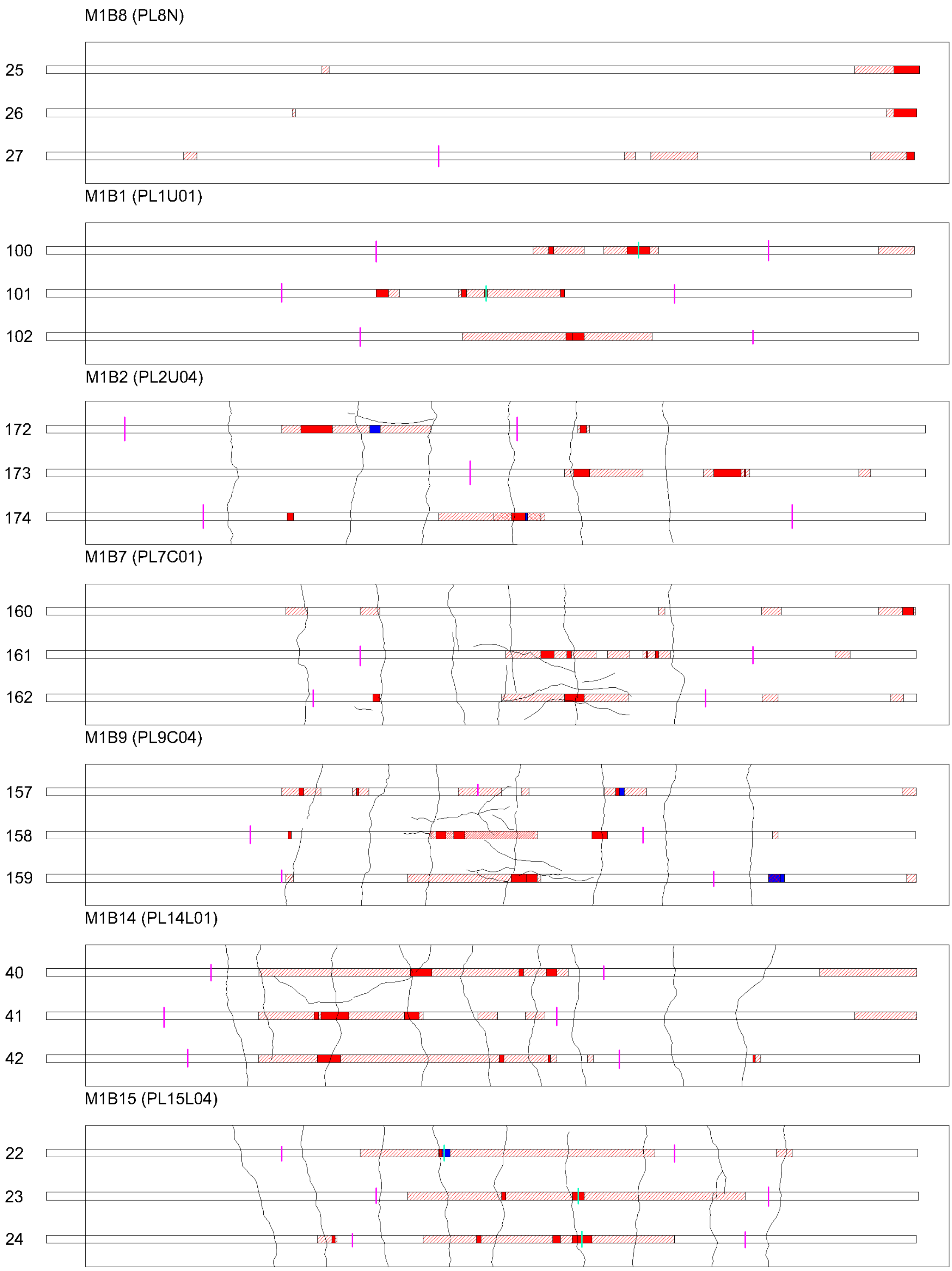

Figure 5.6: Cracks and corrosion pattern in the beams containing plain concrete.

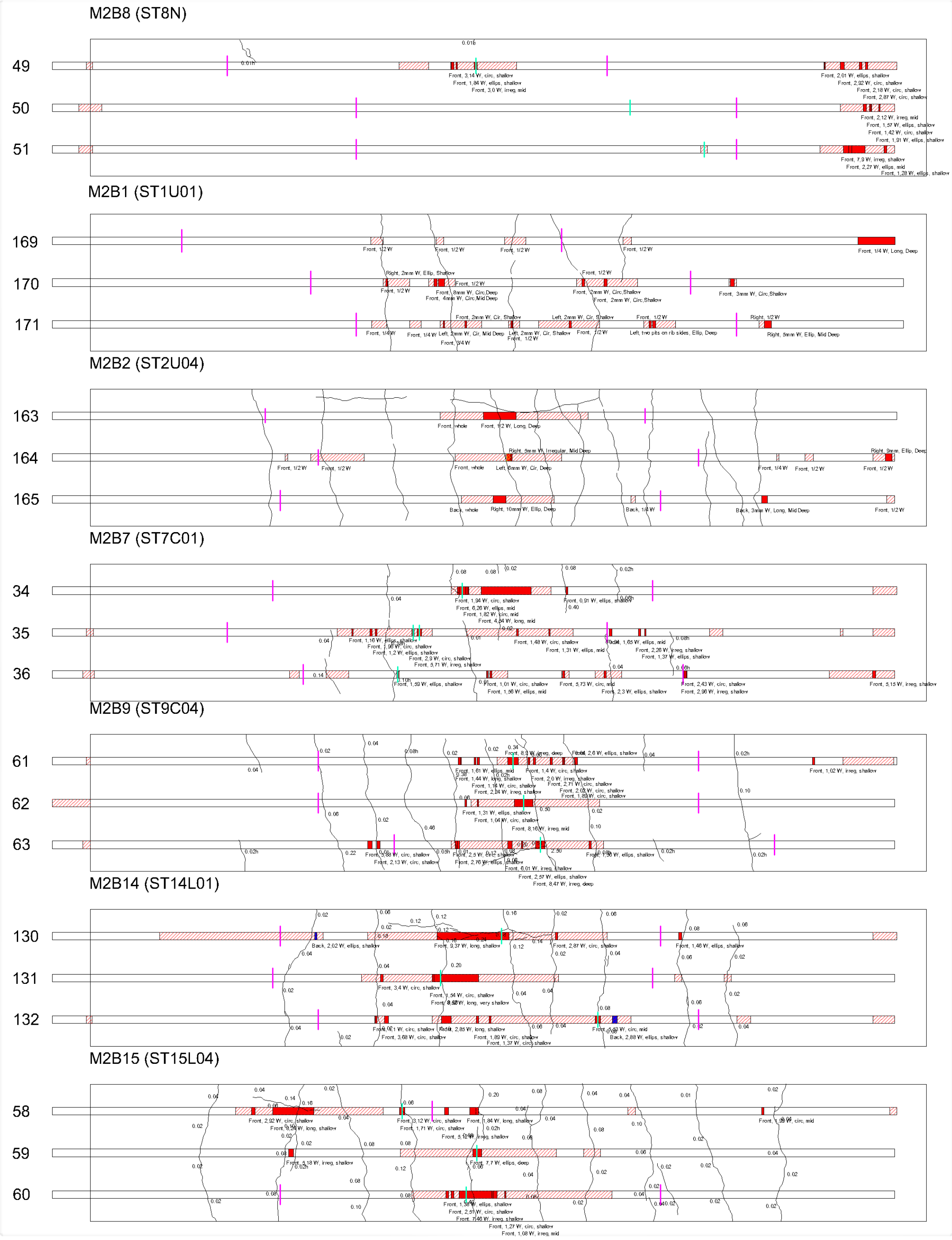

Figure 5.7: Cracks and corrosion pattern in the beams containing steel fibres in the concrete.

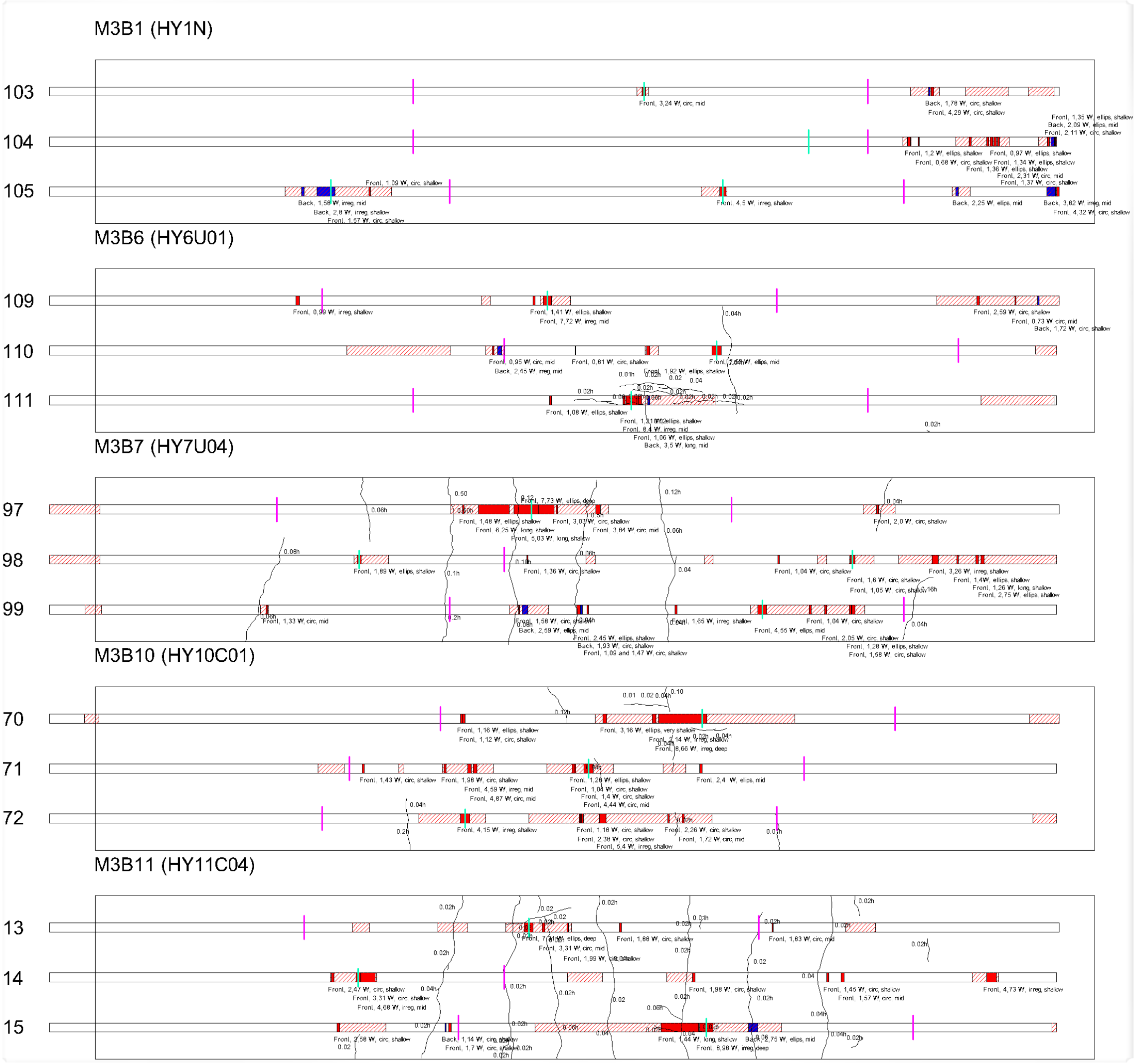

Figure 5.8: Cracks and corrosion pattern in the beams containing a hybrid between steel and PVA fibres in the concrete.

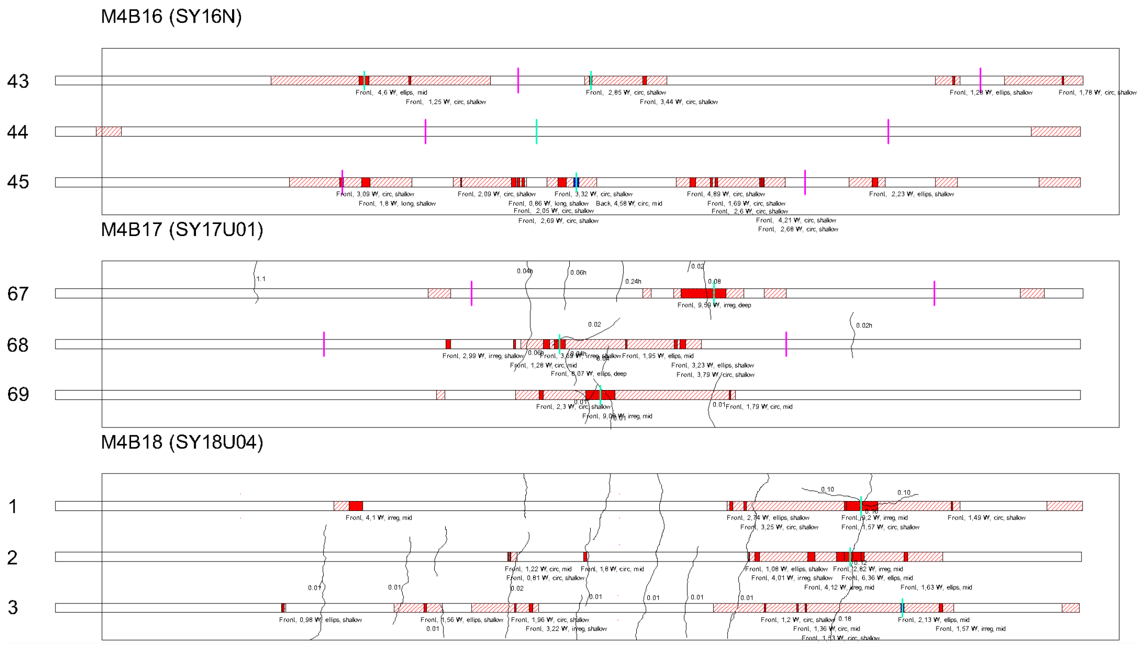

Figure 5.9: Cracks and corrosion pattern in the beams containing synthetic PVA fibres in the concrete.

5.3 Relation between critical corrosion level and target crack width

In this section, the critical corrosion levels of rebars in plain concrete and fibre reinforced concrete under the same target crack width were compared to each other. Figures 5.10-5.13 show how the critical corrosion level for each concrete mixture relate to the target crack widths, the beams have been loaded to. The definition of the y-axis is defined as the sum of bars, in a certain interval and for the specific concrete mixture, divided by the total amount of bars in the specific concrete mixture, which is also called the relative frequency.

The Figure 5.10 shows that for uncracked beams, the corrosion level in the critical section is between 0-10%, independent of concrete mixture. By comparing Figure 5.11 and Figure 5.12, for PL and ST beams, the relative frequency of critical corrosion level less than 10% under target crack width 0.1 mm is larger than that under 0.4 mm target crack, and the relative frequency of critical corrosion level within 10-20% under target crack width 0.1 mm is less than that under target crack width 0.4 mm. Further from Figure 5.11, under the target crack width 0.1 mm, the relative frequency of critical corrosion level less than 10% in ST beam is larger than that in PL beam, and the relative frequency of critical corrosion level within 10-20% in ST beam is less that in PL beam. Figure 5.11 shows that the majority of the bars in beams with synthetic PVA fibres are located in range of 20-30% under the target crack width 0.1 mm, but in Figure 5.12 the critical corrosion level for synthetic PVA fibres are not above 20% under the target crack width 0.4 mm. Note, however, that there were only three beams with synthetic PVA fibres, including one uncracked beam.

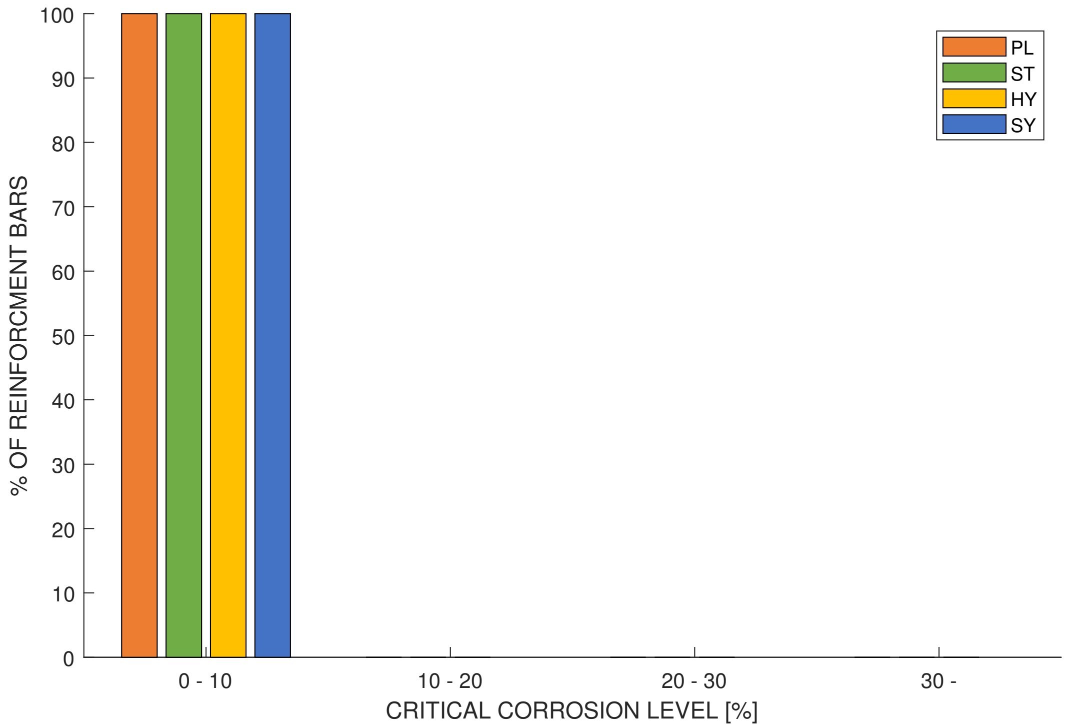

Figure 5.10: Histograms of critical corrosion level for the bars in the uncracked beams, i.e. target crack width of 0 mm.

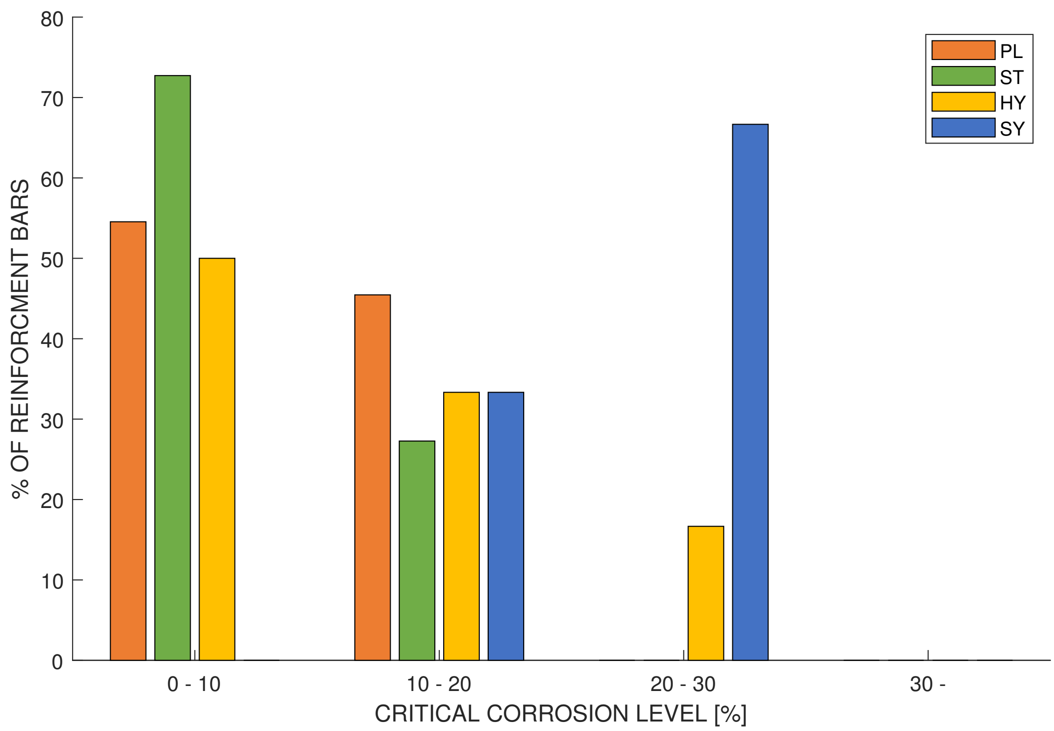

Figure 5.11: Histograms of critical corrosion level for the bars in the beams with a target crack width of 0.1 mm.

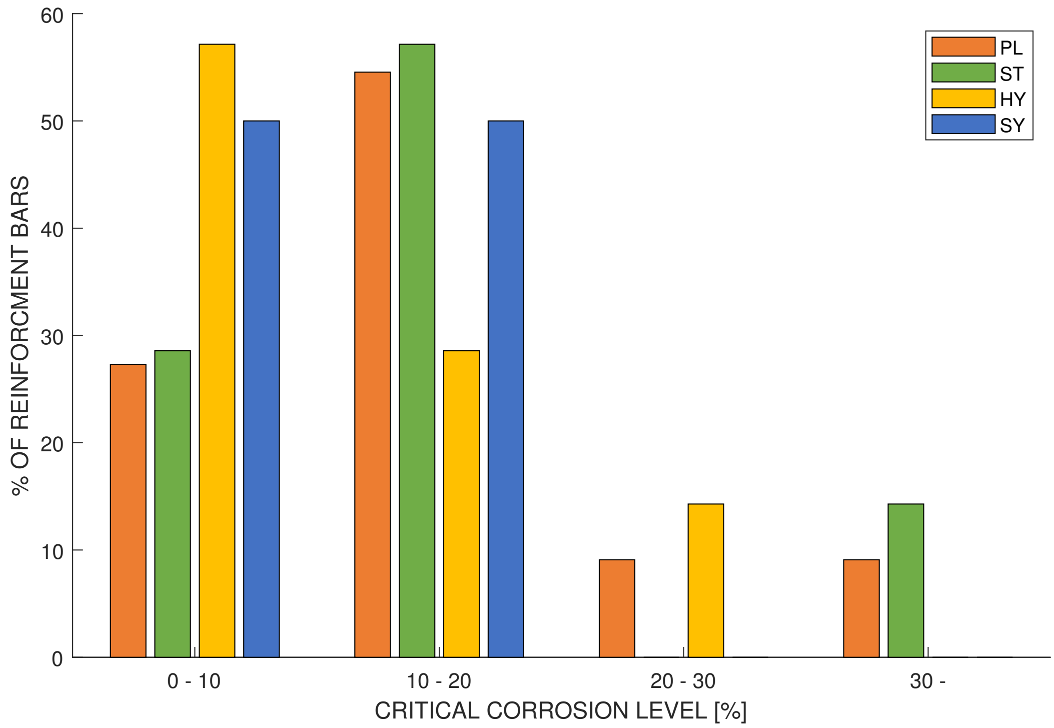

Figure 5.12: Histograms of critical corrosion level for the bars in the beams with a target crack width of 0.4 mm.

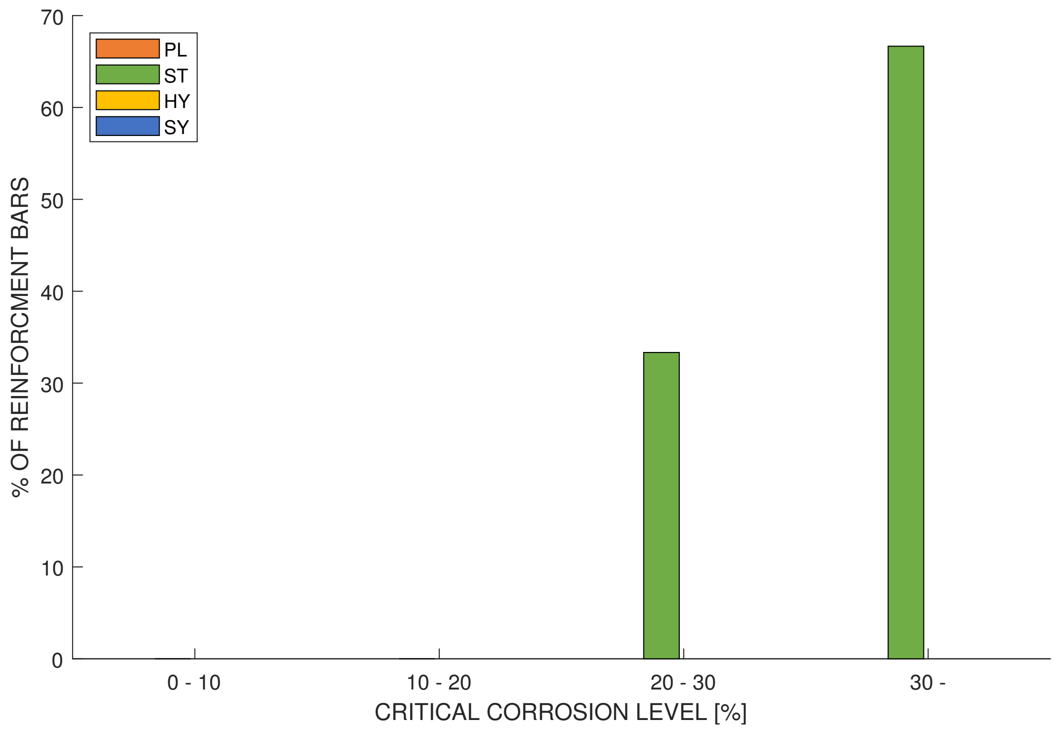

Figure 5.13: Histogram of critical corrosion levels for the bars in the beam loaded to a maximum crack width of 0.8 mm. It should be noted that this only represent one beam that was loaded to 0.8mm by mistake.

The histograms of critical corrosion level under different maximum transverse crack width, independent of the concrete, is shown in Figure 5.14. The y-axis is defined as the sum of bars in a certain interval of critical corrosion level divided by the total number of bars.

As the number of specimens with 0.1 mm and 0.4 mm is close, the relative frequency of critical corrosion level under 0.1 mm and 0.4 mm is compared. From this figure, the relative frequency of critical corrosion level less than 10% is larger under 0.1 mm than that under 0.4 mm, and the relative frequency of critical corrosion level within 10-20% under 0.1 mm is a little less than that under 0.4 mm. However, the relative frequency of critical corrosion level within 20-30% under 0.1 mm is a little larger than that under 0.4 mm. It seems there is no obvious dependence of the critical corrosion level on the maximum crack width 0.1 mm and 0.4 mm. However, all the bars in the beam reaching the maximum crack width 0.8 mm by accident have the critical corrosion level greater than 20%.

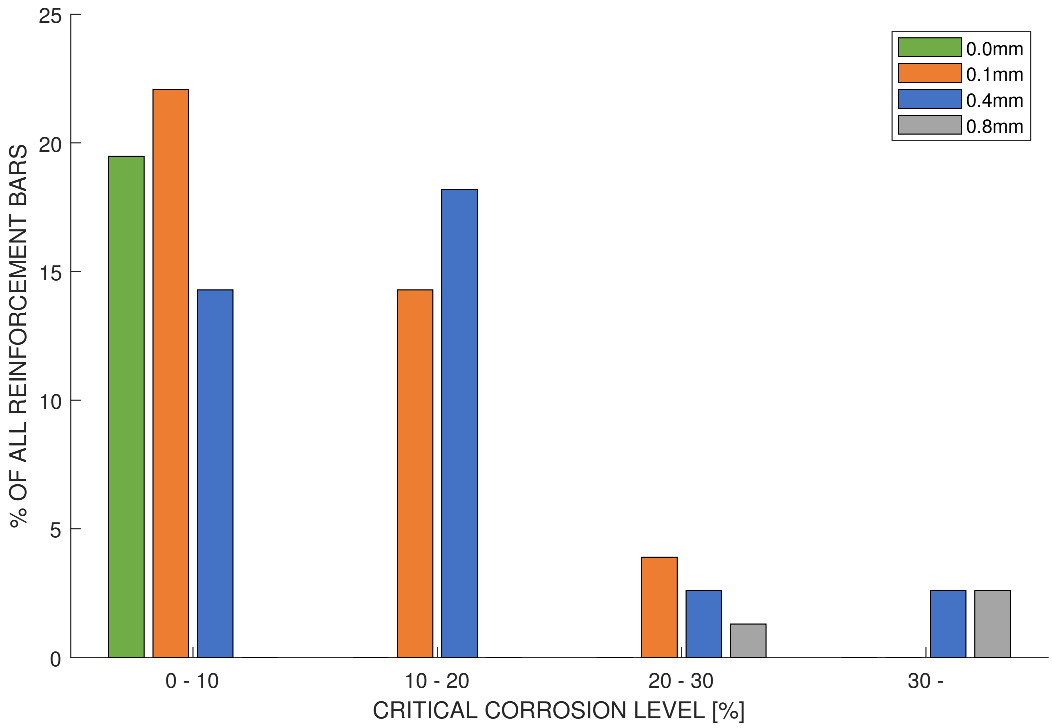

Figure 5.14: Histograms of critical corrosion level for all bars, independent on fibre type

5.4 Comparison of critical corrosion levels in all beams

In Figure 5.15 the critical corrosion level for all bars in each beam, are presented. The figure shows that the critical corrosion levels are less or similar for the bars in the fibre reinforced concrete compared to the bars in plain concrete, if the beams have the same loading conditions. It can be seen that the plain reinforced concrete specimens have a slightly larger critical corrosion level than the specimens containing fibres. The specific colour represent the location of the rebar in the beam, see section 5.2.

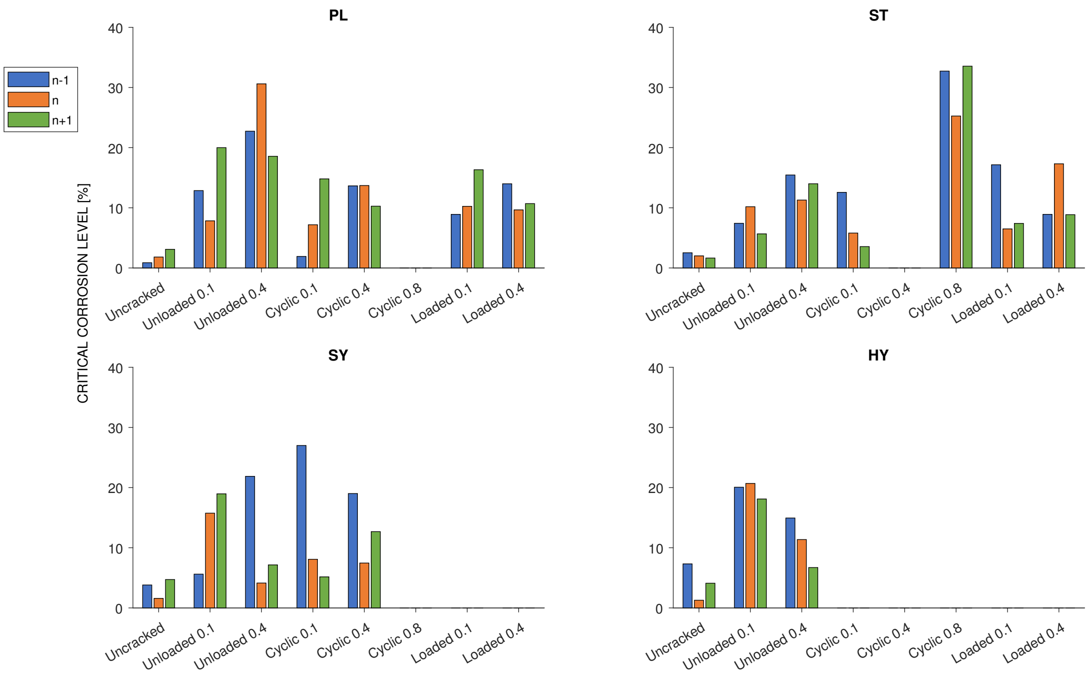

Figure 5.15: Histograms of critical corrosion level for all bars in each beam.

5.5 Relation between the sum of crack width and critical corrosion level

It is of interest to see how the type of fibre influence the corrosion level and the maximum transverse crack width. In order to demonstrate a relationship, all transverse cracks within a certain length are summed up. It was decided to investigate four different intervals, from the critical section. The intervals can be seen as a distance from the critical section in both directions. In other words, the interval 100 mm has a total length of 200 mm where the critical section is located in the middle of the length, see Figure 5.16. The four types of intervals were performed in an attempt to show within how far from the critical section does the cracks influence.

Figure 5.17 shows the relation between the critical corrosion level and the sum of cracks form four different intervals. It is difficult to see any clear connections. Therefore it was decided to divide this graph according to load conditions and target crack width. This is visualized for each interval from the critical section in Figures 5.18-5.25. The critical corrosion level for each rebar can be seen in Appendix A.

The crack widths after the exposure period was not measured for the beams that contained plain concrete. Therefore, it is only a comparison between the mixtures with different kinds of fibres. The diagrams show no obvious correlation between transverse crack widths and corrosion level in the critical section. The four different intervals only indicate that the sum of transverse crack widths increases with a wider interval.

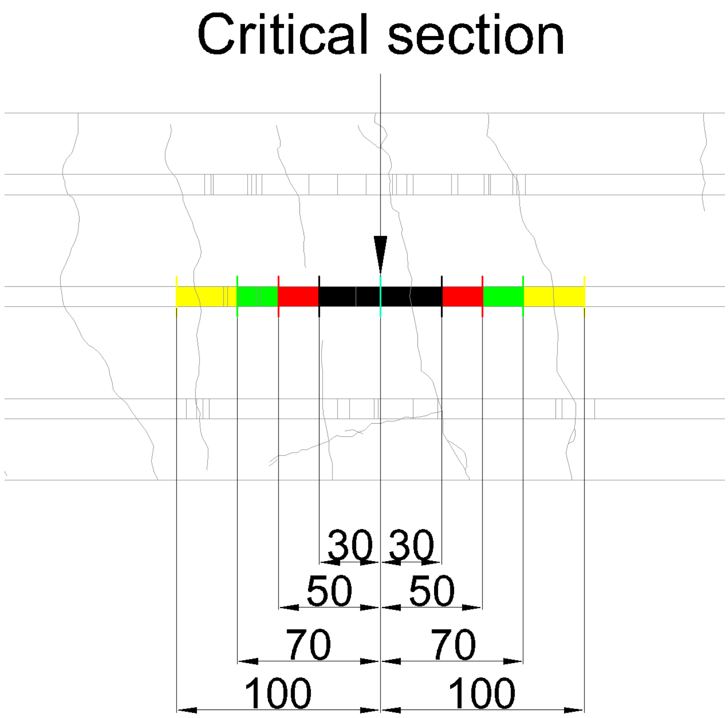

Figure 5.16: Definition of the investigated intervals 100mm (yellow), 70mm (green), 50mm (red) and 30mm (black).

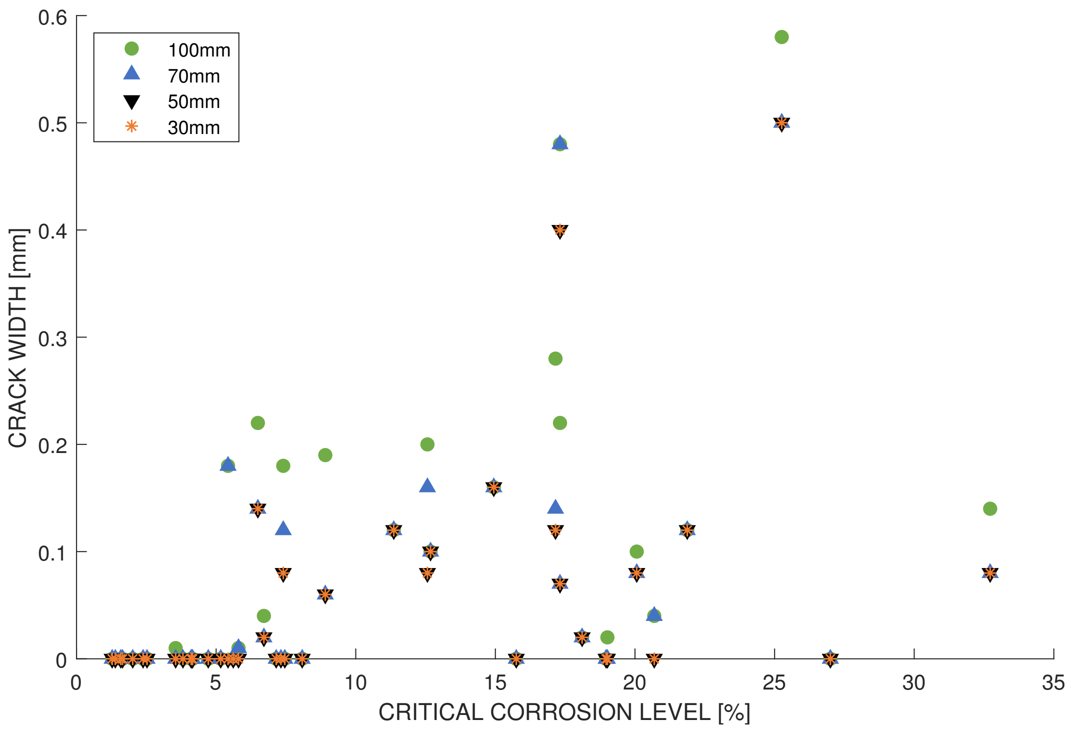

Figure 5.17: Critical corrosion level compared with the summarized transverse crack widths for four different intervals. Note that the values for 50mm and 30mm intervals often coinciding, which result in mixed markers.

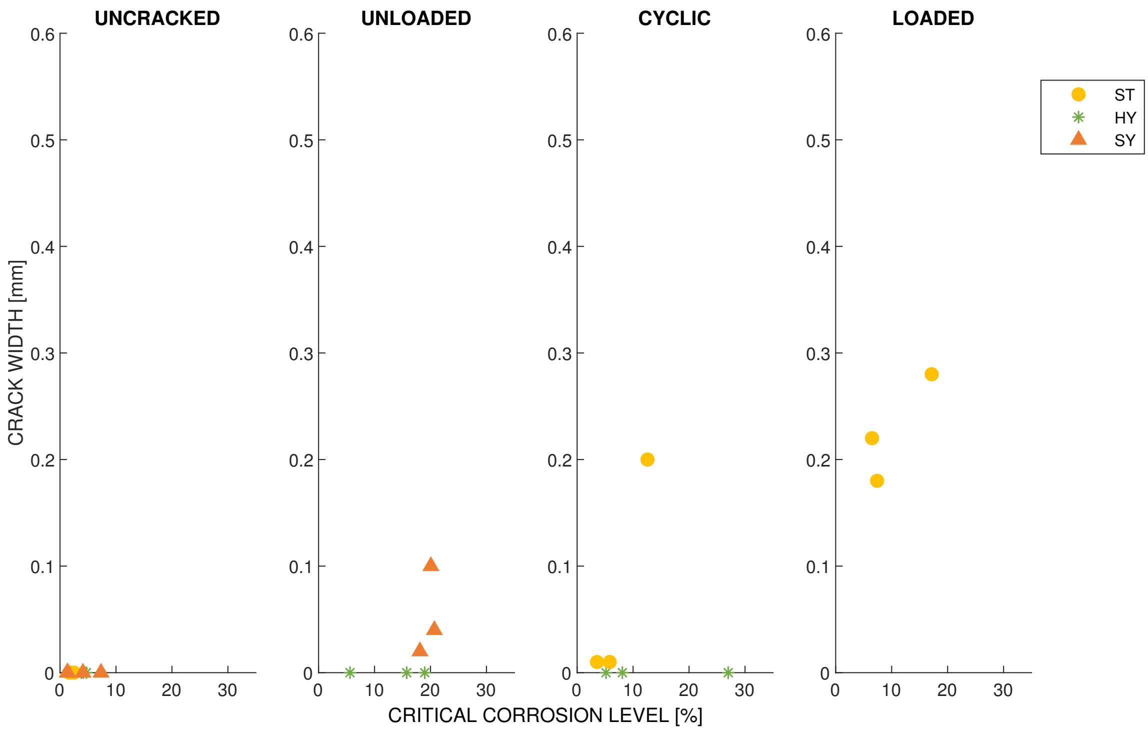

Figure 5.18: Critical corrosion level for the bars with target crack width of 0.1mm vs. sum of the crack widths in the interval of 100mm.

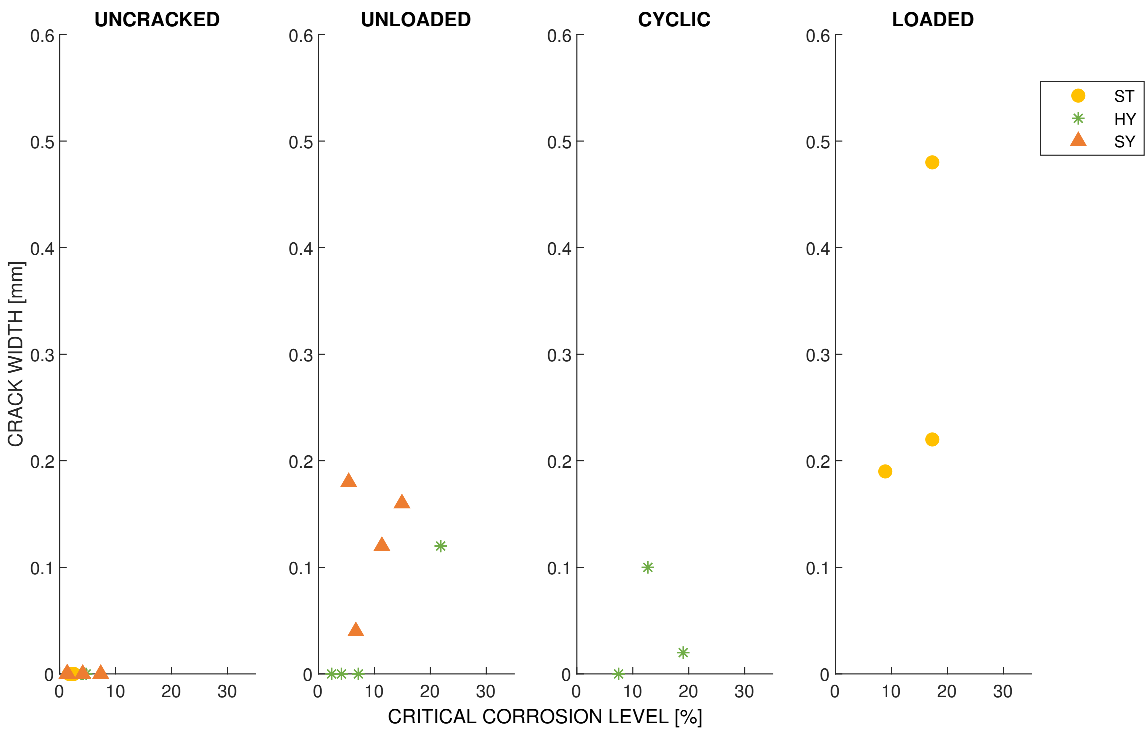

Figure 5.19: Critical corrosion level for the bars with target crack width of 0.4mm vs. sum of the crack widths in the interval of 100mm.

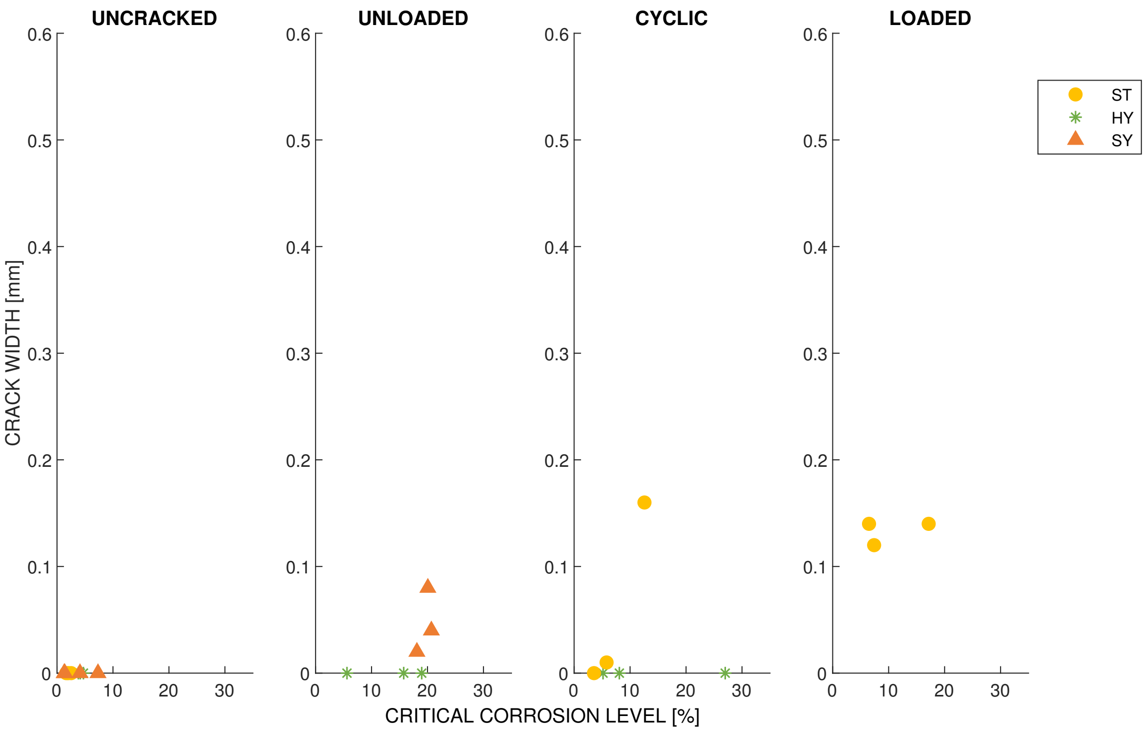

Figure 5.20: Critical corrosion level for the bars with target crack width of 0.1mm vs. sum of the crack widths in the interval of 70mm.

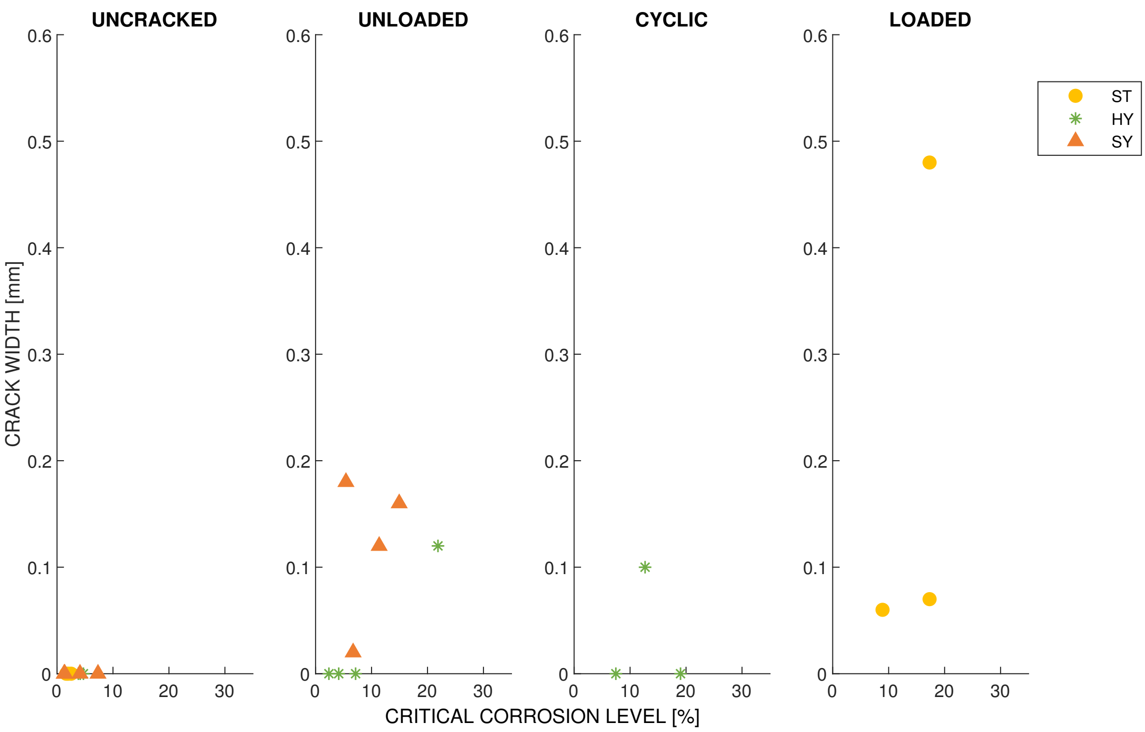

Figure 5.21: Critical corrosion level for the bars with target crack width of 0.4mm vs. sum of the crack widths in the interval of 70mm.

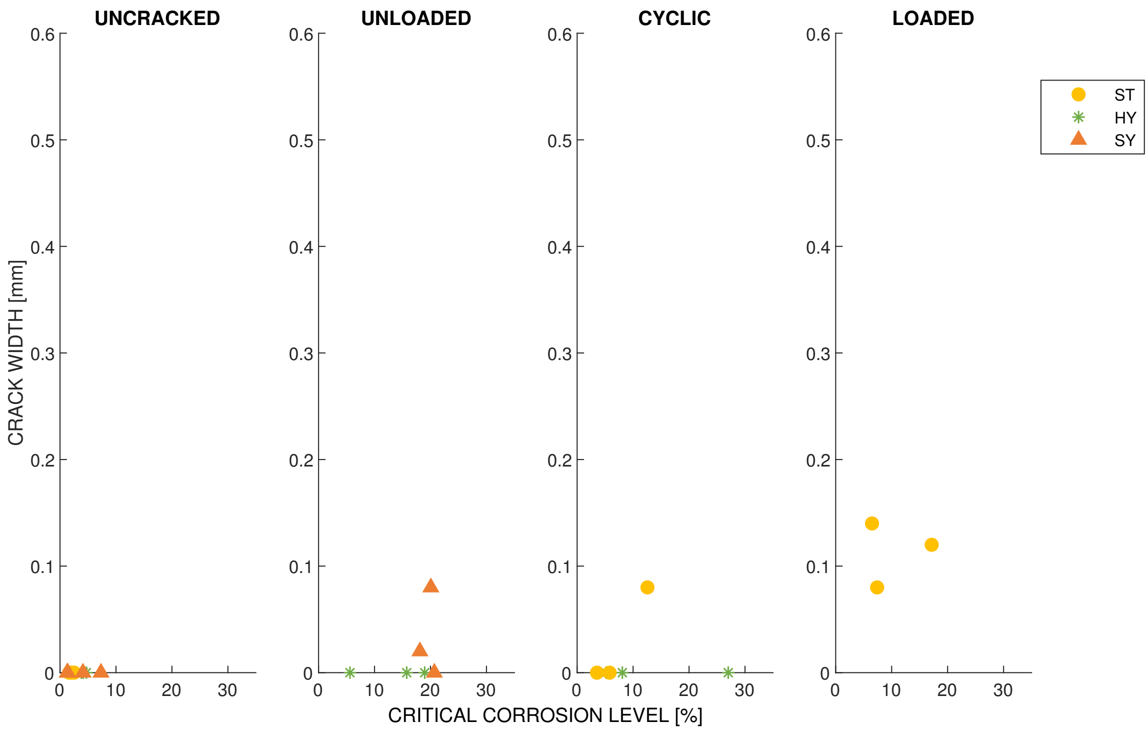

Figure 5.22: Critical corrosion level for the bars with target crack width of 0.1mm vs. sum of the crack widths in the interval of 50mm.

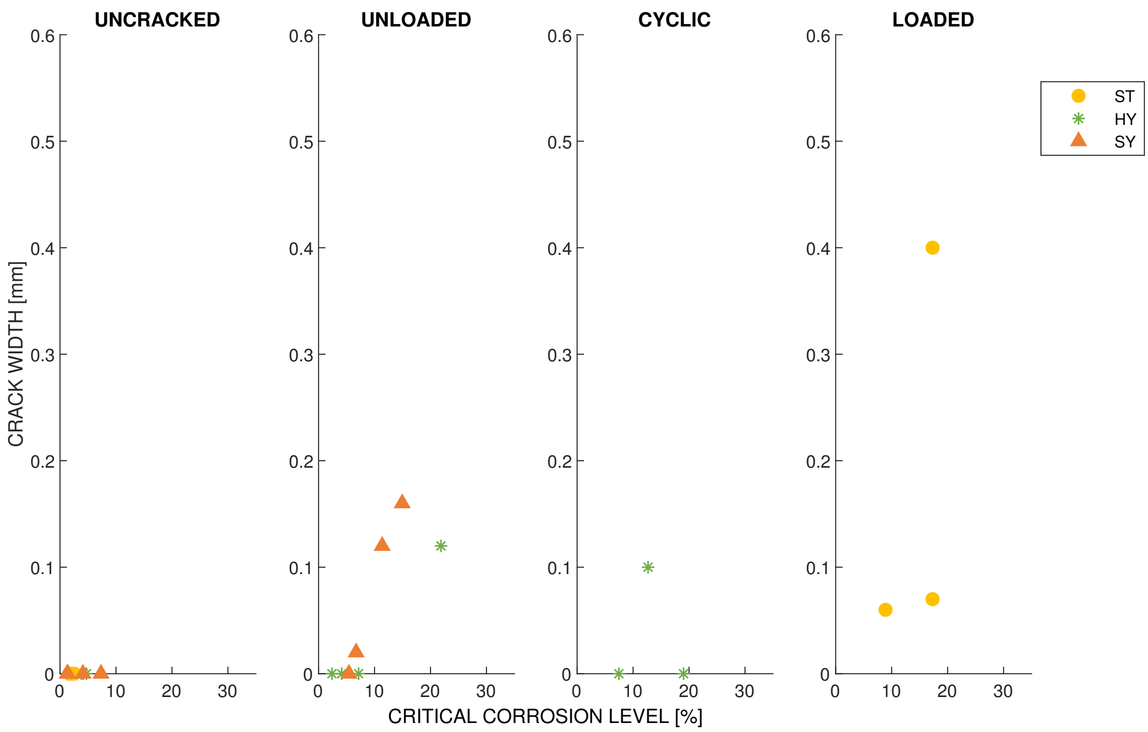

Figure 5.23: Critical corrosion level for the bars with target crack width of 0.4 mm vs. sum of the crack widths in the interval of 50mm.

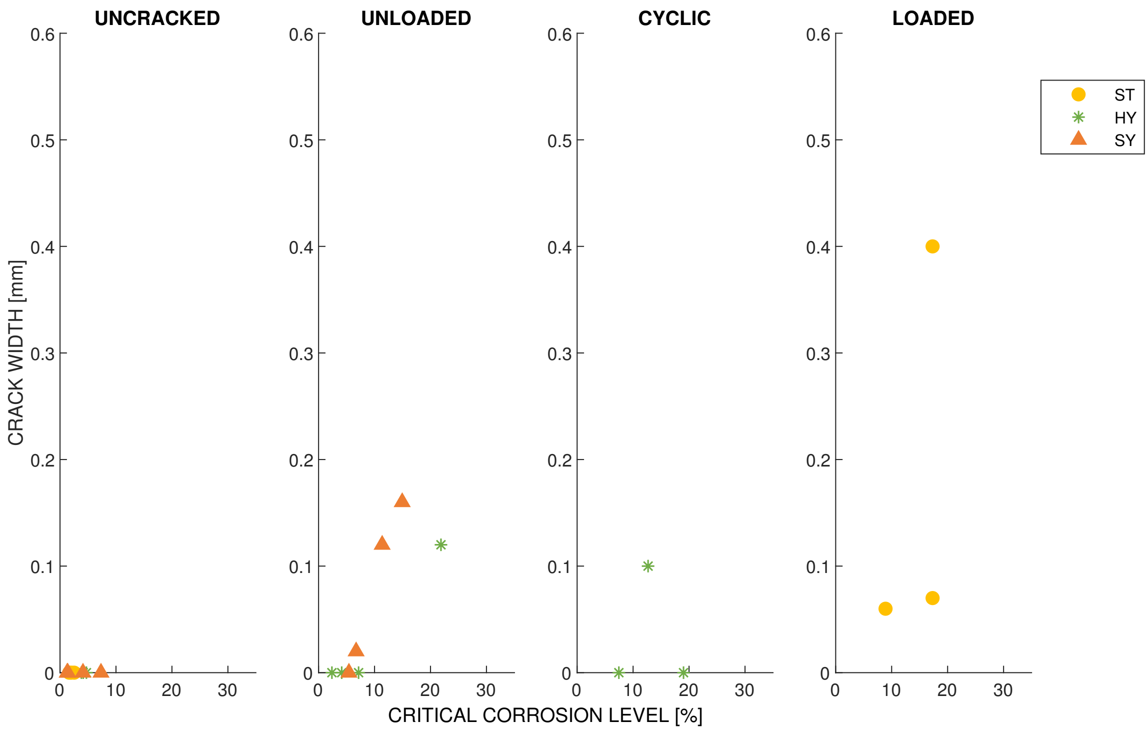

Figure 5.24: Critical corrosion level for the bars with target crack width of 0.1mm vs. sum of the crack widths in the interval of 30mm.

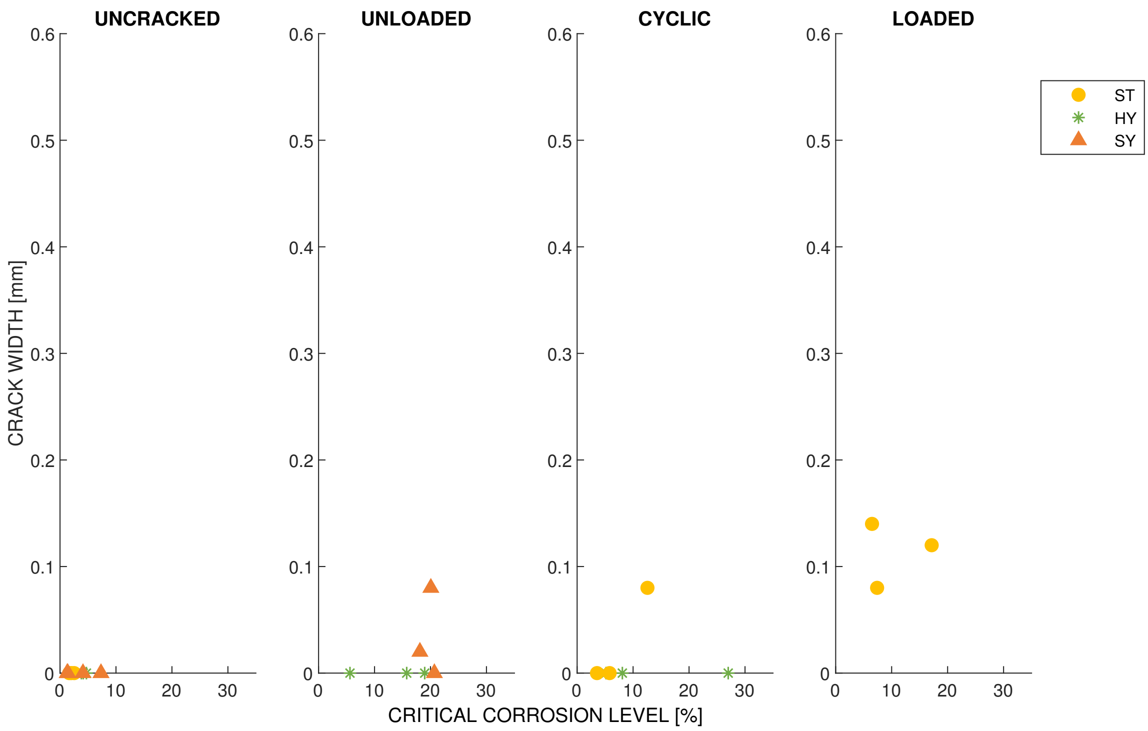

Figure 5.25: Critical corrosion level for the bars with target crack width of 0.4mm vs. sum of the crack widths in the interval of 30mm.

5.6 Corrosion in relation to transverse and longitudinal crack widths

Figure 5.26 shows how the corrosion in the reinforcement depends on the maximum transverse and longitudinal crack widths. It can be seen that the presence of longitudinal cracks, that are caused due to corrosion in the reinforcement, will affect the critical corrosion level, even if the corrosion not increase with a wider longitudinal crack width. But for some places with severe pitting corrosion it doesn't result in any longitudinal cracks. The maximum longitudinal crack width is presented as different colours on the points. The corrosion level for each rebar can be seen in Appendix A.

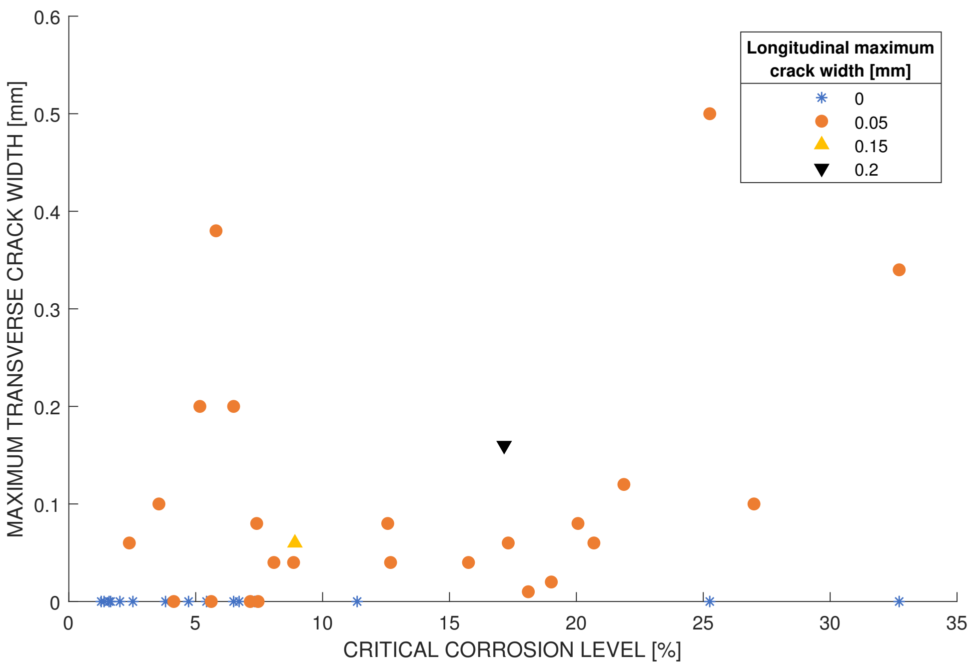

Figure 5.26: Corrosion in relation to transverse and longitudinal crack widths.

5.7 Correlation between critical corrosion level and maximum pit depth

In Figure 5.27 can it be observed that two bars has a critical corrosion level greater than 25% but have a maximum pit depth less than 2.5 mm. This is because there is area loss around the a large portion of cross section, i.e. they have very large pit width. For one bar with the pit depth near four millimeter is the critical corrosion level less than 20%, this is due to there is a hole pit, which has very deep pit depth but very small pit width. Consequently, it is shown that the relation between the critical corrosion level and maximum pit depth depends on the pit morphology.

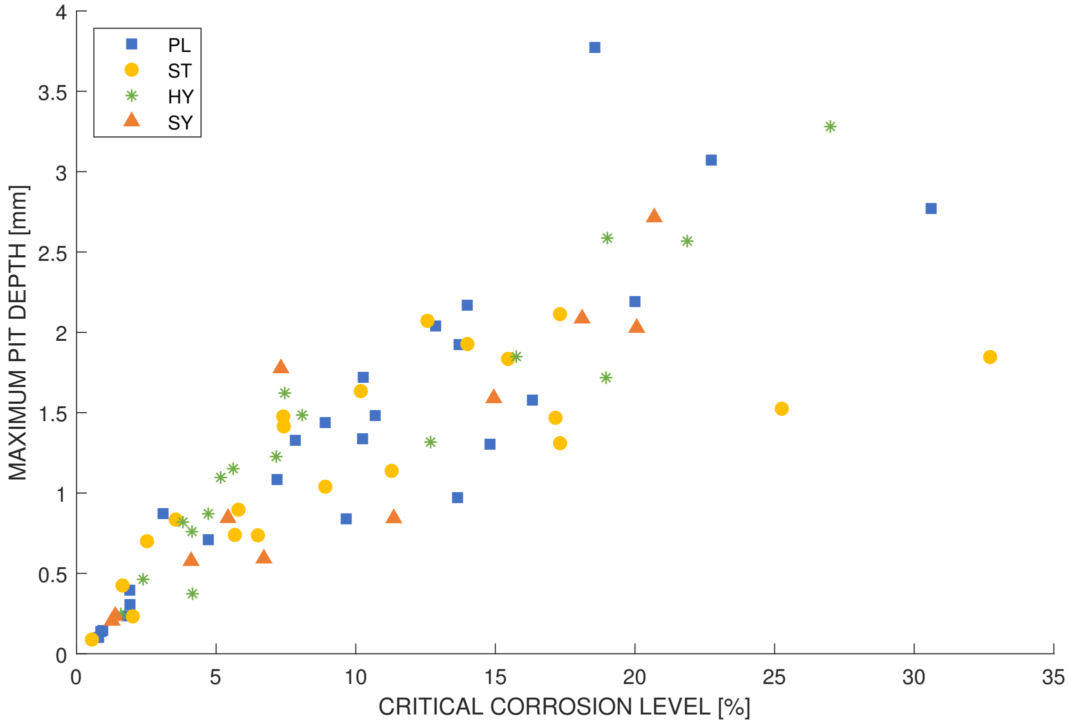

Figure 5.27: The relation between corrosion level in the critical section and maximum pit depth.

5.8 Number of cracks in relation to critical corrosion level

Since the crack widths for plain concrete were not measured after the exposure period, it was decided to compare the number of cracks with relating critical corrosion level for each concrete mixtures, see Figure 5.28. It can be seen that the fibre reinforced concrete beam in the most cases have more cracks than the beams with plain concrete, if the beams have been exposed to the same loading conditions.

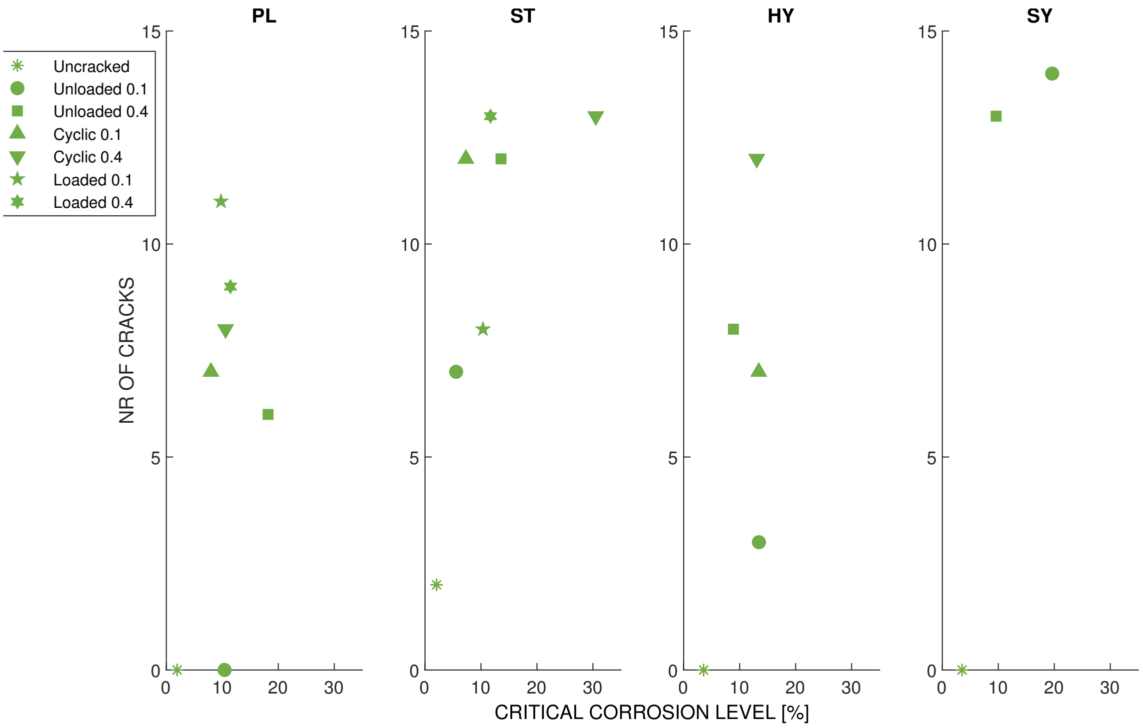

Figure 5.28: Summarized number of cracks in the whole beam compared with the corrosion level in the most critical cross-section.

6
Design procedure on edge beam

This chapter contains a design procedure for a case study where an edge beam constructed with ordinary reinforced concrete will be compared with an edge beam including both traditional reinforcing rebars and fibre reinforcement in the future. This case study can, for example, be carried out in a future master thesis.

The case study will investigate whether the life of the edge beams can be increased by adding fibres into the concrete mixture, which can be performed in a future master thesis. The design of the edge beam including fibers is suggested to have the same dimensions and reinforcement amount as the traditional edge beam.

6.1 Load model for dimensioning of edge beam

Trafikverket (2016) regulates how the edge beam should be designed. Trafikverket (2018) gives advises and is usually used as long as there is no good reason not to use it.

The most common edge beam is designed only for collision load on the railing. According EN 1991-2 (2003, 4.7.3.3(1)) together with Trafikverket (2011, chapter 6, 10 §), a global analysis should be performed with a horizontal accidental force F of 200 kN. However, no higher load needs to be considered than what the rail balusters can transmit. The accidental force F should be applied 100 mm below the top of the selected protective device. The force F and the arising sectional forces are applied as in Figure 6.1.

According to EN 1991-2 (2003, 4.7.3.3(2)) together with Trafikverket (2011, chapter 6, 10 §), the structure should locally be designed to handle an accidental load equivalent to twice the local characteristic capacity of the railing.

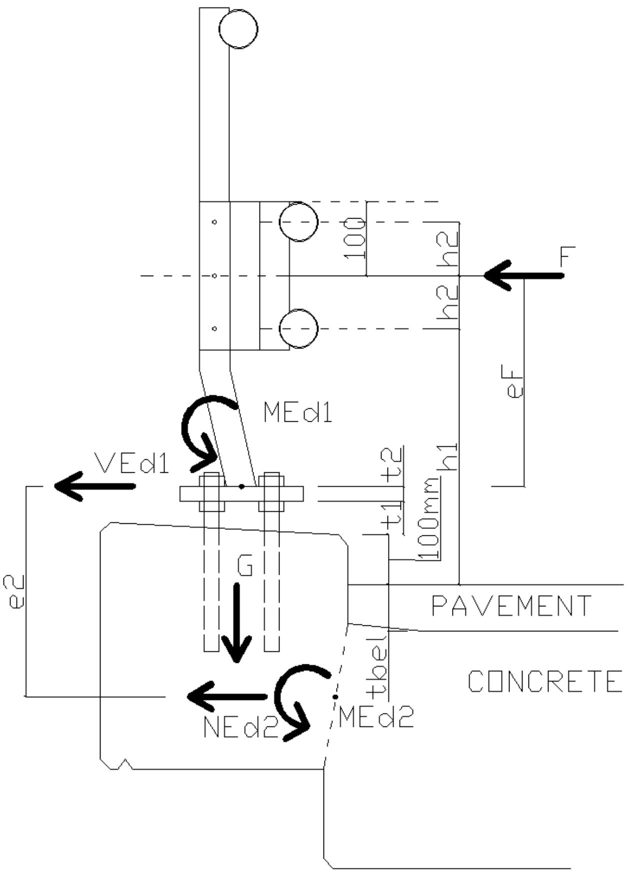

Figure 6.1: Loads acting on the edge beam.

6.1.1 Section forces for the railing baluster

The moment, that occurs when the horizontal accidental force F is applied, acting in the connection of the baluster can be calculated as

$$M_{Ed1} = F \cdot e_F. \tag{6.1}$$

The load bearing capacity for the transverse force, $V_{pl.Rd}$ and $M_{pl.Rd}$, the baluster and the railing, which are in cross-sectional class 1, can according to EN 1993-1-1 (2003) be calculated as

$$V_{pl.Rd} = \frac{A_v \cdot f_{yk.baluster}}{\sqrt{3} \cdot \gamma_{M0}}, \tag{6.2}$$

$$M_{pl.Rd} = \frac{W_{y.pl} \cdot f_{yk.baluster}}{\gamma_{M0}}, \tag{6.3}$$

$$W_{y.pl} = \frac{b^3_{baluster}}{4}. \tag{6.4}$$

Where:
$f_{yk.baluster}$ - The yield strength of the baluster
$b_{baluster}$ - The width of the baluster
A_v - The shear area, cross-sectional area of the baluster

γ_{M0}=1.0 - Partial coefficient of load bearing capacity

The plastic moment capacity based on ultimate tensile strength, f_{uk}, is instead calculated as

$$M_{u.Rd} = \frac{W_{y.pl} \cdot f_{uk}}{\gamma_{M0}}. \tag{6.5}$$

The global design shear force, V_{Ed}, is equal to the maximum shear force based on the yield strength and ultimate tensile strength. Those can be calculated by dividing the plastic moment capacity, for each case, with distance e_F. If V_{Ed} exceeds half of the value of the shear force capacity, $V_{pl.Rd}$, a combination of moment and shear force need to be checked. The baluster is often designed according to the moment, since the moment often is the most critical sectional force.

6.1.2 Dimensioning of the edge beam connection in bridge

From the global designed shear force V_{Ed}, number of balusters, which is required to take up the collision force of 200 kN, can be decided. By knowing the number of balusters and the distance between them the required length of railing, that can handle the collision load, can be defined.

The total self-weight, G_{TOT}, is the sum of the self-weight of the concrete in the edge beam and the self-weight of the railing. The dimensioning moment in the cut, visualized in Figure 6.7, can be calculated as

$$M_{Ed2} = G_{TOT} \cdot \frac{b_{beam}}{2} + \frac{M_{Ed.1} + V_{Ed} \cdot e_2}{L_{cut}} \tag{6.6}$$

where L_{cut} is the considered contributing width in the cut and e_2 is the distance between the centre of the cut and attachment of the baluster.

6.1.3 Required anchorage length for reinforcement

Required anchorage length for reinforcement can be decided according to EN 1992-1-1 (2008). The adhesive strength, f_{bd}, and the base anchorage length, $l_{b.rqd}$, are calculated as

$$f_{bd} = 2.25 \cdot \eta_1 \cdot \eta_2 \cdot \frac{f_{ctk}}{\gamma_{c.acc}}, \tag{6.7}$$

$$l_{b.rqd} = \frac{\phi_s}{4} \cdot \frac{f_{yk.s}}{\gamma_{s.acc} \cdot f_{bd}}. \tag{6.8}$$

Where:
$f_{yk.s}$ - The yield strength of the reinforcement
f_{ctk} - Tensile strength of the concrete
$\gamma_{c.acc}$ - Partial coefficient for concrete in case of accident load
$\gamma_{s.acc}$ - Partial coefficient for steel in case of accident load
ϕ_s - Transverse reinforcement from the bridge deck

η_1=1.0 and η_2=1.0 - Constants during good adhesion conditions (reinforcement anchored in the lowest 250mm of the edge beam) and the diameter of the reinforcement is less than 32 mm.

The design anchorage length are calculated as: $l_{bd.1} = \alpha_1 \cdot \alpha_2 \cdot \alpha_3 \cdot \alpha_4 \cdot \alpha_5 \cdot l_{b.rqd}$. Where the different α depends on the reinforcement, cover thickness and acting load. The minimum anchorage length is determined as

$$l_{bd.min} = max \begin{bmatrix} 0.3 \cdot l_{b.rqd} \\ 10 \cdot \phi_s \\ 100mm \end{bmatrix}. \tag{6.9}$$

The design anchorage length, l_{bd}, when the minimum value is taken into account, is the largest of $l_{bd.1}$ and $l_{bd.min}$.

6.1.4 Control of moment capacity

When checking the moment capacity in the critical section, the effective height for the critical section needs to be calculated as $d_{cut} = b_{cut} - c_d - \frac{\phi_s}{2}$, see Figure 6.2. The moment capacity can be simplified and calculated as

$$M_{Rd2} = A_{si} \cdot \frac{1}{s_s} \cdot \frac{f_{yk.s}}{\gamma_{s.acc}} \cdot 0.9 \cdot d_{cut}. \tag{6.10}$$

Where:
d_{cut} - Effective height in the cut
b_{cut} - Width in the cut
c_d - Cover thickness of concrete
$M_{Rd.2}$ - Moment capacity in the cut
s_s - Spacing of transverse reinforcement
A_{si} - Cross-sectional area of one rebar

The utilization rate is given by comparing it with M_{Ed2}.

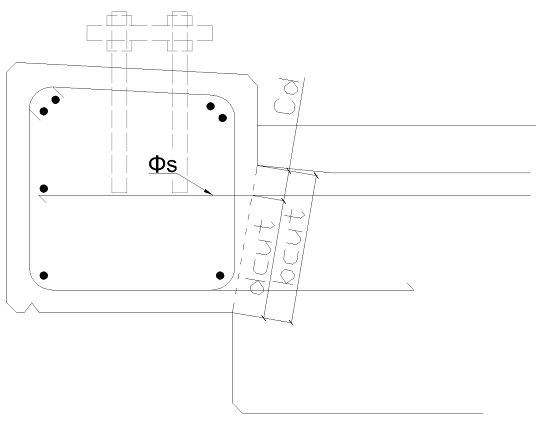

Figure 6.2: Definition of d_{cut}-the effective height in the cut.

6.1.5 Control of bending moment capacity of the edge beam

The edge beam's bending moment capacity can be calculated in a simplified way by assuming the contributing length, L_{cut}, to be one meter. By dividing V_{Ed} with L_{cut}, a line load is obtained, here called $q_{Ed.k}$. The acting bending moment can then be calculated as

$$M_{Ed.k} = q_{Ed.k} \cdot 0.5 \cdot (0.5 \cdot L_{cut})^2. \tag{6.11}$$

There are three rebars along the edge of the beam, see Figure 6.3. The area A_s is given by the sum of the area of those rebars. The bending moment capacity is

$$M_{Rd.k} = A_s \cdot 0.9 \cdot d_h \cdot \frac{f_{yk.s}}{\gamma_{s.acc}} \tag{6.12}$$

where d_h is the efficient height in the cross-section.

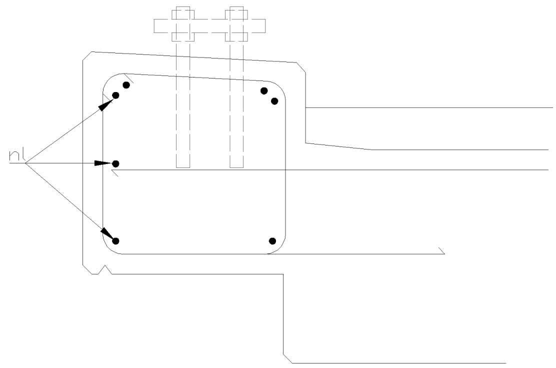

Figure 6.3: Reinforcement along the edge beam

6.1.6 Check of torque capacity of the edge beam

The shear force acting on the edge beam is also creating a torque, which needs to be designed for. It depends on the vertical and the horizontal components of the shear force. The horizontal shear force is subdivided into $V_{Ed.h.1}$ and $V_{Ed.h.2}$, and the total shear force is calculated as

$$V_{Ed.h} = 0.5 \cdot V_{Ed.h.1} + V_{Ed.h.2}. \tag{6.13}$$

Where $V_{Ed.h.1}$ is the shear force due to the line load, determined as

$$V_{Ed.h.1} = q_{Ed.k} \cdot (0.5 \cdot L_{cut}) \tag{6.14}$$

and $V_{Ed.h2}$ is derived from the moment which acting on the edge beam, M_{Ed2}, and calculated as

$$V_{Ed.h.2} = \frac{T_{Ed}}{2 \cdot A_k}. \tag{6.15}$$

The vertical component of the shear force is determined as

$$V_{Ed.v} = \frac{T_{Ed}}{2 \cdot A_k}. \tag{6.16}$$

Where T_{Ed} and A_k are determined as

$$T_{Ed} = 0.5 \cdot M_{Ed2} \cdot L_{cut}, \tag{6.17}$$

$$A_k = Z_v \cdot Z_h. \tag{6.18}$$

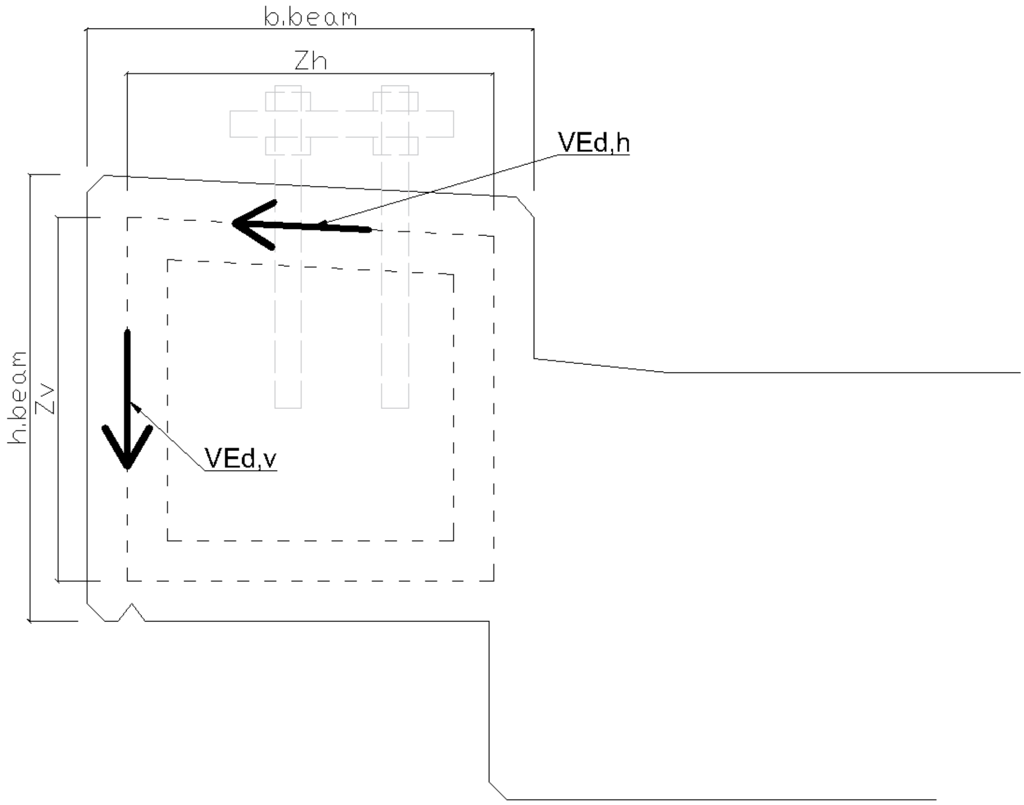

Figure 6.4: Torque in the edge beam.

It can be assumed that the safe side of the shear reinforcement is required and control of shear resistance is performed according to EN 1992-1-1 (2008), which can be determined as

$$V_{Rds.v} = A_{sw} \cdot 0.9 \cdot \frac{d_v}{s_b} \cdot f_{yk.s}, \tag{6.19}$$

$$V_{Rds.h} = A_{sw} \cdot 0.9 \cdot \frac{d_h}{s_b} \cdot f_{yk.s}. \tag{6.20}$$

Where:
A_{sw} - The area of the shear reinforcement
d_v/d_h - The efficient height for each direction
s_b - The spacing between the shear reinforcement

In addition of the control of the concrete and the reinforcement capacity in the beam, the balusters connection needs to be designed. This is done by checking the spalling, checking the bolts for the rail attachment, checking the bolt's insertion length, and checking possible cone fracture.

6.2 Further analysis in case study

A possible design of dimensions and reinforcement arrangement is shown in Figure 6.5, Figure 6.6 and Figure 6.7. The suggestion is based on an existing non-load carrying edge beam, i.e. it is not included in the load carrying system. A non-load carrying edge beam is one of the most common types in Sweden and therefore a suitable choice of design. The non-load carrying edge beam is designed with just an accidental load as in chapter 6.

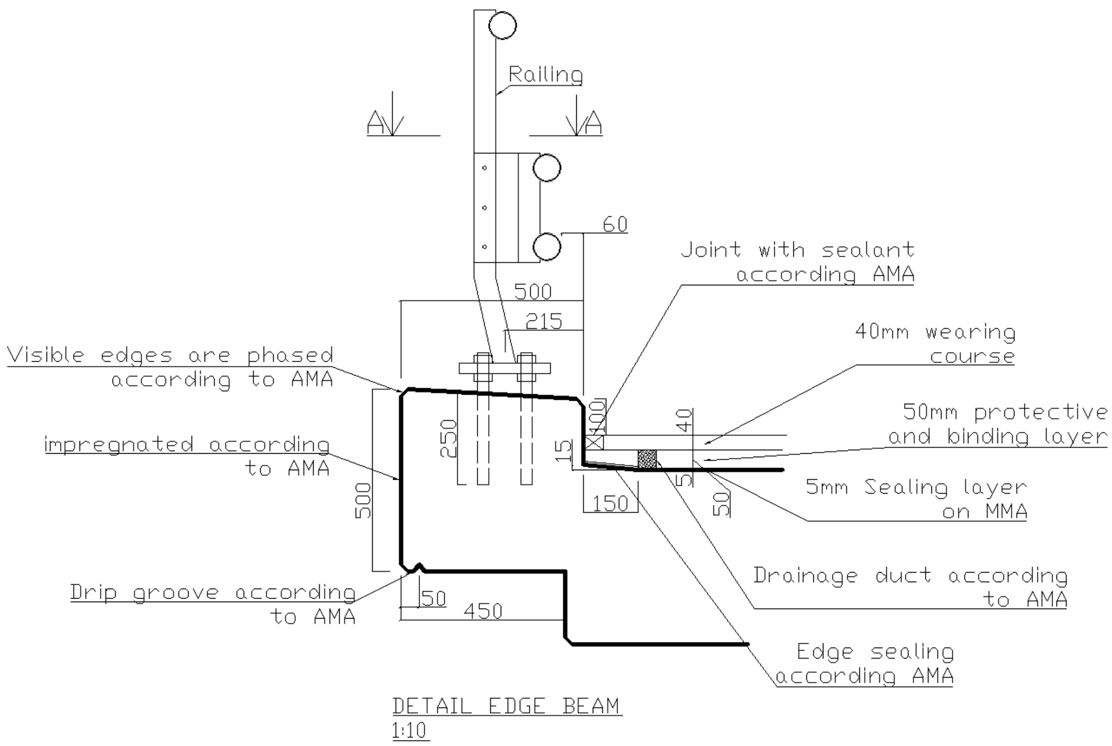

Figure 6.5: A detail of the designed edge beam.

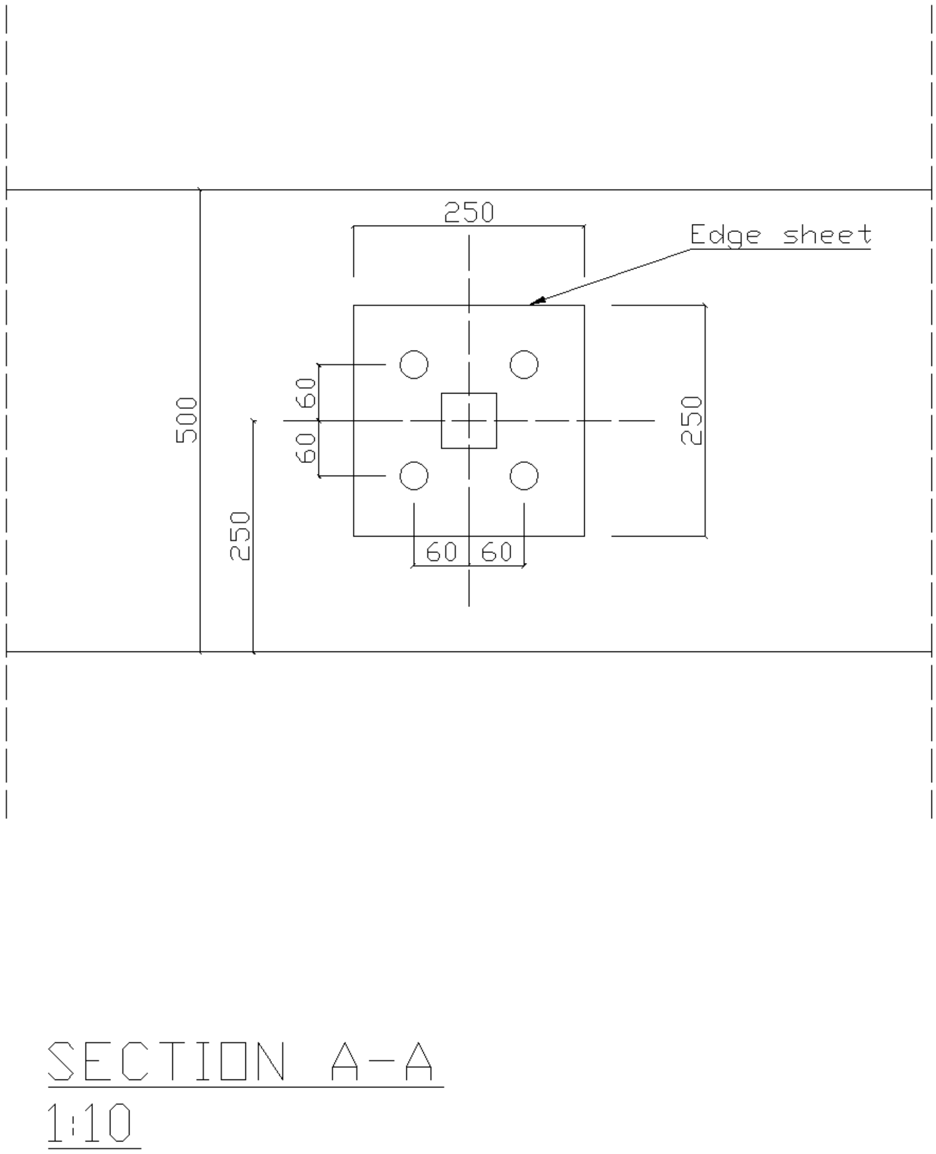

Figure 6.6: Section A-A of the designed edge beam.

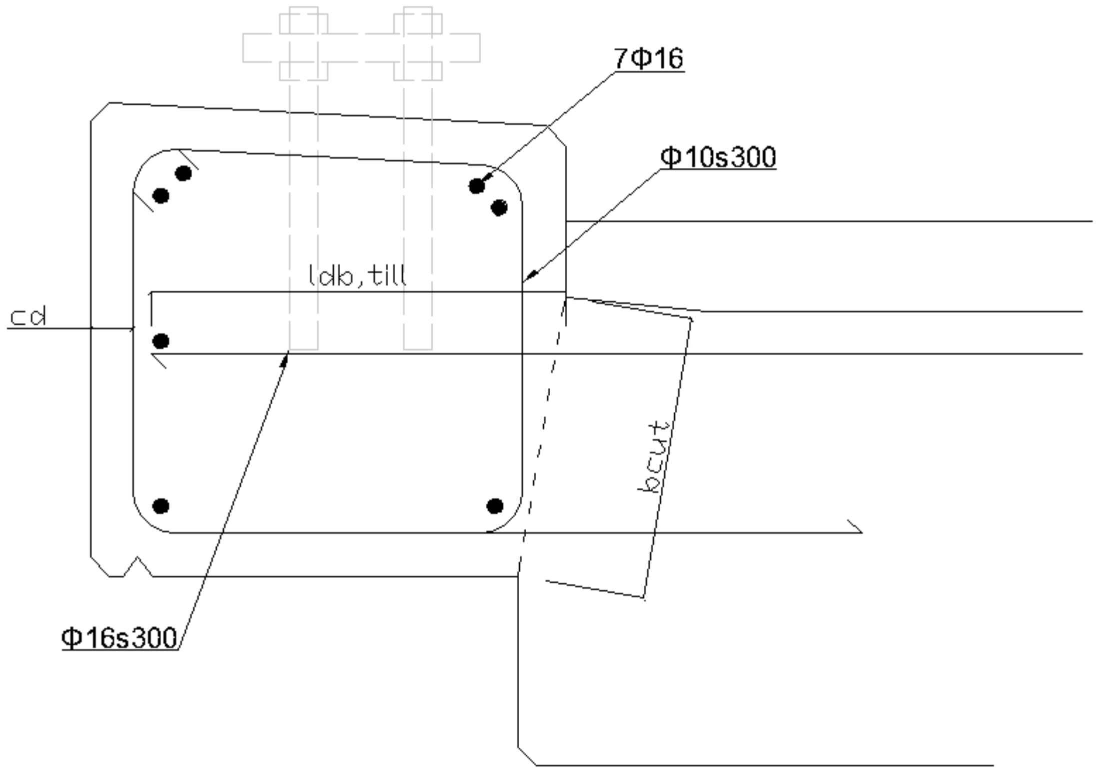

Figure 6.7: The reinforcement layout in the designed edge beam. Where *bcut* stands for the width in the connection between the edge beam and slab, and $lbd, till$ stands for the transverse reinforcement from the bridge deck.

7 Discussion

This chapter discusses the results of this master thesis. It is based on the literature study and the performed experiments.

7.1 Measurements

This master thesis is performed as a part of a bigger project where the whole project was based on laboratory studies. Some experiments on reported beams in this project had already been completed for other studies. Consequently, that led to the crack widths for plain concrete were not measured after the exposure period, which made it difficult to make a comparison between plain concrete and fibre reinforced concrete regarding the relation between transverse crack width and critical corrosion level.

It was first decided not to focus on the longitudinal cracks, although measurements of those were taken. Subsequently, the results showed that longitudinal cracks had a major influence on the corrosion, which is further discussed in section 7.2. The measurements would probably have been performed more carefully concerning longitudinal cracks.

The number of concrete beams of the same type varied between the different concrete mixtures. This leads to the result being difficult to interpret due to lack of number of specimens for some concrete mixtures, especially for the beams with synthetic fibres since there were only three beams of that type.

Since the crack width is not constant over a crack can it be difficult to know if the measured crack width is accurate for the specific crack. Further, there was sometimes loss of concrete in areas near a crack which must be taken into account, with other words, the crack width at some locations may include loss of concrete. Therefore, it is necessary to critically evaluate the data when the results are interpreted.

7.2 Analysis of the result

In the figures drawn in AutoCAD, it can be seen, that the location of cracks and corrosion often correspond to each other. Except from that, it could also be seen that there are cracks that have not induced on the reinforcement bars. This could be explained by that the reinforcement sacrificing one area and let it corrode first.

By analyzing the critical corrosion levels and the beams' target crack width or loading conditions, it seems that the fibre reinforced concrete beams have slightly less corrosion than the concrete beams with no fibres. This indicates that the fibres have influence on the corrosion, but it is difficult to define exactly why the corrosion became less for the fibre reinforce concrete. One factor could be the crack width, since fibres generally decreases the crack width. More factors could be involved, but it is difficult to determine them since no crack widths for the beams with no fibres where available.

It seems as longitudinal cracks and transverse cracks together, affect the corrosion rate in the steel, see Figure 5.26. Although the transverse cracks are small, they promote corrosion initiation, which leads to the longitudinal cracks. The longitudinal cracks can, in turn, increase the corrosion rate. It can be noted that the longitudinal cracks, in the studied specimens, have occurred due to the formation of rust. But at the same time was it possible to see that some deep corrosion pits did not always lead to longitudinal cracks.

The analysis of the result showed that the correlation between visible cracks and corrosion is complicated, which agrees with literature. Moreover, there is a need to do further studies for a clearer correlation between cracks and corrosion. Suggestions for further studies is presented in section 8.2.

7.3 Impact of fibres

Although the fibres can contribute to the strength of concrete structures, it can be discussed whether the aesthetic look is desirable when steel fibres are included in the concrete mixture. The steel fibres tend to give rise to superficial corrosion, see section 5.1, which appears in the typical orange colour. The superficial corrosion, seen in this study, coincides with that previously described in subsection 2.2.3. The visible corrosion can also affect the public's perception of strength since corrosion usually is perceived as a weakness in the material. Meanwhile, for mixtures that only consist of synthetic fibre, no surface corrosion can be seen. From that point of view, synthetic fibres can be used to avoid surface corrosion which also was described in literature, however, they lack the high strength that steel fibers provide.

Previous research projects, described in Berrocal et al. (2017), have shown that fibre reinforced concrete has less pitting corrosion but more scattered corrosion with more pits but smaller. However, in this study, it is impossible to draw any conclusions regarding that, since the thesis mainly compared different types of fibres in the concrete mixtures.

8

Conclusions and suggestions for further studies

This chapter presents the conclusions and the suggestions for further studies.

8.1 Conclusions

From this study, the following conclusions were drawn:

- Most corrosion occurred near the pre-existing crack. However, some cracks did not induce corrosion of rebars. That is probably caused due to that the corrosion induced earliest at the widest crack width may delay and suppress corrosion at other cracks. It is difficult to estimate the rebar degradation based on measurements of surface cracks.

- It is not sufficient to focus on the transverse cracks only, since when corrosion-induced longitudinal cracks appear, they also influence the corrosion process. But some deep and severe pits, caused by corrosion, did not induce any longitudinal cracks.

- It is probably suitable to use fibre reinforced concrete instead of plain concrete in edge beams, as the structural capacity increases. But it should be noted that steel fibres affect the aesthetic of the edge beam due to surface corrosion, and may therefore not be a good choice.

- The type of fibre in the concrete mixture doesn't seem to influence the degree of critical corrosion level considerably.

- The transverse crack widths were slightly larger for steel fibre reinforced concrete compared to the other fibre reinforced mixtures, but the critical corrosion level seems to be similar regardless of fibre type.

This study showed that the corrosion level of most bars in fibre reinforced concrete is less than in plain concrete under the same loading condition and target crack width. It should be noted that the loading level is higher in fibre reinforced concrete beams than plain reinforced beams to reach the same target crack width. Furthermore, under the same corrosion degree, the residual structural capacity of fibre reinforced concrete would be higher than plain reinforced concrete due to the shear resistance provided by fibres. Although no dependency of the corrosion level on the maximum crack width 0.1 mm and 0.4 mm was found in this thesis, all cracked beams had larger corrosion degree than uncracked beams, and the beam with 0.8 mm crack width had the most severe corrosion degree, which indicates that controlling crack width is still necessary.

Finally, it can be concluded that the subject treated in this thesis is broad and complex. Further research is needed to possibly find a more specific connection between cracks and corrosion.

8.2 Suggestion for further studies

Further studies on how fibres can reduce the crack with can be done by doing a case study of an edge beam. In short terms, it is suggested to develop a FE-model where fibres are included and examine how the volume of fibres affects the crack width. It can also be investigated how the length of the fibres, the type of fibre and the shape of the fibre affect the result.

Although it is possible to design an edge beam to obtain smaller crack width, there are more aspects that need to be taken into account. The economical aspect is of big importance in the design, which includes both material costs, maintenance cost and the cost a traffic disruption would lead to. These aspect need to be evaluated and compared to the hopefully extended service-life, which an edge beam with fibres would have. A suggestion to the case study is thus to examine whether it is economically viable to include fibres in order to extend the service-life.

Bibliography

Ahlström, L. U. (2011), 'Corrosion of Steel in Concrete at various moisture and chloride levels', *Energiforsk AB* pp. 633–647.
URL: *http://doi.wiley.com/10.1002/9780470872864.ch49*

Al-emrani, M., Engström, B., Johansson, M. & Johansson, P. (2013), Bärande konstruktioner, Technical report, Bygg- och miljöteknik, Göteborg.

Andisheh, K., Scott, A. & Palermo, A. (2016), 'Modeling the influence of pitting corrosion on the mechanical properties of steel reinforcement', *Materials and Corrosion* **67**(11), 1220–1234.

Balouch, S. U., Forth, J. P. & Granju, J. L. (2010), 'Surface corrosion of steel fibre reinforced concrete', *Cement and Concrete Research* **40**(3), 410–414.
URL: *http://dx.doi.org/10.1016/j.cemconres.2009.10.001*

Berrocal, C. G., Löfgren, I. & Lundgren, K. (2018), 'The effect of fibres on steel bar corrosion and flexural behaviour of corroded RC beams', *Engineering Structures* **163**(15 May 2018), 409–425.

Berrocal, C. G., Löfgren, I., Lundgren, K. & Tang, L. (2015), 'Corrosion initiation in cracked fibre reinforced concrete: Influence of crack width, fibre type and loading conditions', *Corrosion Science* **98**, 128–139.

Berrocal, C. G., Lundgren, K. & Löfgren, I. (2017), 'Fibrer i anläggningskonstruktioner', *Bygg och Teknik* **7**(Betong), 30–33.
URL: *https://research.chalmers.se/publication/252633*

Creaform (2019), 'HandySCAN 3D'.
URL: *https://www.creaform3d.com/en/metrology-solutions/portable-3d-scanner-handyscan-3d*

Domone, P. & Illston, J. (2010), *Construction materials: Their nature and behaviour: Fourth edition*, Spon press.

EN 1991-2 (2003), Eurocode 1: Actions on structures - Part 2: Traffic loads on bridges, Standard, European Committee for Standardization.

EN 1992-1-1 (2008), Eurocode 2 - Design of concrete structures, Standard, European Committee for Standardization.

EN 1993-1-1 (2003), Eurocode 3: Design of steel structures - Part 1-1: General rules and rules for buildings, Standard, European Committee for Standardization.

Fernandez, I., Lundgren, K. & Zandi, K. (2018), 'Evaluation of corrosion level of naturally corroded bars using different cleaning methods, computed tomography, and 3D optical scanning', *Materials and Structures/Materiaux et Constructions* **51**(3), 1–13.
URL: *https://doi.org/10.1617/s11527-018-1206-z*

Hwang, J. P., Jung, M. S., Kim, M. & Ann, K. Y. (2015), 'Corrosion risk of steel fibre in concrete', *Construction and Building Materials* **101**, 239–245.
URL: *http://dx.doi.org/10.1016/j.conbuildmat.2015.10.072*

Löfgren, I. (2005), Fibre-reinforced concrete for industrial construction - A fracture mechanics approach to material testing and structural analysis, PhD thesis, Chalmers university of technology, Göteborg.

Mattsson, H.-Å. & Sundquist, H. (2007), 'The Real Service Life and Repair Costs for Bridge Edge Beams', *Restoration of buildings and monuments,* **13**(4), 215–228.
URL: *https://www.kth.se/polopoly_fs/1.517556.1550156610!/The%20Real%20Service%20Life%20and%20Repair%20Costs%20for%20Bridge%20Edge%20Beams.pdf*

Nationalencyklopedin (2019), 'hydrolys - Uppslagsverk - NE.se'.
URL: *https://www.ne.se/uppslagsverk/encyklopedi/lång/hydrolys*

Noushini, A., Samali, B. & Vessalas, K. (2013), 'Effect of polyvinyl alcohol (PVA) fibre on dynamic and material properties of fibre reinforced concrete', *Construction and Building Materials* **49**, 374–383.
URL: *http://dx.doi.org/10.1016/j.conbuildmat.2013.08.035*

Park, W. S. & Yun, H. D. (2011), 'Seismic performance of pseudo strain-hardening cementitious composite coupling beams with different reinforcement details', *Composites Part B: Engineering* .

Pettersson, L. & Sundquist, H. (2014), Optimala kantbalkssystem, Technical report, KTH, Civil and Architectural Engineering, Stockholm.

Polymer Properties Database (2017), 'PVA Fibers'.
URL: *http://polymerdatabase.com/Fibers/PVA.html*

Shaikh, F. U. A. (2018), 'Effect of Cracking on Corrosion of Steel in Concrete', *International Journal of Concrete Structures and Materials* **12**(1).
URL: *https://doi.org/10.1186/s40069-018-0234-y*

SS-EN 14889-1:2006 (2006), 'SVENSK STANDARD Fibrer för betong – Del 1 : Stålfibrer – Definitioner , specifikationer och överensstämmelse Fibres for concrete – Part 1 : Steel fibres – Definitions , specifications and conformity'.

Suryanto, B., Wilson, S. & McCarter, W. (2015), 'Self-healing of Micro-cracks in Engineered Cementitious Composites', *Civil Engineering Dimension* **Vol. 17, N**.

Tahershamsi, M., Fernandez, I., Lundgren, K. & Zandi, K. (2017), 'Investigating correlations between crack width, corrosion level and anchorage capacity', *Struc-*

ture and Infrastructure Engineering **13**(10), 1294–1307.
URL: *http://dx.doi.org/10.1080/15732479.2016.1263673*

Trafikverket (2011), Trafikverkets föreskrifter om ändring i Vägverkets föreskrifter (VVFS 2004:43) om tillämpningen av europeiska beräkningsstandarder, Standard, Trafikverket.

Trafikverket (2016), Krav Brobyggande, Technical report, Trafikverket.
URL: *http://dokument.trafikverket.se/Versioner.aspx?spid=289&dokumentId=TDOK 2016%3A0204*

Trafikverket (2018), Råd Brobyggande TDOK 2016:2003, Technical Report TDOK 2016:0203, Trafikverket.

Tuutti, K. (1982), 'Corrosion of steel in concrete structures, swedish cement and concrete research institute'.

Vägverket (2008), BaTMan - MÄTNING OCH BEDÖMNING AV BROARS TILLSTÅND exklusive Metodbeskrivningar, Technical report, Vägverket.

Wang, Q., Sun, W., Guo, L., Gu, C. & Zong, J. (2018), 'Prediction of chloride ingress in steel fibre reinforced concrete under bending load', *Ceramics - Silikaty* **62**(1), 59–66.

Zhang, P., Song, H., Ng, S. & Wang, X.-H. (2018), 'Fiber-Reinforced Concrete with Application in Civil Engineering', *Advances in Civil Engineering* **2018**, 1–4.

Zhu, C., Zhang, J., Peng, J., Cao, W. & Liu, J. (2018), 'Physical and mechanical properties of gypsum-based composites reinforced with PVA and PP fibers', *Construction and Building Materials* **163**, 695–705.
URL: *https://doi.org/10.1016/j.conbuildmat.2017.12.168*

Zhu, W., François, R., Coronelli, D. & Cleland, D. (2013), 'Effect of corrosion of reinforcement on the mechanical behaviour of highly corroded RC beams', *Engineering Structures* **56**(March 2018), 544–554.
URL: *http://dx.doi.org/10.1016/j.engstruct.2013.04.017*

List of Figures

List of Tables

A

Results - MATLAB analysis

This appendix presents all data given from the analysis done in MATLAB. All reinforcement parts, that have been scanned, are named according to Figure A.1.

Figure A.1: Definitions of the naming of the different parts of a reinforcement bar n. Black, vertical lines correspond to cuts. One or two parts of a reinforcement bar, have normally been scanned.

Beam nr:	Bar nr:	Pith depth in critical section [mm]	Maximum pit depth [mm]	Critical area [mm^2]	Corrosion level [%]
M1B2 (PL2U04)	172_3	0,10150	0,10150	78,896	0,792%
M1B1 (PL1U01)	102_1	0,14457	0,14457	77,740	0,938%
M1B9 (PL9C04)	157_1	0,70958	0,70958	76,842	4,719%
M1B9 (PL9C04)	157_2	0,97137	0,97137	68,650	13,646%
M1B9 (PL9C04)	158_2	1,92370	1,92370	71,174	13,702%
M1B9 (PL9C04)	159_2	1,72000	1,72000	71,376	10,268%
M1B7 (PL7C01)	160_2	0,30599	0,30599	78,440	1,913%
M1B7 (PL7C01)	161_2	1,08400	1,08400	75,013	7,182%
M1B7 (PL7C01)	162_2	1,24790	1,30390	68,670	14,808%
M1B1 (PL1U01)	101_2	1,32810	1,32810	73,069	7,836%
M1B1 (PL1U01)	100_2	2,03960	2,03960	69,079	12,860%
M1B15 (PL15L04)	22_2	1,99960	2,16890	69,295	13,993%
M1B15 (PL15L04)	23_2	0,83944	0,83944	72,395	9,659%
M1B15 (PL15L04)	24_2	1,48200	1,48200	72,889	10,697%
M1B8 (PL8N)	25_2	0,13860	0,13860	78,850	0,870%
M1B8 (PL8N)	26_2	0,23558	0,23558	77,057	1,818%
M1B8 (PL8N)	27_1	0,39537	0,39537	79,873	1,906%
M1B8 (PL8N)	27_2	0,87195	0,87195	77,893	3,099%
M1B2 (PL2U04)	174_2	3,77300	3,77300	65,733	18,563%
M1B14 (PL14L01)	40_2	0,83554	1,43850	71,640	8,906%
M1B14 (PL14L01)	41_2	1,33780	1,33780	70,603	10,244%
M1B14 (PL14L01)	42_1	1,56350	1,57840	65,889	16,327%
M1B1 (PL1U01)	102_2	2,19160	2,19160	63,265	19,999%
M1B2 (PL2U04)	172_2	2,81340	3,07180	61,902	22,733%
M1B2 (PL2U04)	173_2	2,77070	2,77070	55,028	30,607%
M2B1 (ST1U01)	171_1	0,08822	0,08822	79,403	0,550%
M2B1 (ST1U01)	171_2	0,73921	0,73921	75,183	5,671%
M2B14 (ST14L01)	130_2	1,46830	1,46830	65,936	17,154%
M2B14 (ST14L01)	131_2	0,73680	0,73680	73,395	6,494%
M2B14 (ST14L01)	132_2	1,47640	1,47640	73,414	7,404%
M2B1 (ST1U01)	169_3	1,41450	1,41450	73,740	7,424%
M2B1 (ST1U01)	170_2	1,63420	1,63420	72,324	10,180%
M2B2 (ST2U04)	164_2	1,01670	1,13810	69,975	11,286%
M2B2 (ST2U04)	165_2	1,92720	1,92720	69,269	13,997%
M2B2 (ST2U04)	163_2	1,83470	1,83470	68,388	15,453%
M2B7 (ST7C01)	34_2	2,06830	2,07170	70,664	12,567%
M2B7 (ST7C01)	35_2	0,86338	0,89623	73,965	5,801%
M2B7 (ST7C01)	36_2	0,83486	0,83486	76,996	3,550%
M2B8 (ST8N)	49_2	0,70015	0,70015	77,207	2,525%
M2B8 (ST8N)	50_2	0,23250	0,23250	77,199	2,013%
M2B8 (ST8N)	51_2	0,42454	0,42454	78,156	1,648%
M2B15 (ST15L04)	58_1	1,03930	1,03930	71,514	8,909%
M2B15 (ST15L04)	59_	2,11330	2,11330	65,721	17,315%
M2B15 (ST15L04)	60_2	1,31020	1,31020	71,985	8,857%
M2B9 (ST9C04)	61_2	1,84630	1,84630	51,846	32,720%

	Plain
	Steel fiber
	Hybrid
	Syntethic

M2B9 (ST9C04)	62_2	1,52450	1,52450	57,228	25,256%
M2B9 (ST9C04)	63_2	2,60080	2,60080	51,829	33,543%
M3B7 (HY7U04)	98_1	0,46298	0,46298	77,861	2,385%
M3B7 (HY7U04)	98_2	0,76004	0,76004	76,976	4,137%
M3B1 (HY1N)	103_2	0,81913	0,81913	78,562	3,811%
M3B1 (HY1N)	104_2	0,24728	0,24728	77,782	1,585%
M3B1 (HY1N)	105_1	0,37370	0,37370	73,699	4,156%
M3B1 (HY1N)	105_2	0,87126	0,87126	74,669	4,718%
M3B6 (HY6U01)	109_2	1,15140	1,15140	74,341	5,612%
M3B11 (HY11C04)	13_2	2,58680	2,58680	62,716	19,012%
M3B11 (HY11C04)	14_1	1,53770	1,62250	73,426	7,459%
M3B11 (HY11C04)	15_2	1,31720	1,31720	69,883	12,679%
M3B7 (HY7U04)	99_2	1,22680	1,22680	73,090	7,151%
M3B6 (HY6U01)	110_2	1,68520	1,84880	66,158	15,749%
M3B6 (HY6U01)	111_2	1,38660	1,71810	62,569	18,965%
M3B10 (HY10C01)	70_2	3,25600	3,28070	58,927	26,998%
M3B10 (HY10C01)	71_2	1,22880	1,48500	71,558	8,082%
M3B10 (HY10C01)	72_2	1,02890	1,09680	74,840	5,164%
M3B7 (HY7U04)	97_2	2,51850	2,56760	61,323	21,872%
M4B18 (SY18U04)	3_2	0,84438	0,84438	73,865	5,427%
M4B18 (SY18U04)	3_1	0,59282	0,59282	73,707	6,710%
M4B18 (SY18U04)	2_2	0,84305	0,84305	69,804	11,362%
M4B18 (SY18U04)	1_3	1,37950	1,59030	66,736	14,944%
M4B17 (SY17U01)	69_	2,08610	2,08610	62,434	18,106%
M4B16 (SY16N)	43_1	1,76530	1,77640	71,944	7,320%
M4B16 (SY16N)	43_2	0,23538	0,23538	74,8480	1,389%
M4B16 (SY16N)	44_2	0,20532	0,20532	78,6680	1,277%
M4B16 (SY16N)	45_2	0,57700	0,57700	74,1820	4,104%
M4B17 (SY17U01)	67_2	1,64910	2,02820	63,1950	20,063%
M4B17 (SY17U01)	68_2	2,69230	2,71570	61,3760	20,690%

B
Graphs of all results

The data, given from Figures 5.6-5.9 and Appendix A, are summarized and presented in several graphs. In following appendix are all graphs, that were performed, shown.

B.1 Corrosion levels vs. crack width in different intervals

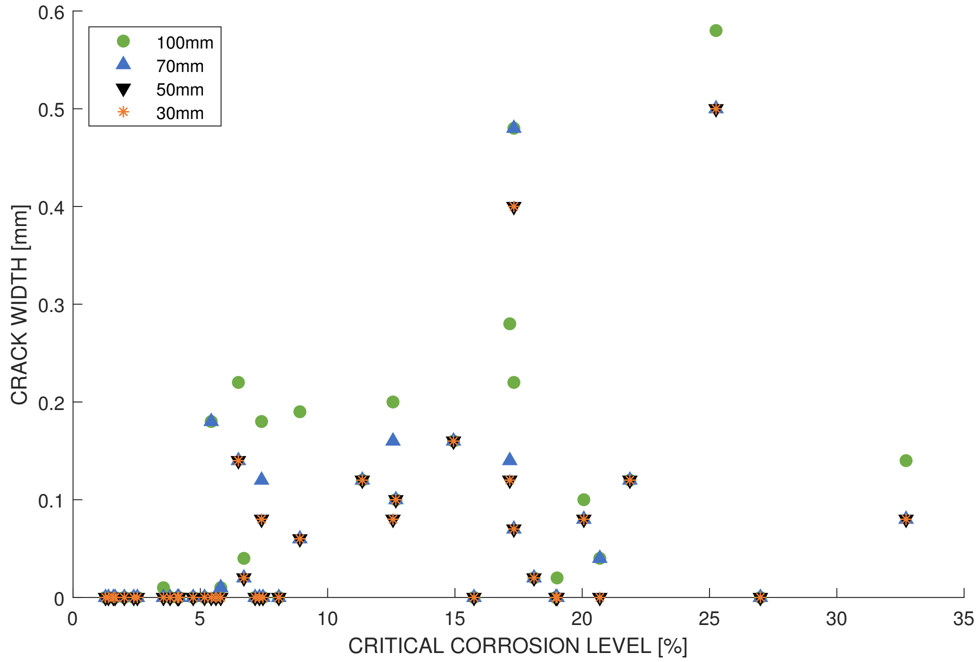

Figure B.1: Corrosion vs. crack width for different intervals from the critical section

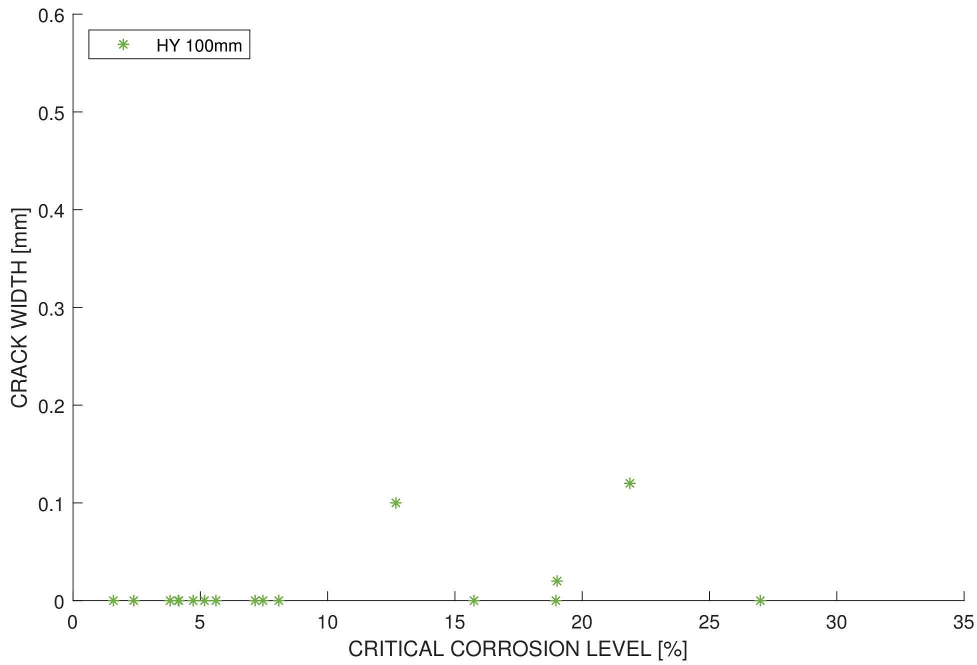

Figure B.2: Corrosion vs. crack width for hybrid fibres in an interval of 100mm from the critical section

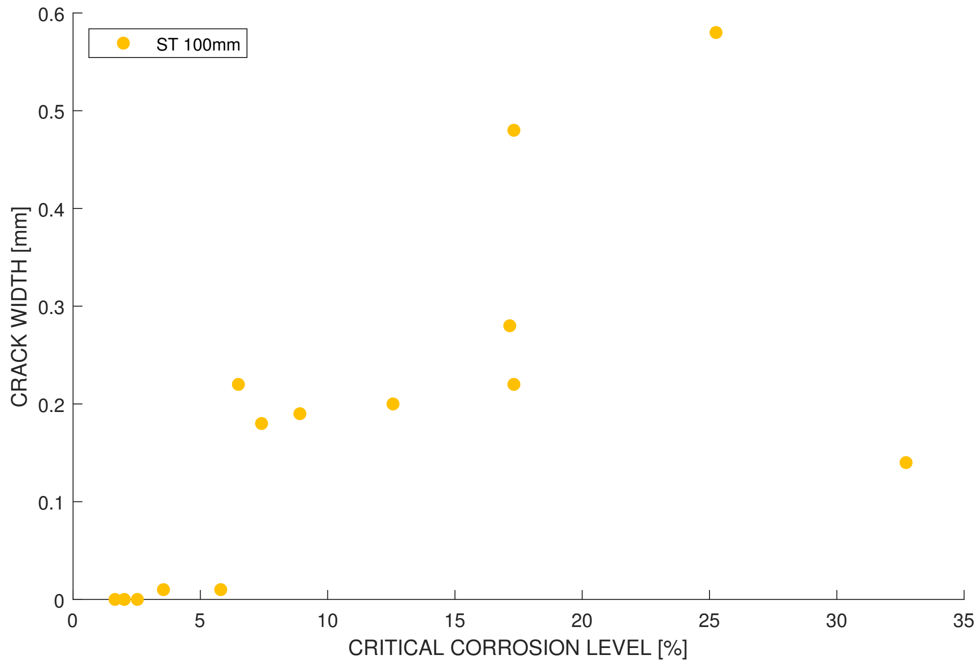

Figure B.3: Corrosion vs. crack width for steel fibres in an interval of 100mm from the critical section

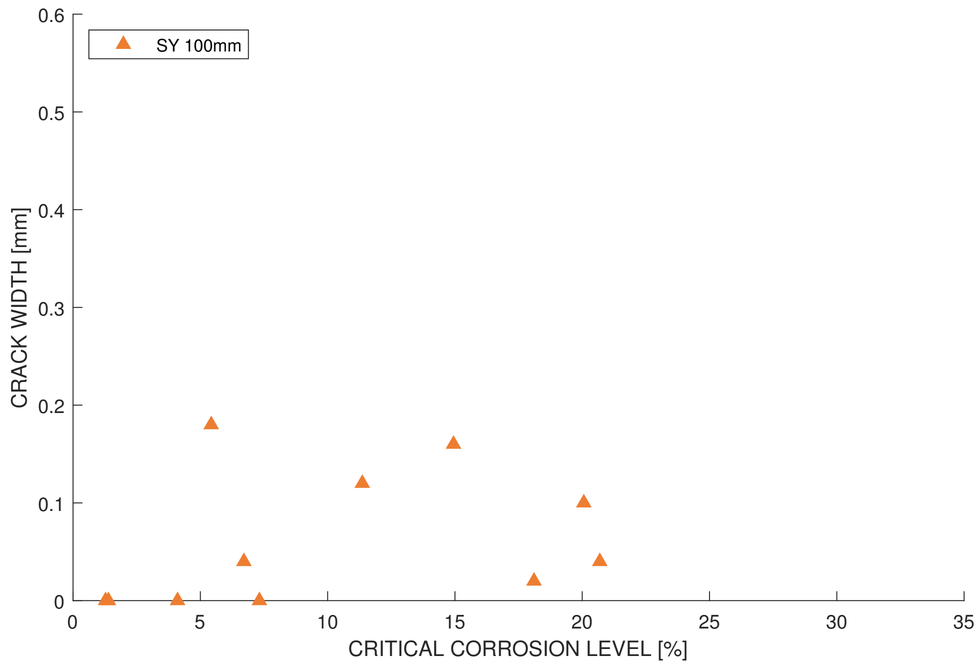

Figure B.4: Corrosion vs. crack width for synthetic fibres in an interval of 100mm from the critical section

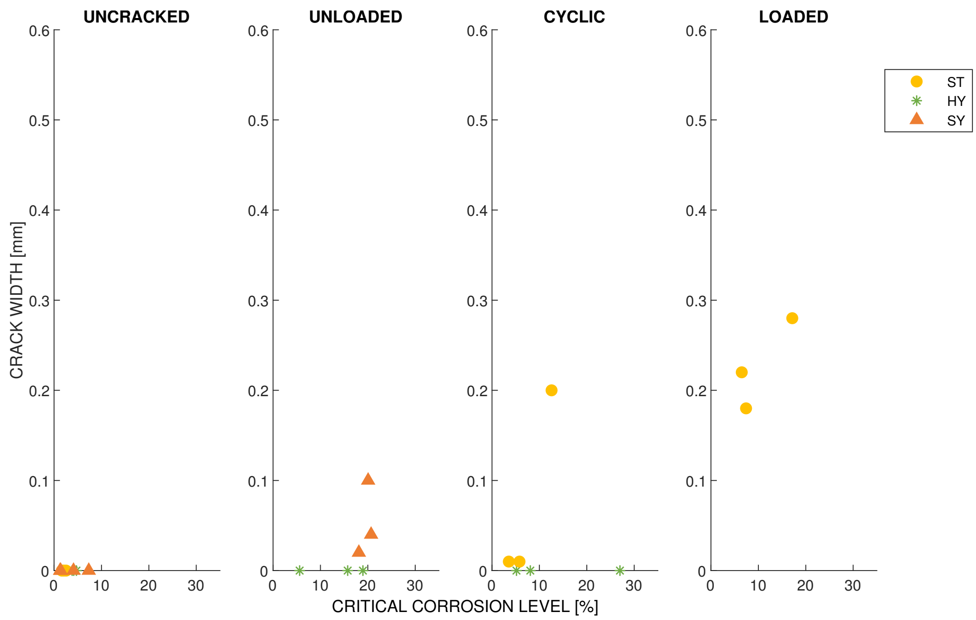

Figure B.5: Corrosion for the bars with target crack width of 0.1mm vs. crack width all mixtures of fibres in an interval of 100mm from the critical section.

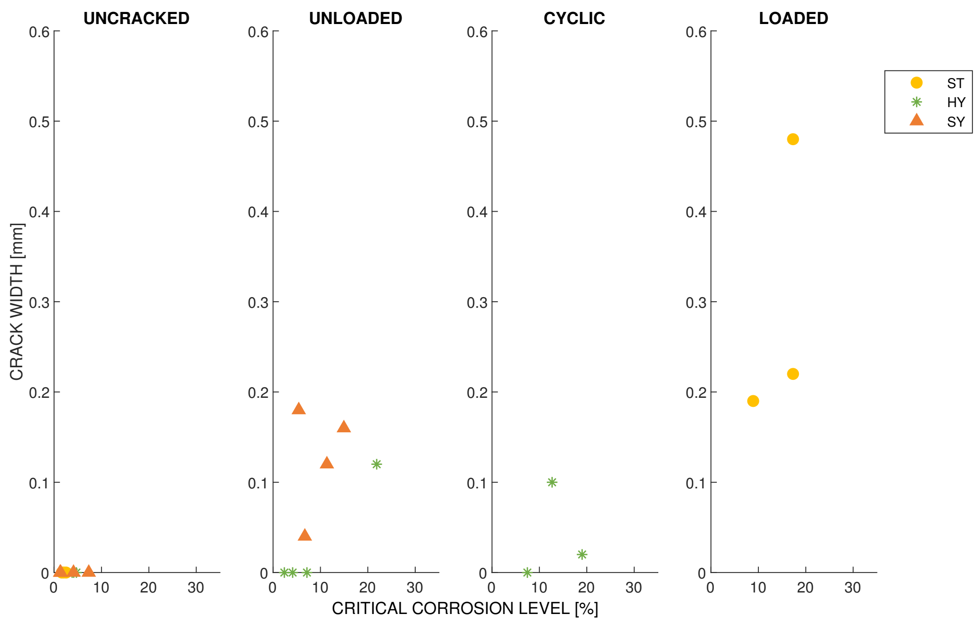

Figure B.6: Corrosion for the bars with target crack width of 0.4mm vs. crack width all mixtures of fibres in an interval of 100mm from the critical section.

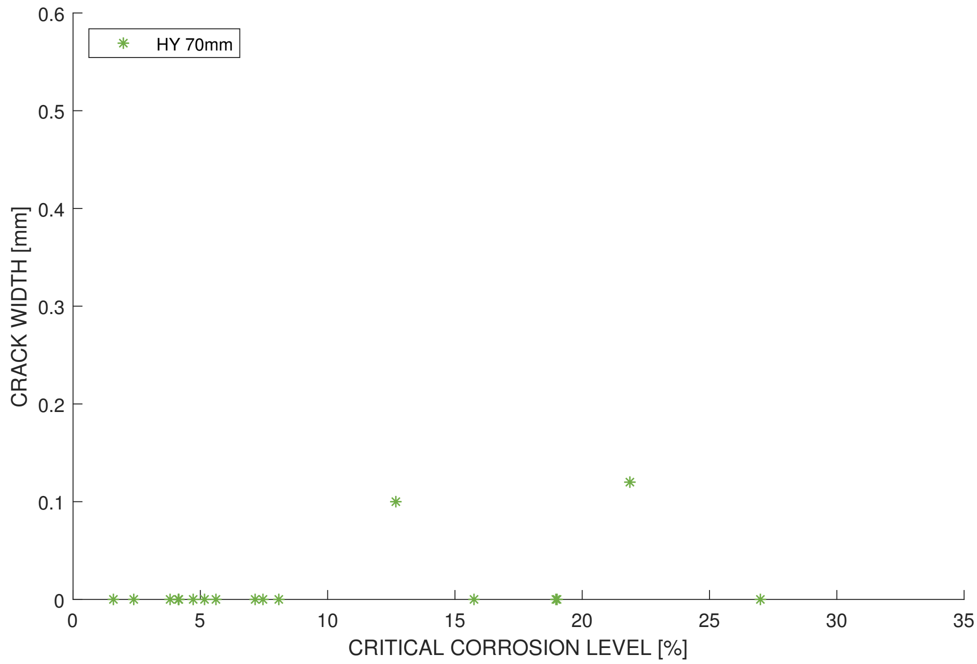

Figure B.7: Corrosion vs. crack width for hybrid fibres in an interval of 70mm from the critical section

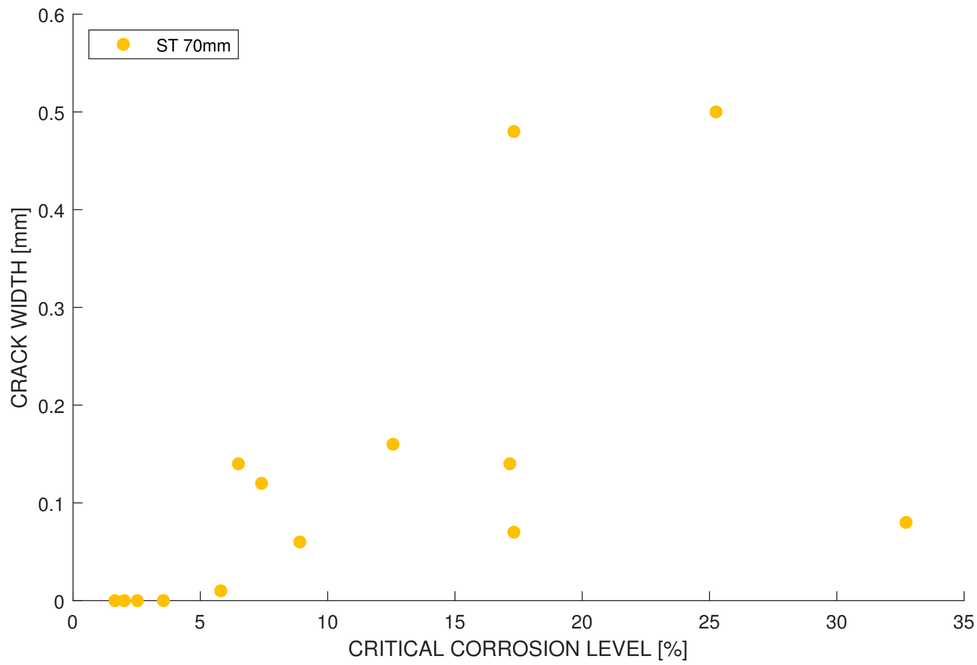

Figure B.8: Corrosion vs. crack width for steel fibres in an interval of 70mm from the critical section

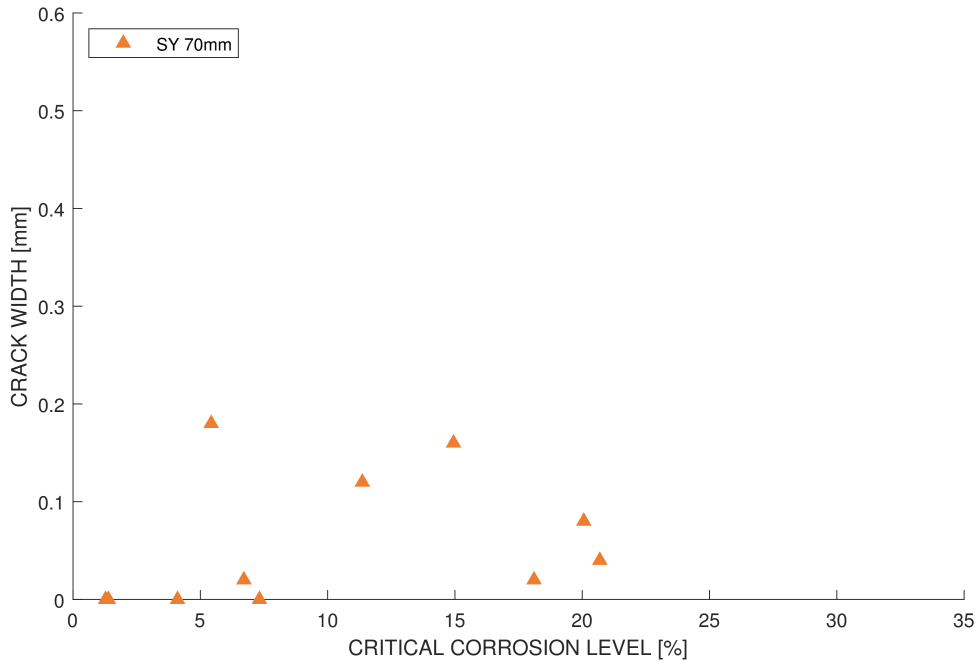

Figure B.9: Corrosion vs. crack width for synthetic fibres in an interval of 70mm from the critical section

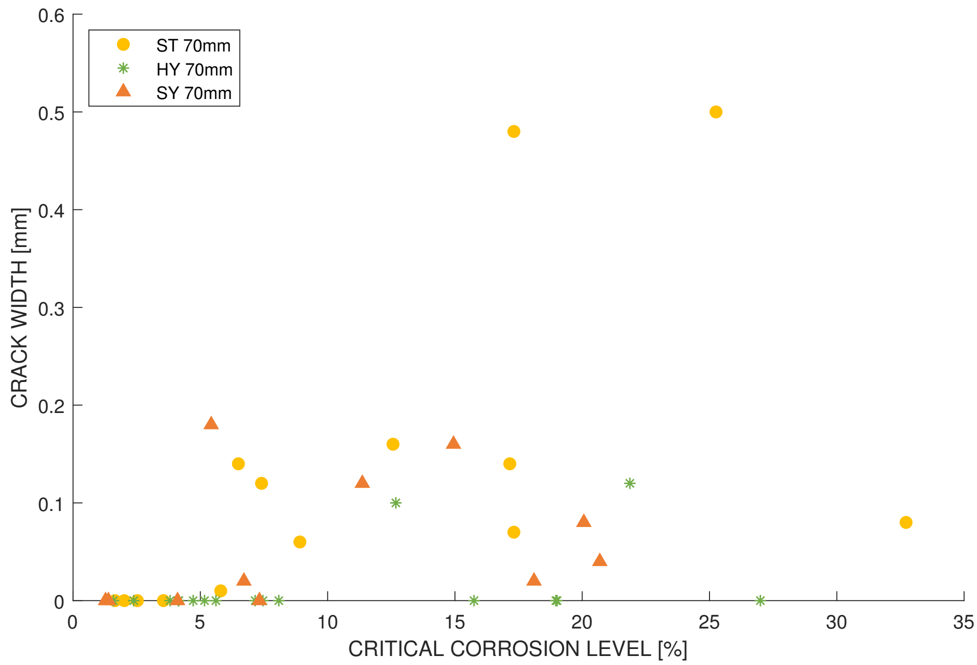

Figure B.10: Corrosion vs. crack width for all mixtures of fibres in an interval of 70mm from the critical section

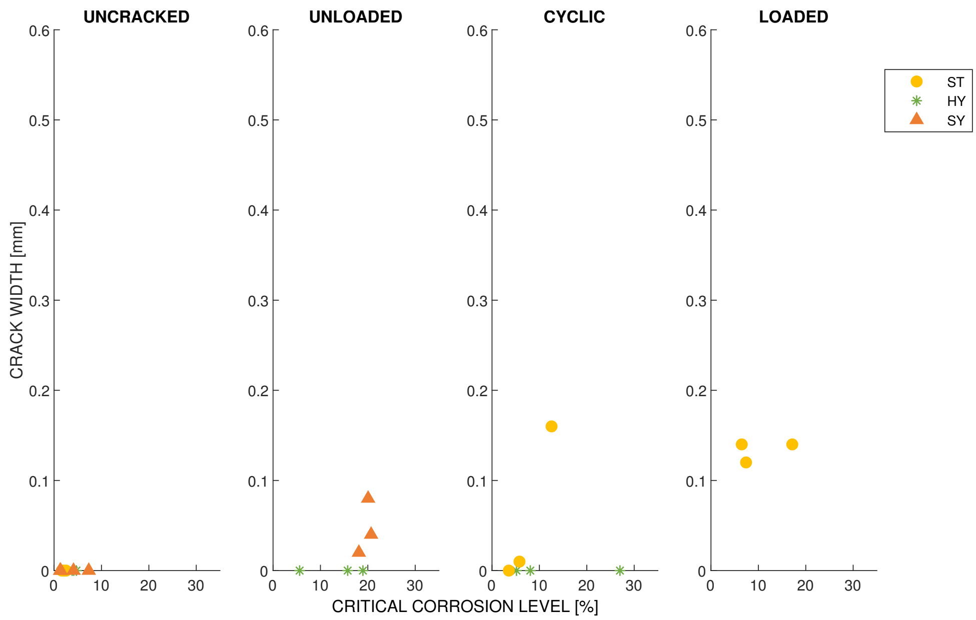

Figure B.11: Corrosion for the bars with target crack width of 0.1mm vs. crack width for all mixtures of fibres in an interval of 70mm from the critical section presented in a subplot.

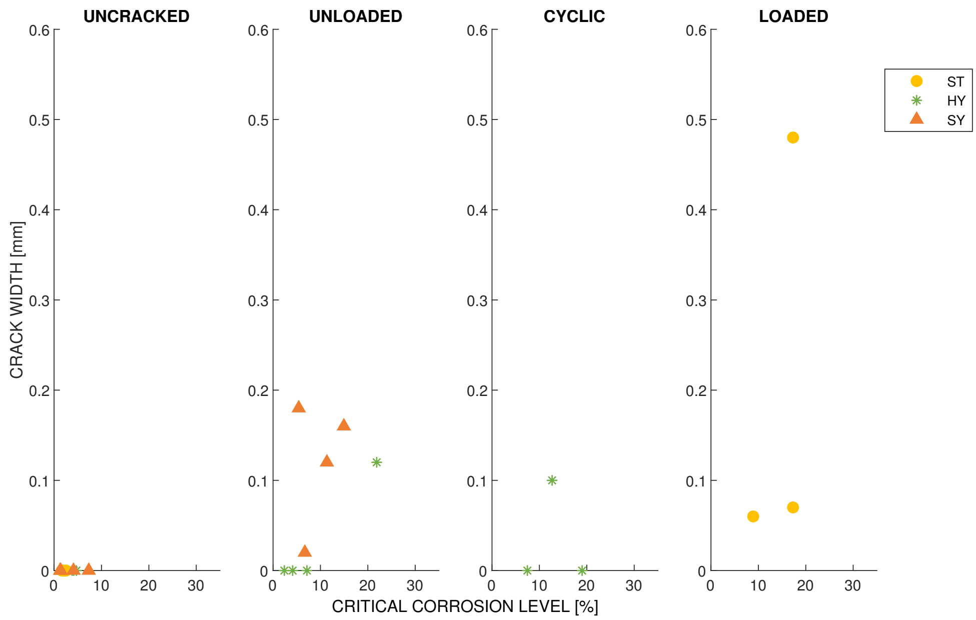

Figure B.12: Corrosion for the bars with target crack width of 0.4mm vs. crack width for all mixtures of fibres in an interval of 70mm from the critical section presented in a subplot.

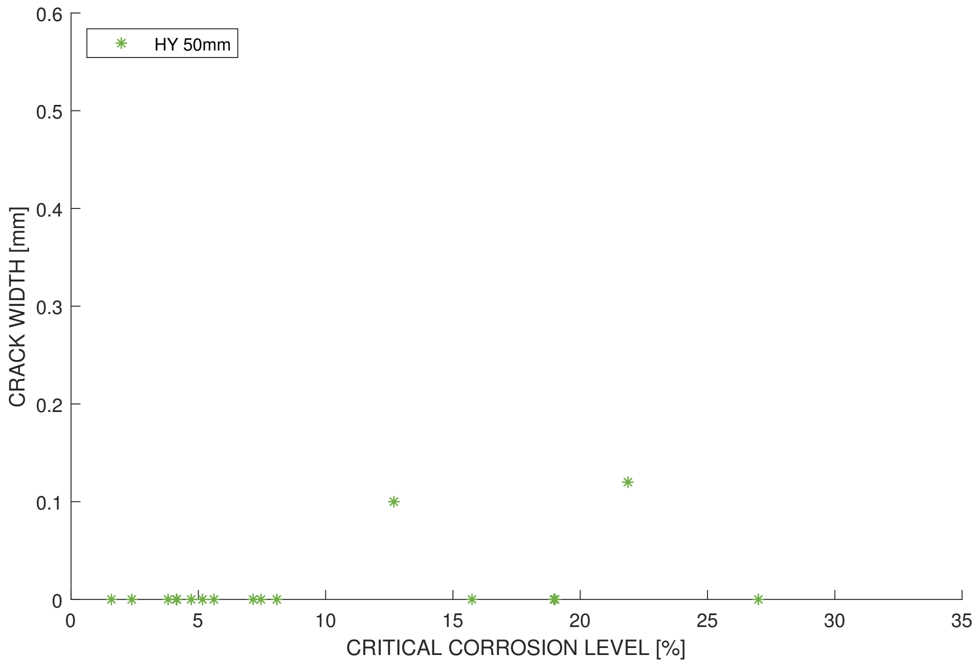

Figure B.13: Corrosion vs. crack width for hybrid fibres in an interval of 50mm from the critical section

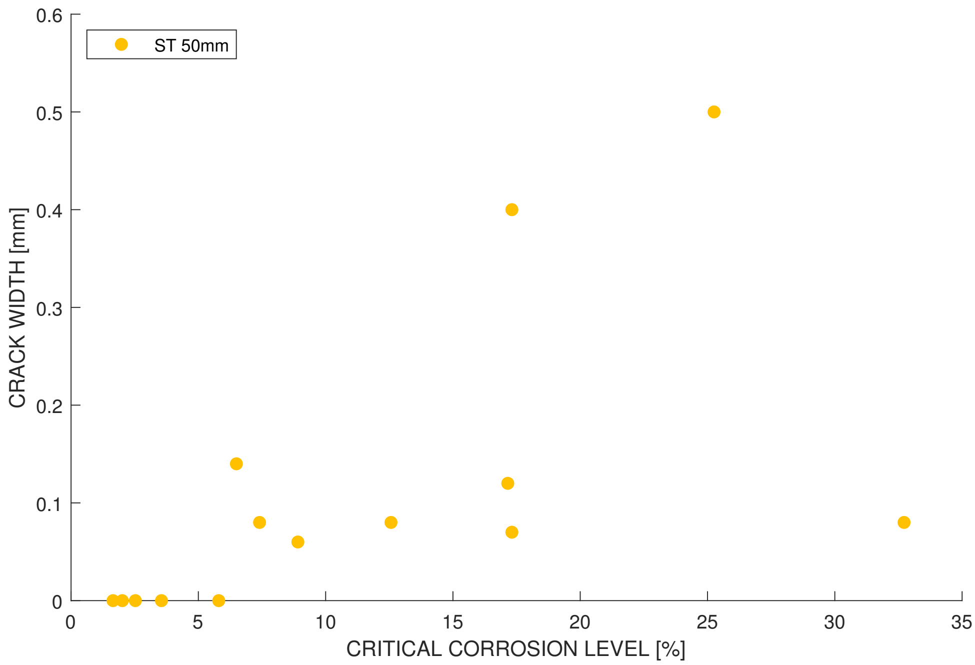

Figure B.14: Corrosion vs. crack width for steel fibres in an interval of 50mm from the critical section

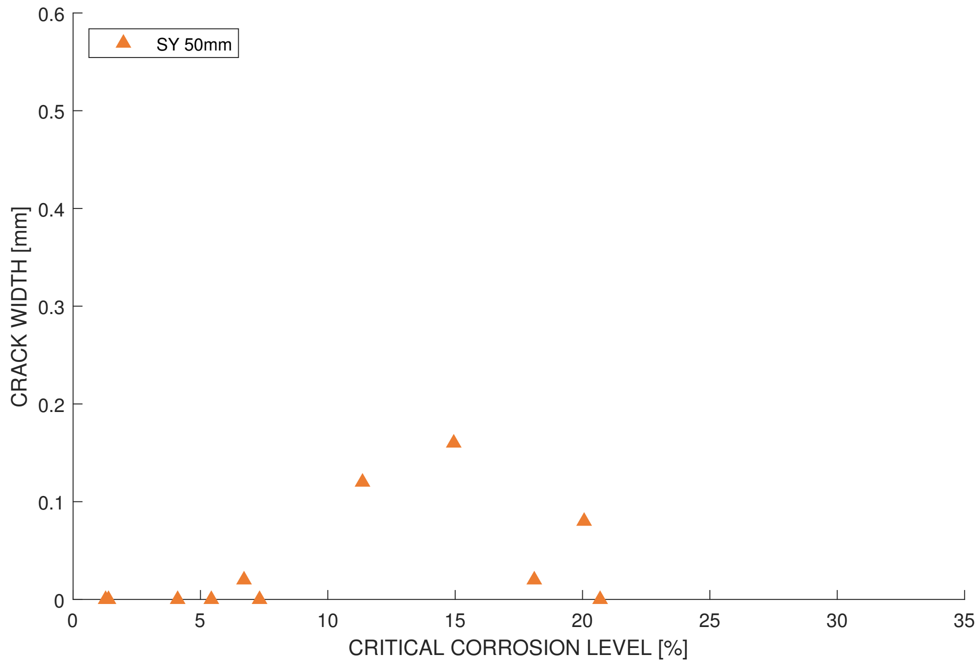

Figure B.15: Corrosion vs. crack width for synthetic fibres in an interval of 50mm from the critical section

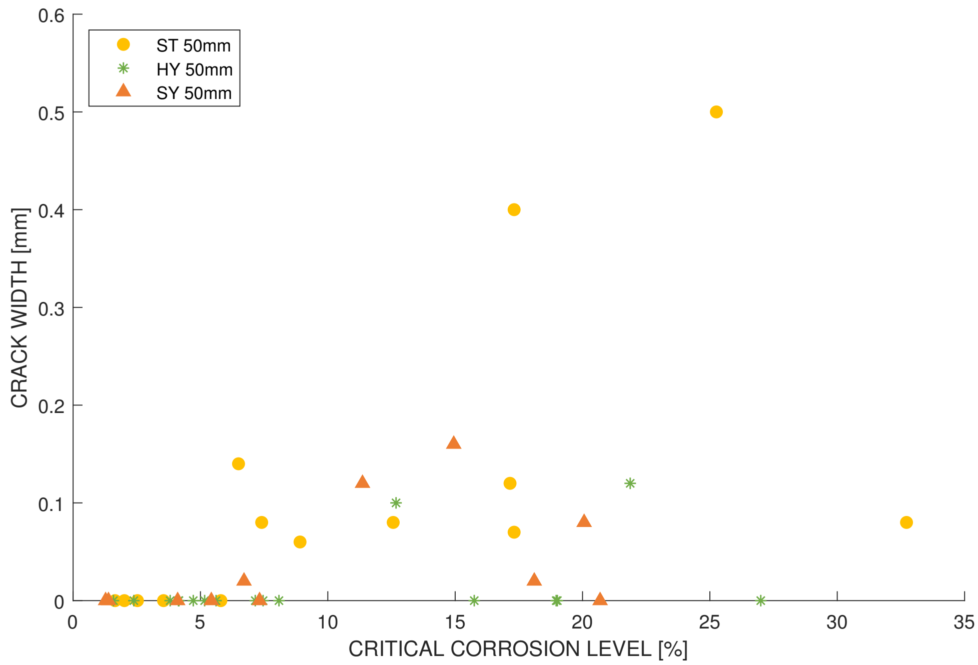

Figure B.16: Corrosion vs. crack width for all mixtures of fibres in an interval of 50mm from the critical section

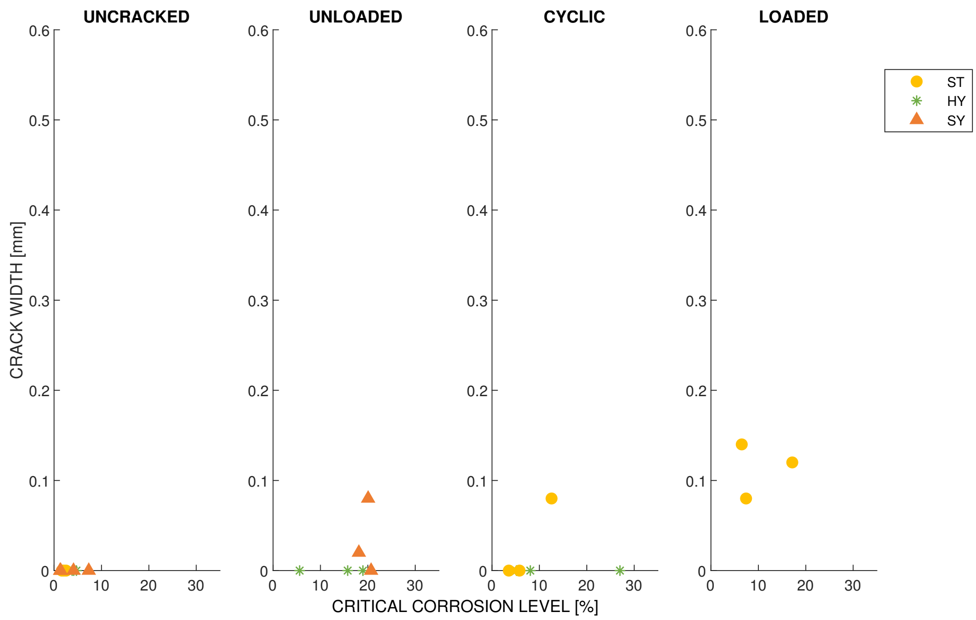

Figure B.17: Corrosion for the bars with target crack width of 0.1mm vs. crack width for all mixtures of fibres in an interval of 50mm from the critical section presented in a subplot.

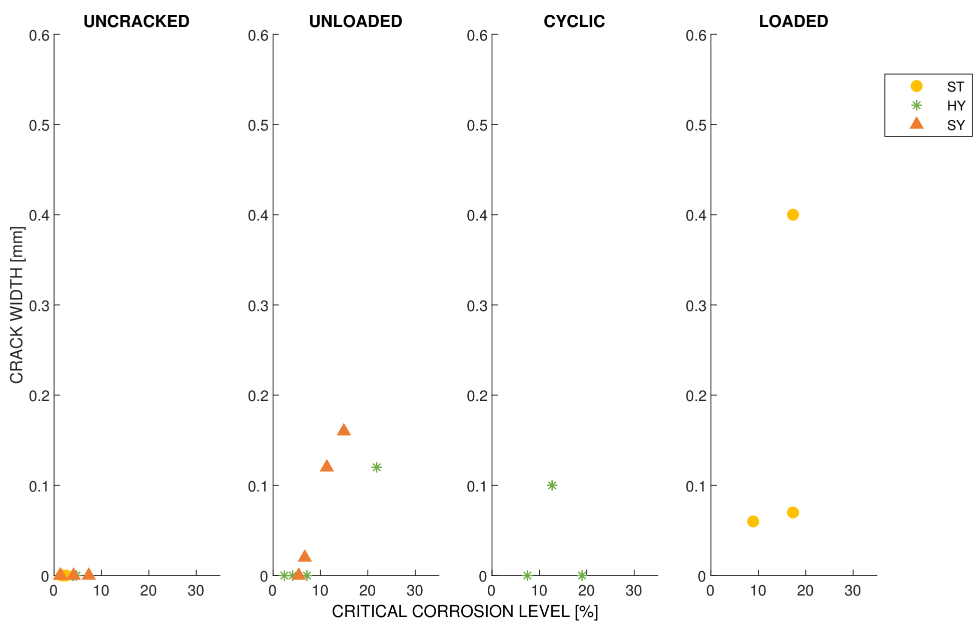

Figure B.18: Corrosion for the bars with target crack width of 0.4mm vs. crack width for all mixtures of fibres in an interval of 50mm from the critical section presented in a subplot.

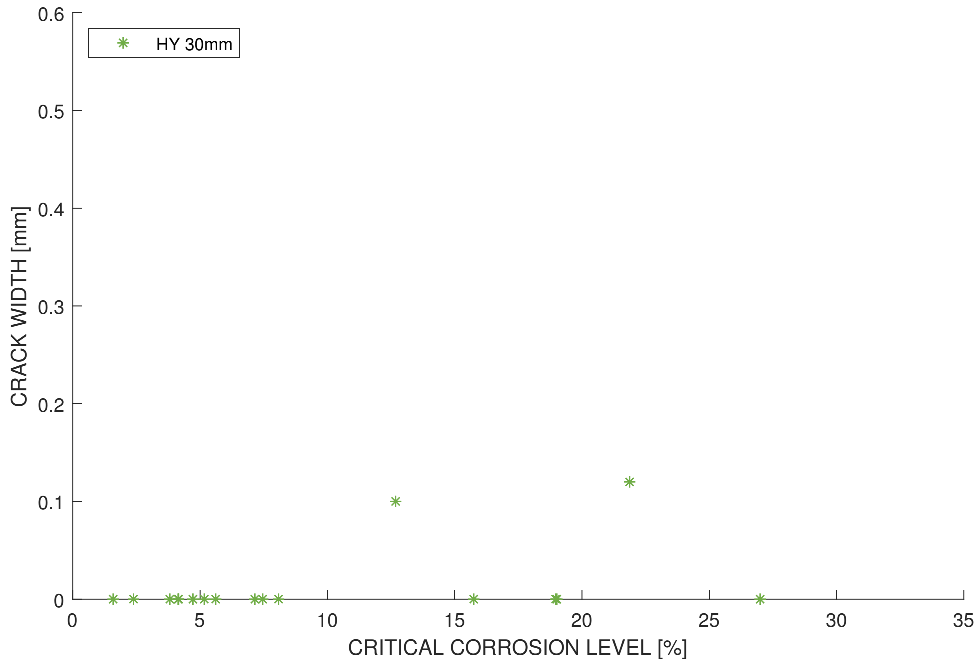

Figure B.19: Corrosion vs. crack width for hybrid fibres in an interval of 30mm from the critical section

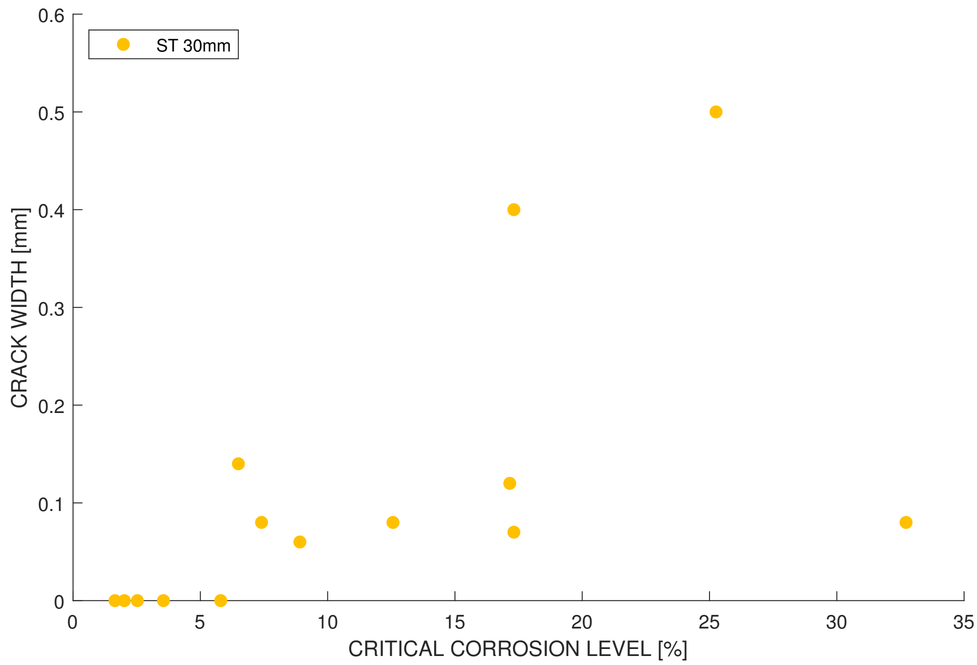

Figure B.20: Corrosion vs. crack width for steel fibres in an interval of 30mm from the critical section

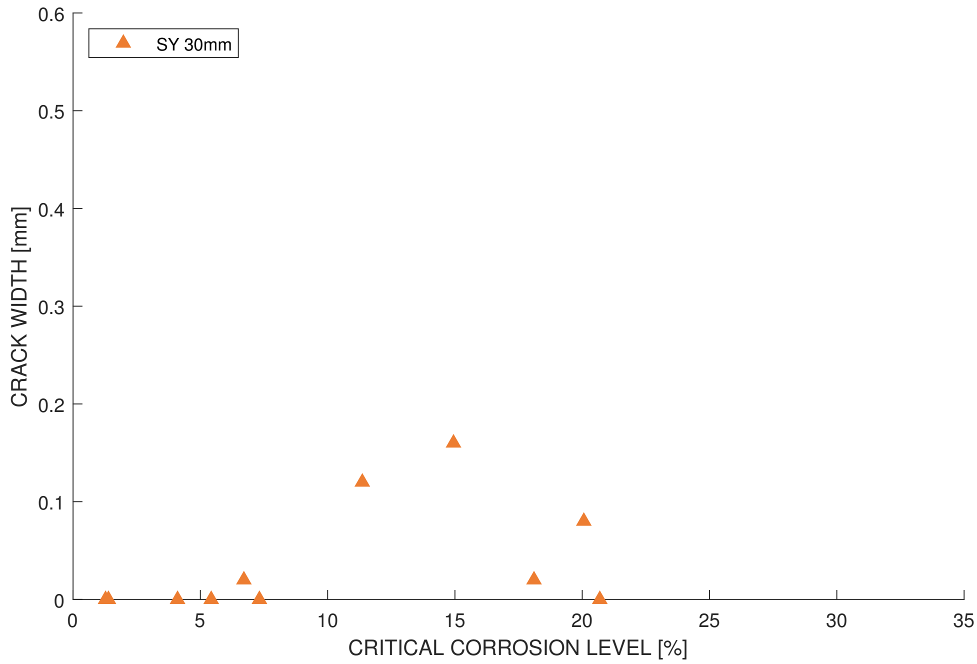

Figure B.21: Corrosion vs. crack width for synthetic fibres in an interval of 30mm from the critical section

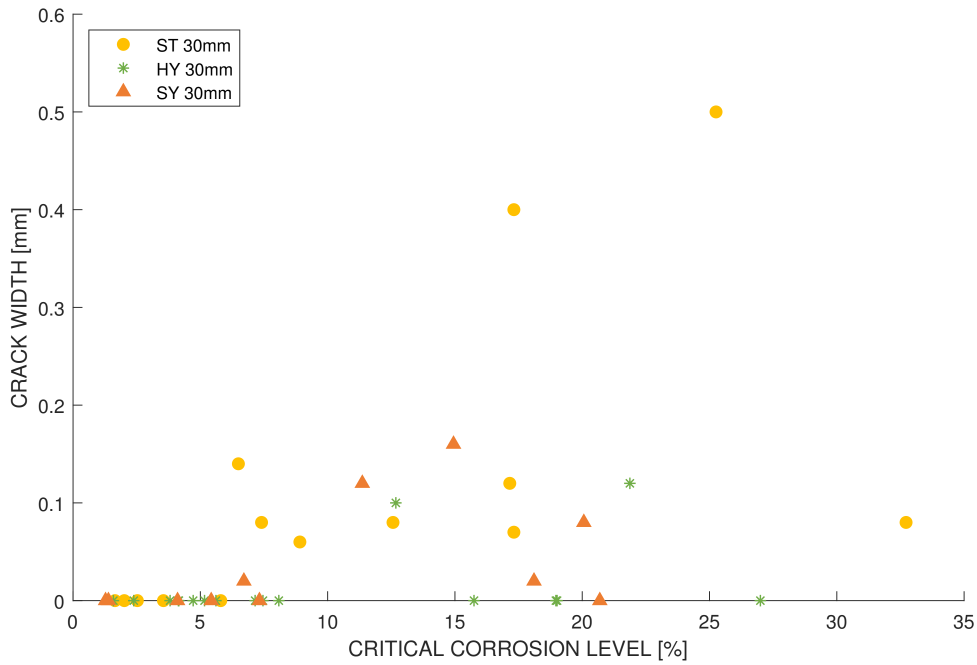

Figure B.22: Corrosion vs. crack width for all mixtures of fibres in an interval of 30mm from the critical section

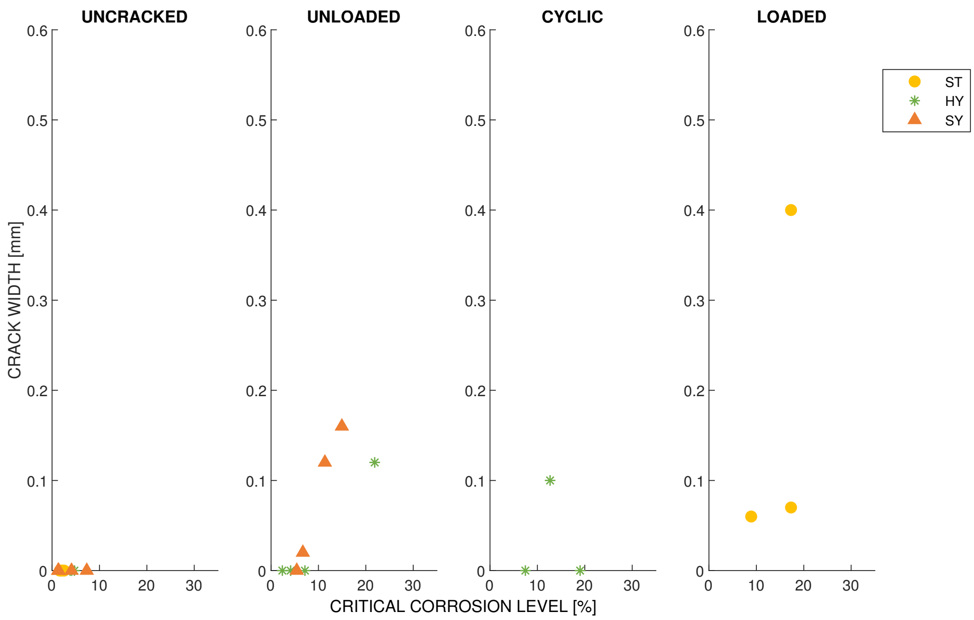

Figure B.23: Corrosion for the bars with target crack width of 0.1mm vs. crack width for all mixtures of fibres in an interval of 30mm from the critical section presented in a subplot.

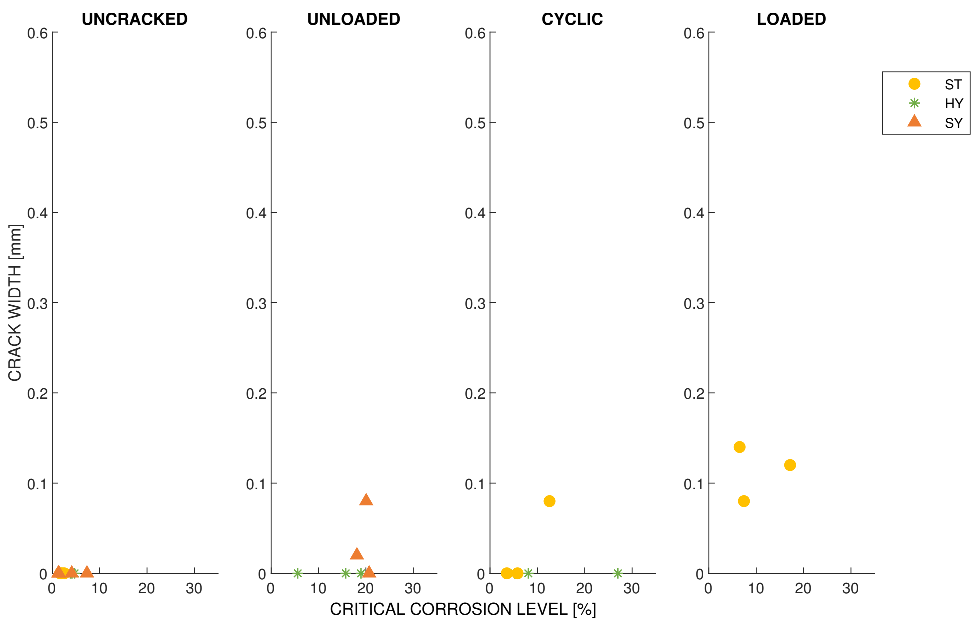

Figure B.24: Corrosion for the bars with target crack width of 0.4mm vs. crack width for all mixtures of fibres in an interval of 30mm from the critical section presented in a subplot.

B.2 Pit depth vs. crack widths in different intervals

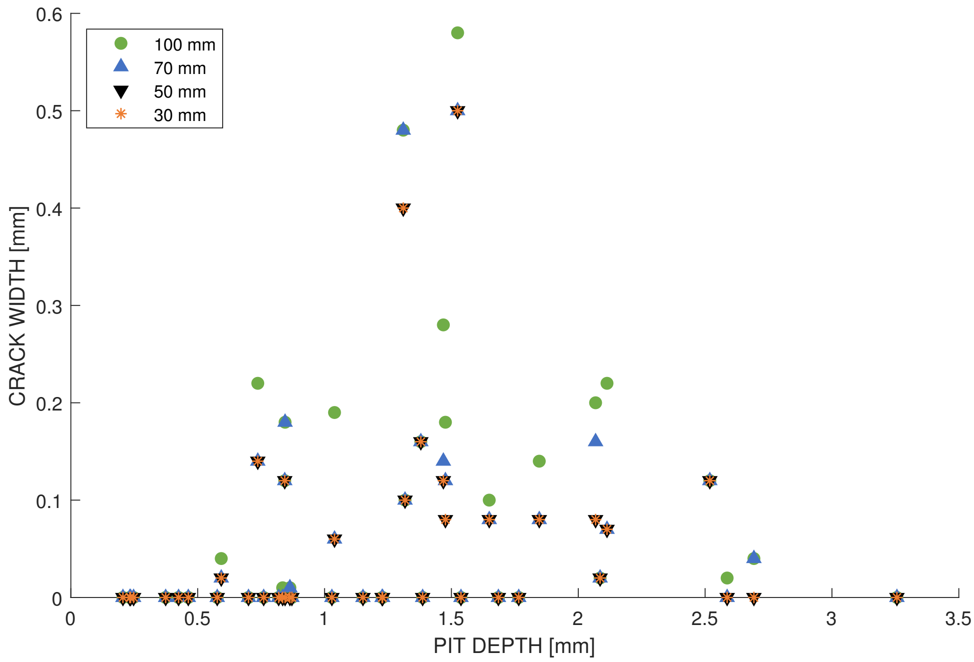

Figure B.25: Pit depth vs. crack width for all intervals from the critical section

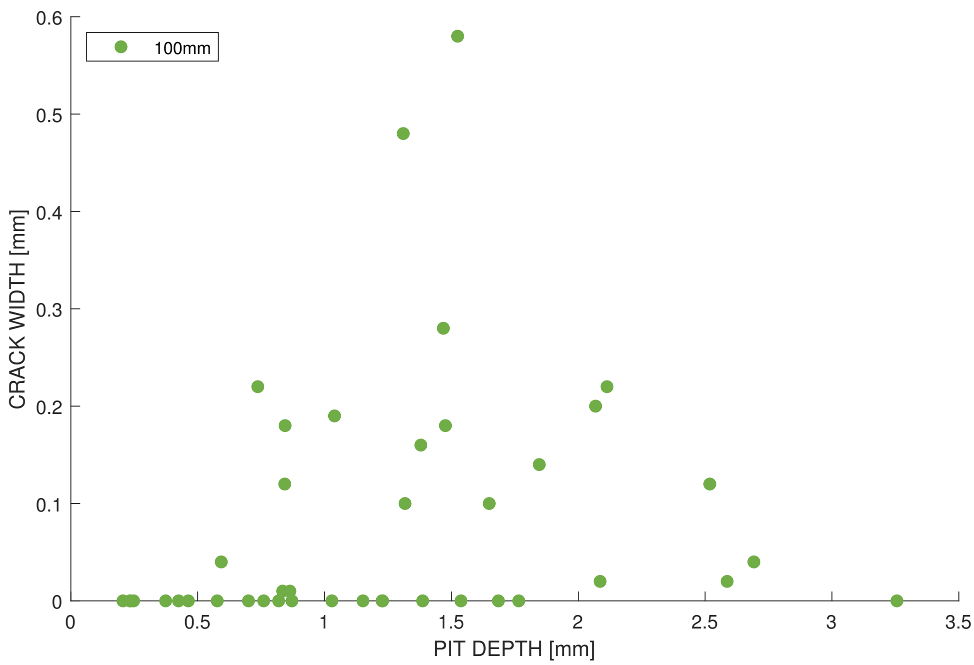

Figure B.26: Pit depth vs. crack width for an interval of 100mm from the critical section

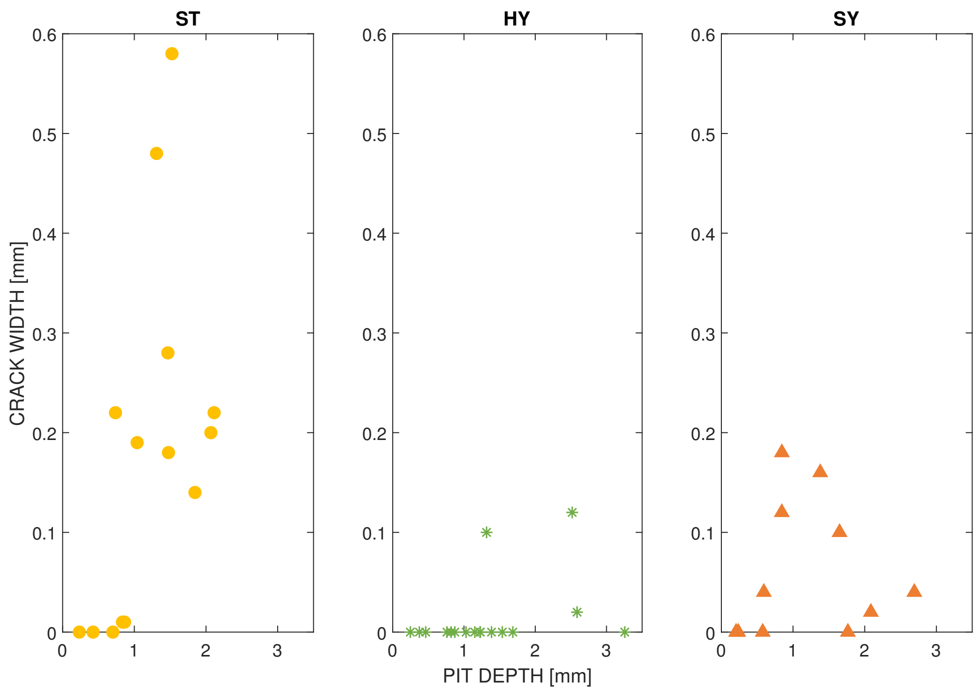

Figure B.27: Pit depth vs. crack width for different fibres in an interval of 70mm from the critical section.

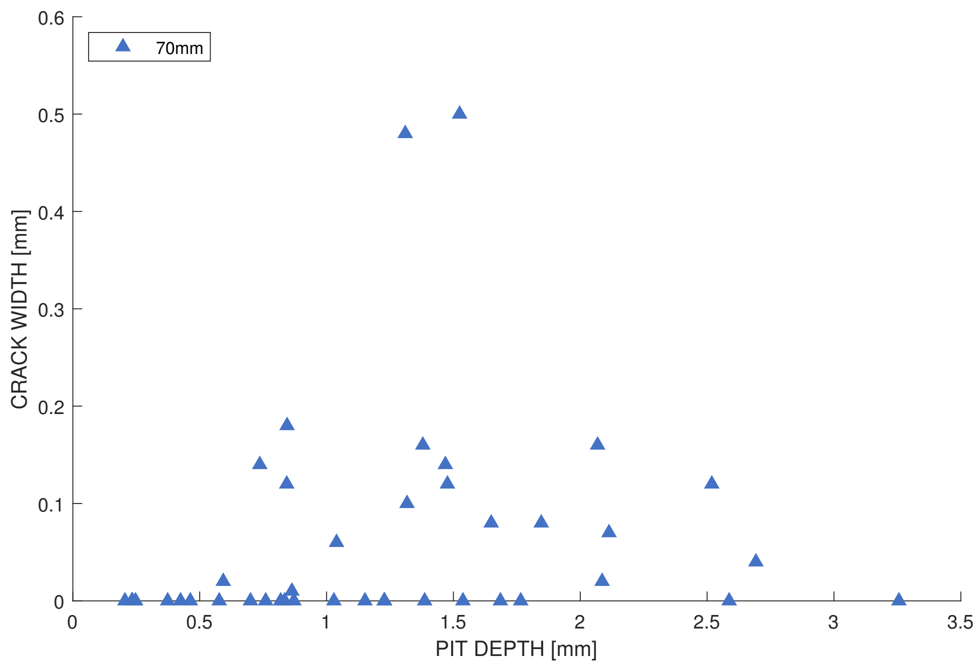

Figure B.28: Pit depth vs. crack width for an interval of 70mm from the critical section

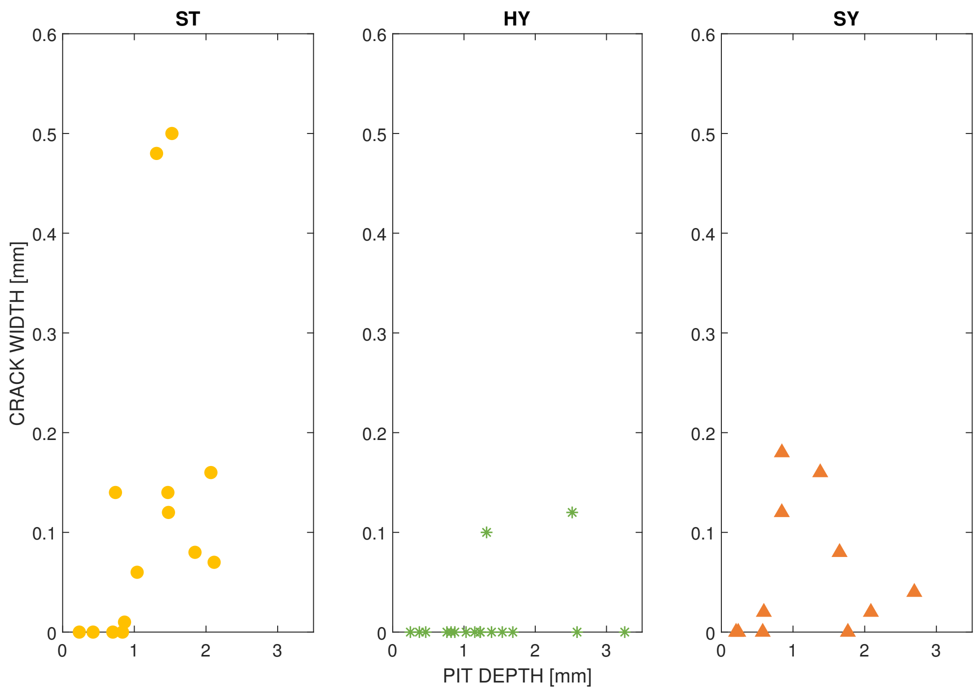

Figure B.29: Pit depth vs. crack width for different fibres in an interval of 70mm from the critical section.

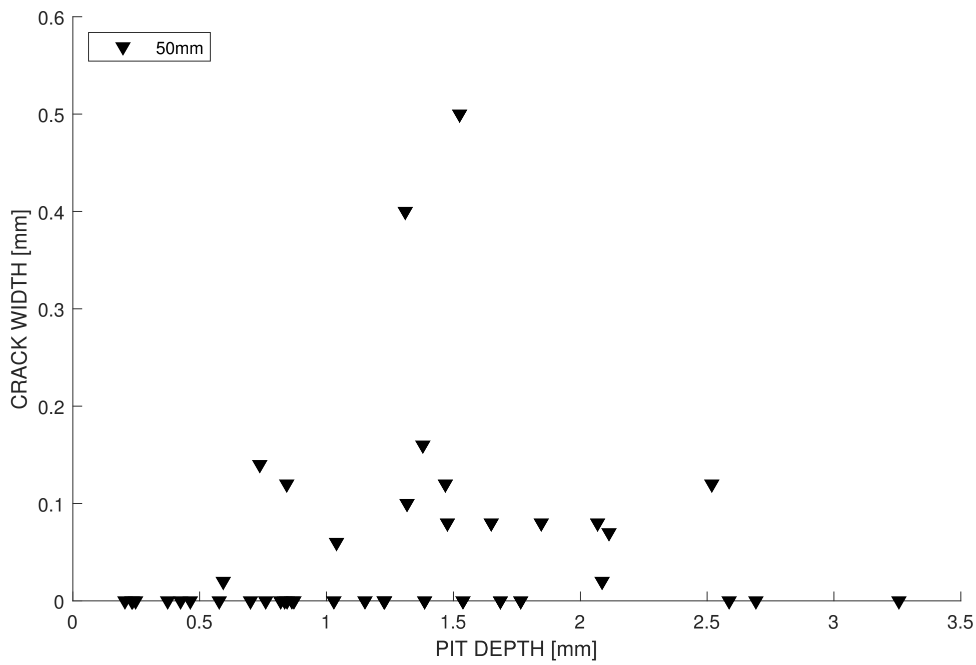

Figure B.30: Pit depth vs. crack width for an interval of 50mm from the critical section

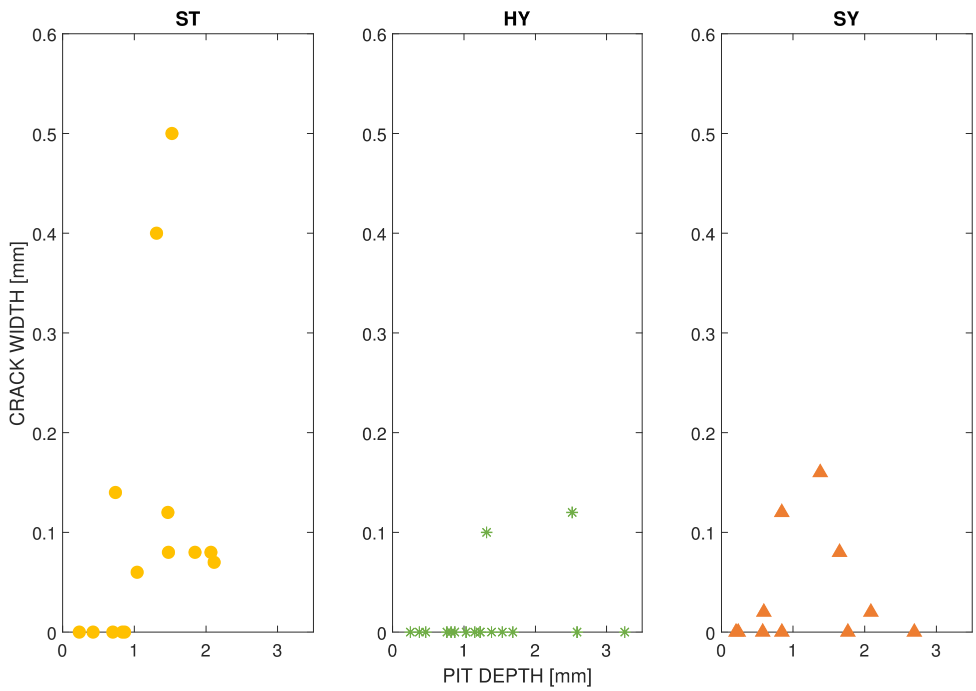

Figure B.31: Pit depth vs. crack width for different fibres in an interval of 50mm from the critical section.

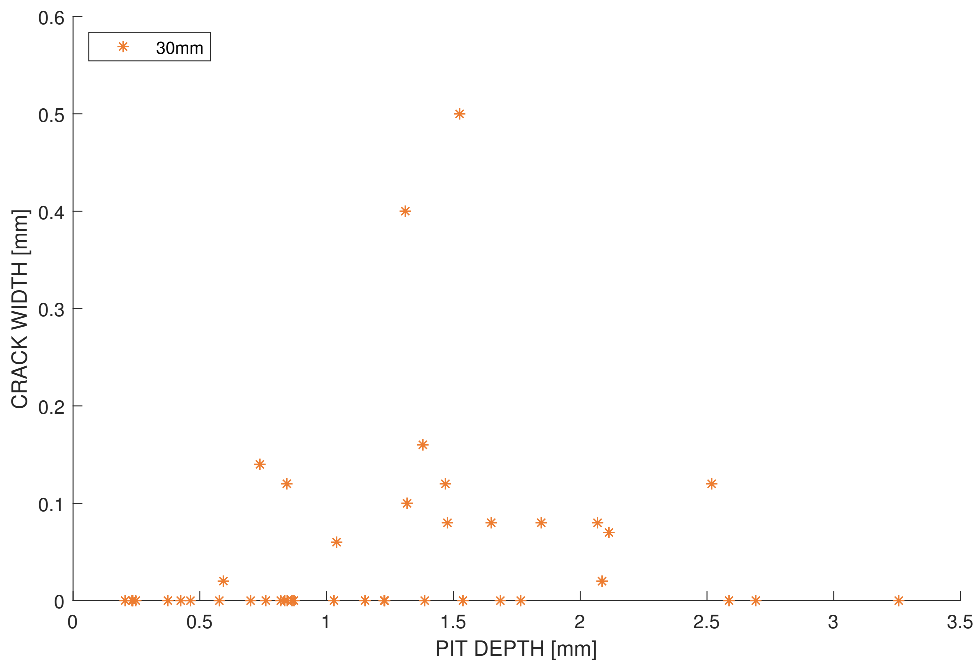

Figure B.32: Pit depth vs. crack width for an interval of 30mm from the critical section

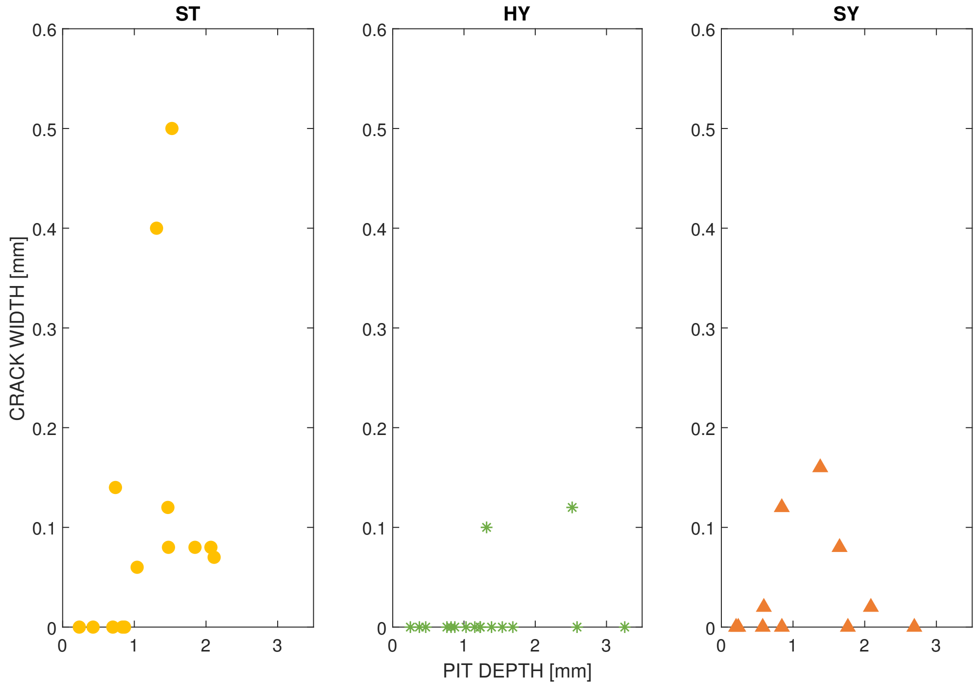

Figure B.33: Pit depth vs. crack width for different fibres in an interval of 30mm from the critical section.

B.3 Critical section area vs. crack width in different intervals

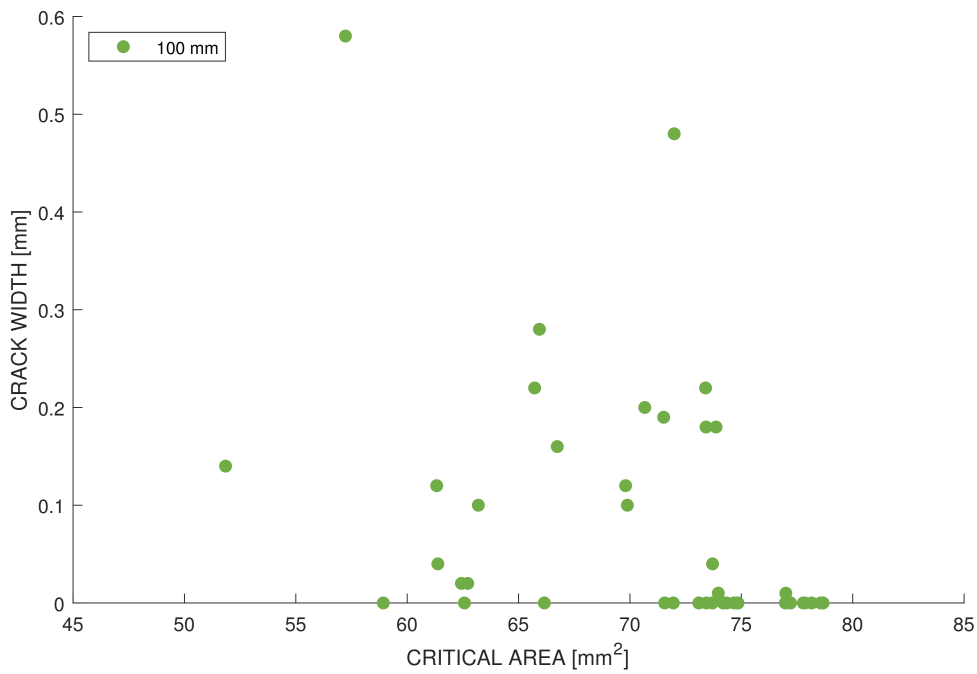

Figure B.34: Critical section area vs. crack width for an interval of 100mm from the critical section.

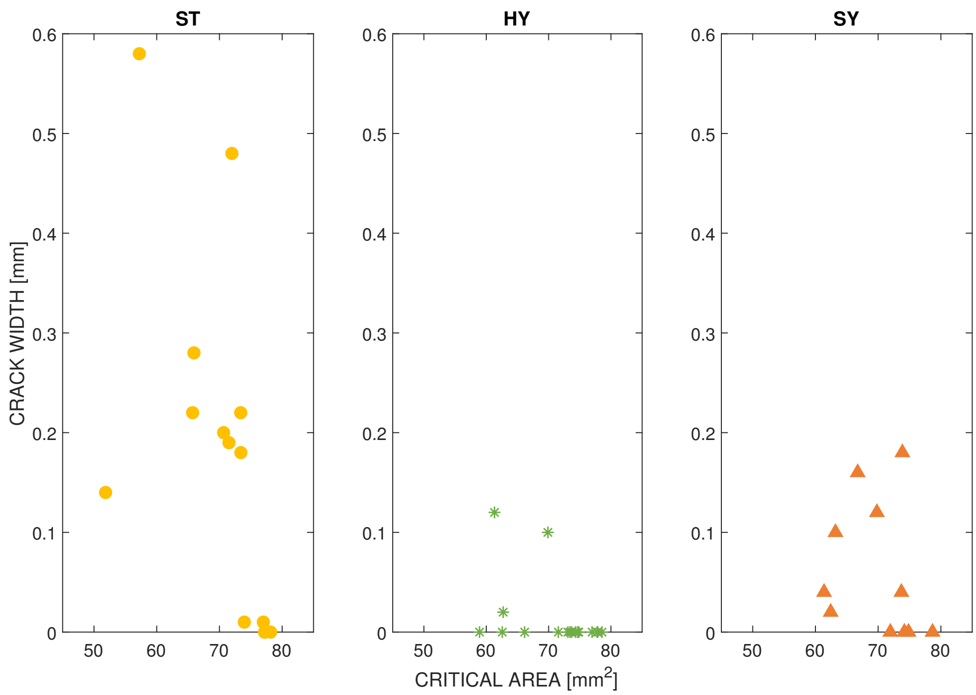

Figure B.35: Critical section area vs. crack width for different fibres in an interval of 100mm from the critical section.

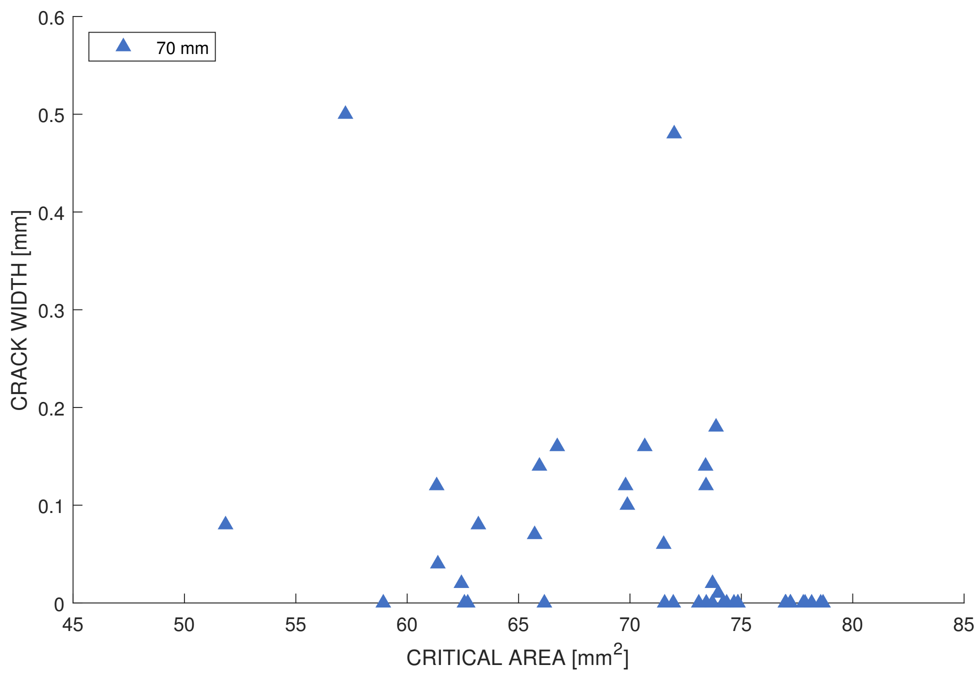

Figure B.36: Critical section area vs. crack width for an interval of 70mm from the critical section.

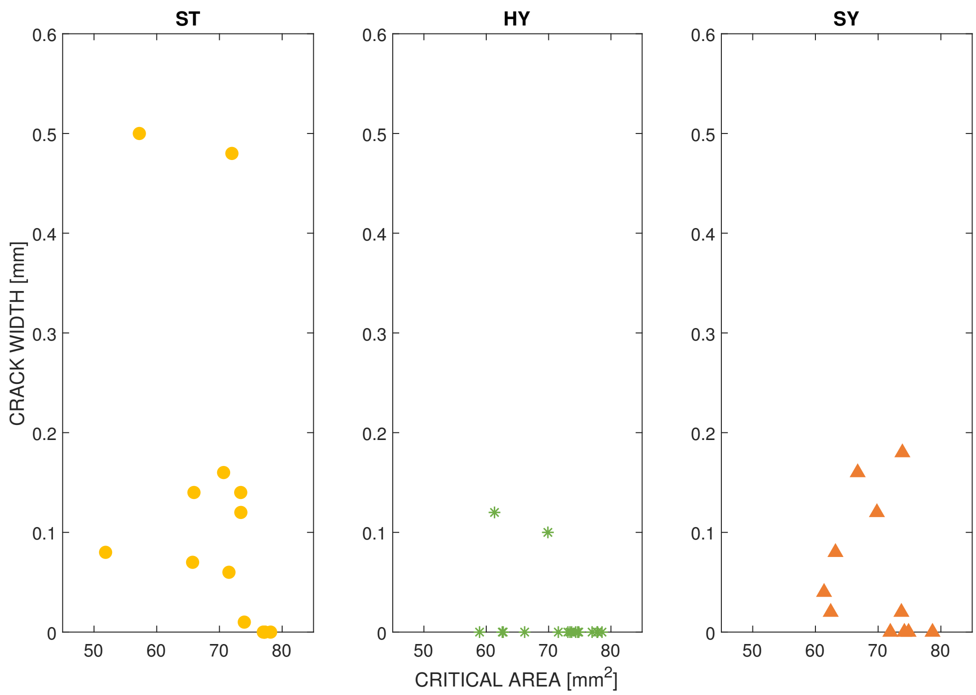

Figure B.37: Critical section area vs. crack width for different fibres in an interval of 70mm from the critical section.

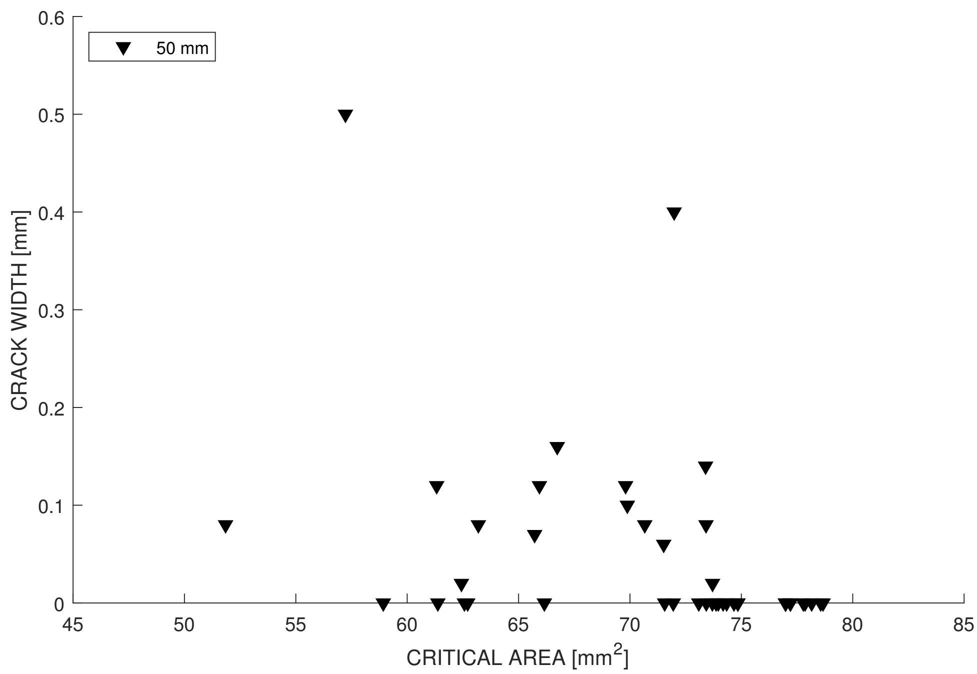

Figure B.38: Critical section area vs. crack width for an interval of 50mm from the critical section.

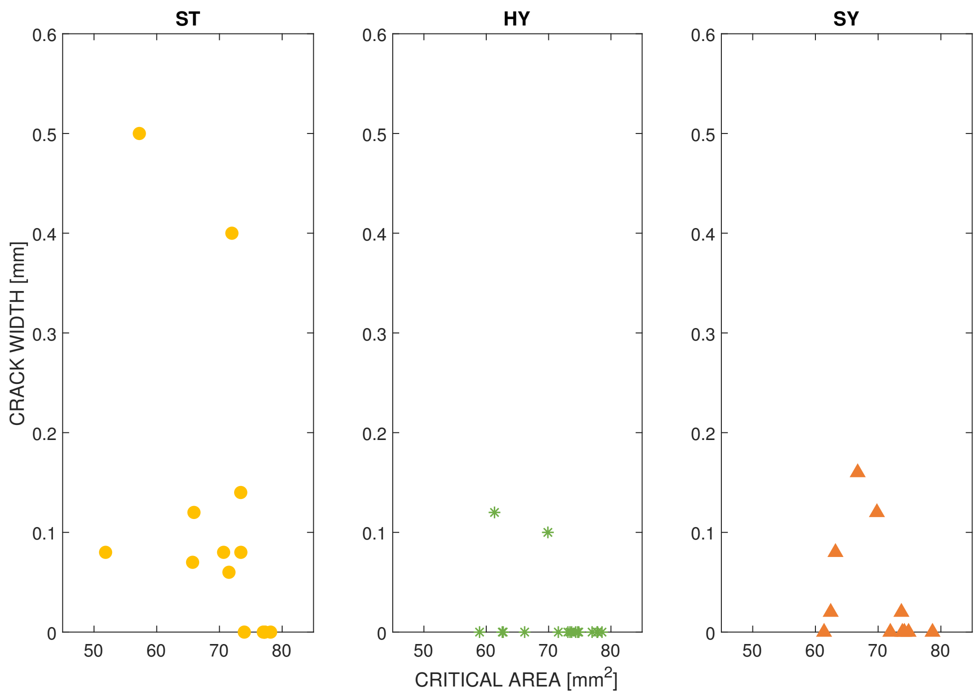

Figure B.39: Critical section area vs. crack width for different fibres in an interval of 50mm from the critical section.

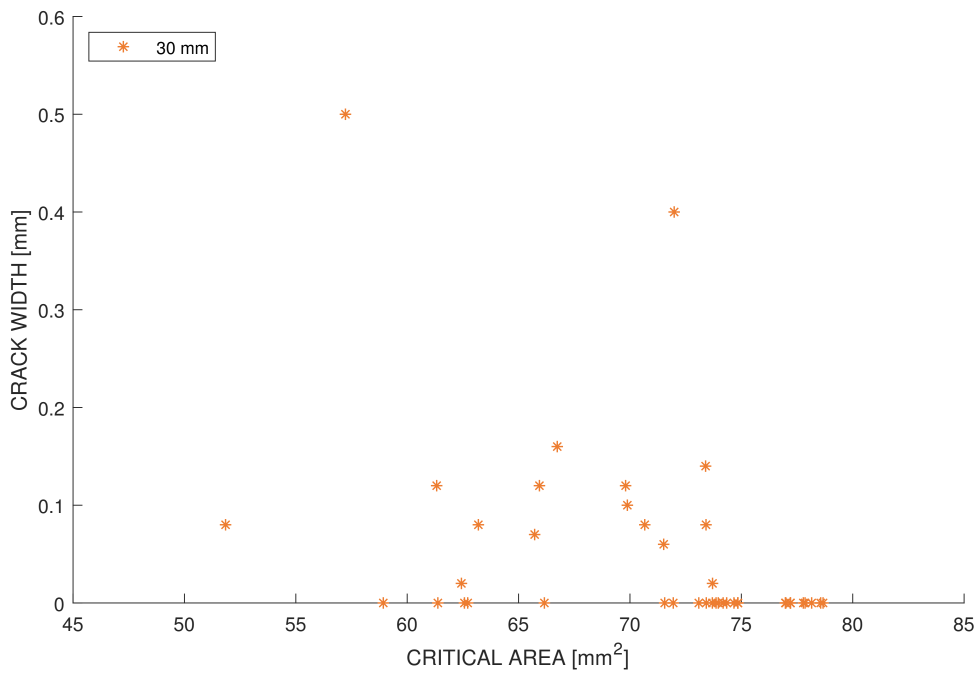

Figure B.40: Critical section area vs. crack width for an interval of 30mm from the critical section.

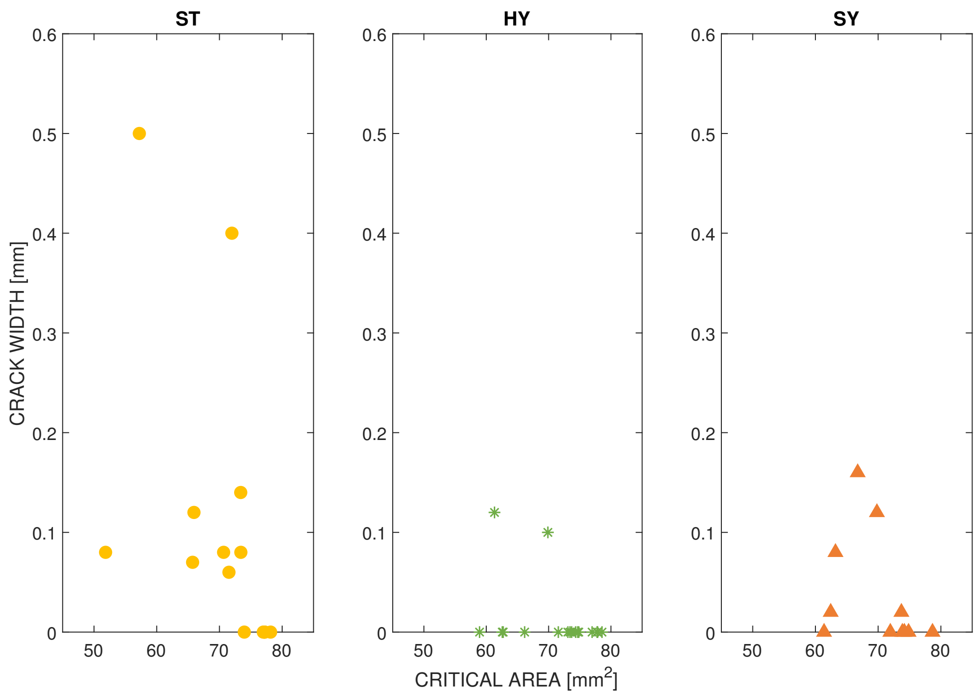

Figure B.41: Critical section area vs. crack width for different fibres in an interval of 30mm from the critical section.

B.4 Mass loss vs. the sum of all cracks in the scanned area

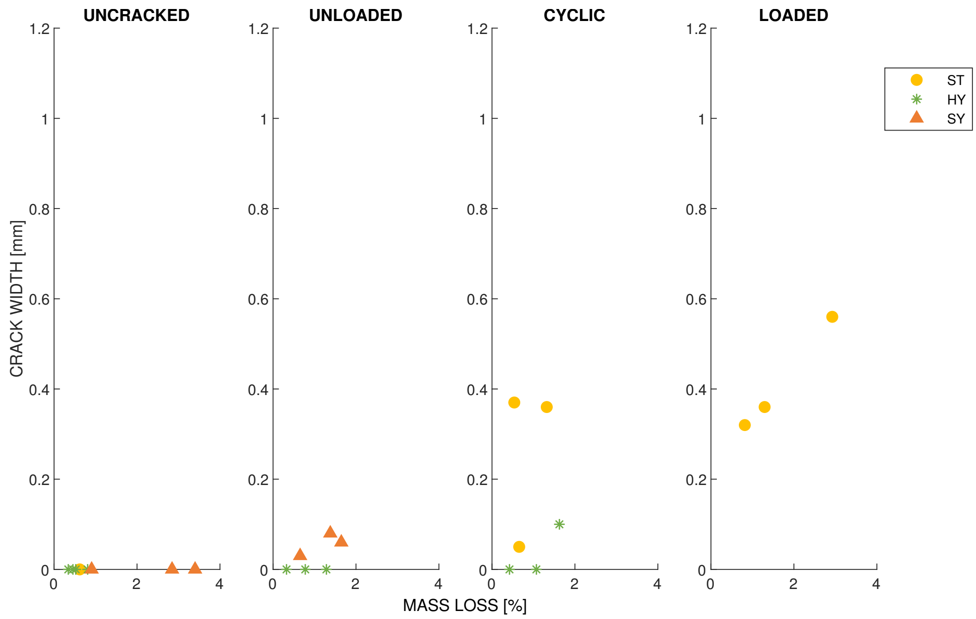

Figure B.42: Mass loss for the bars with target crack width of 0.4 mm vs. the sum of all cracks in the scanned area

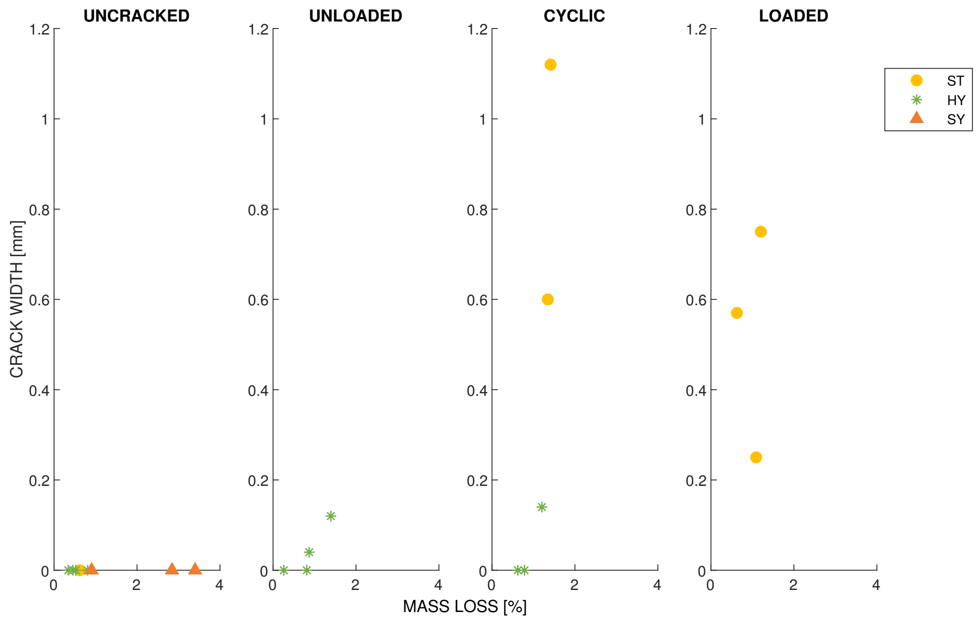

Figure B.43: Mass loss for the bars with target crack width of 0.4 mm vs. the sum of all cracks in the scanned area

B.5 Number of cracks in the scanned area vs. corrosion level

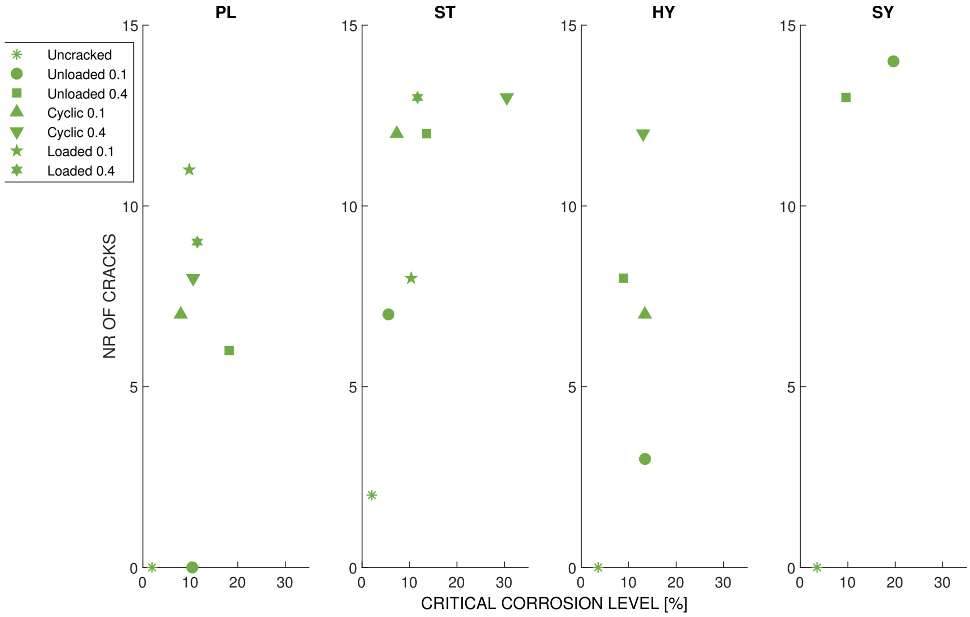

Figure B.44: Number of cracks in the whole beam vs. the corrosion level for plain concrete and each kind of fibres

B.6 Target crack width vs. corrosion

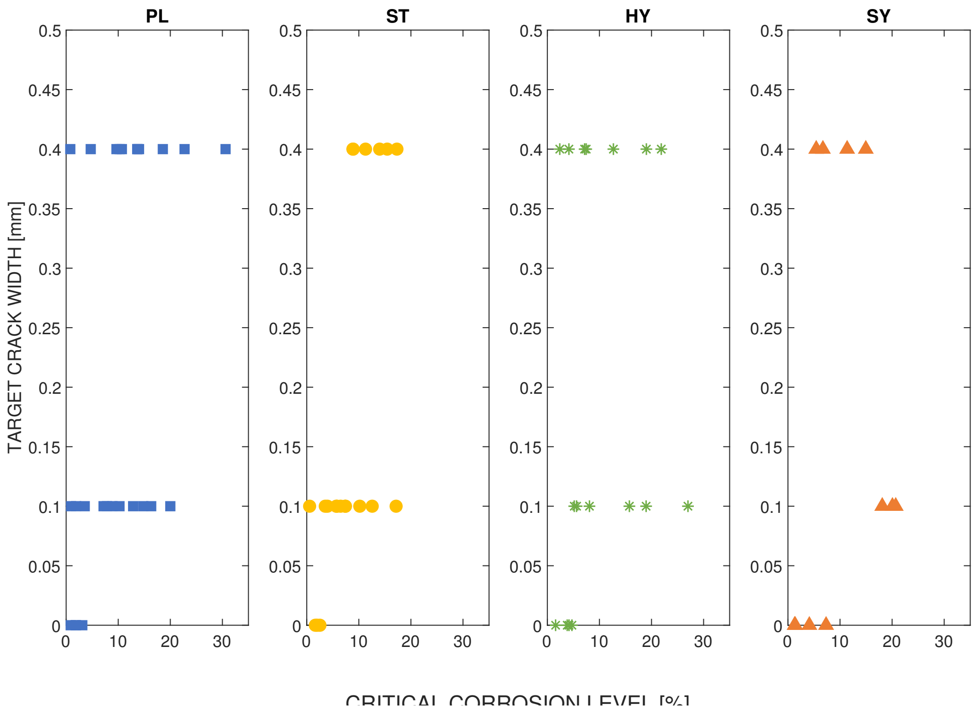

Figure B.45: Target crack width vs. corrosion for each type of concrete mixture

B.7 Corrosion distribution for the scanned bars

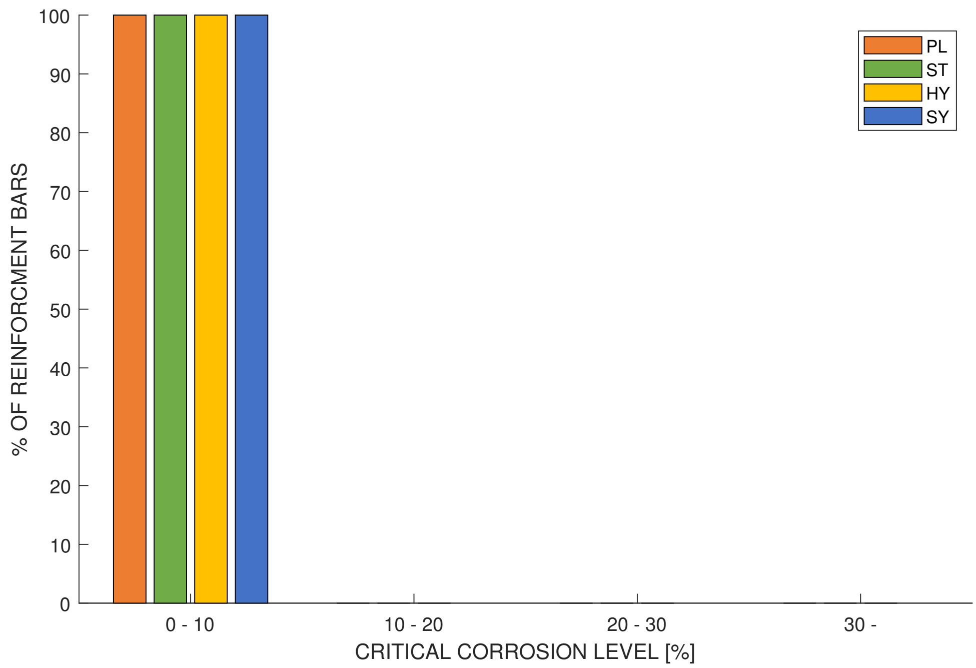

Figure B.46: Histograms of critical corrosion level for the bars in the uncracked beams, i.e. target crack width of 0 mm.

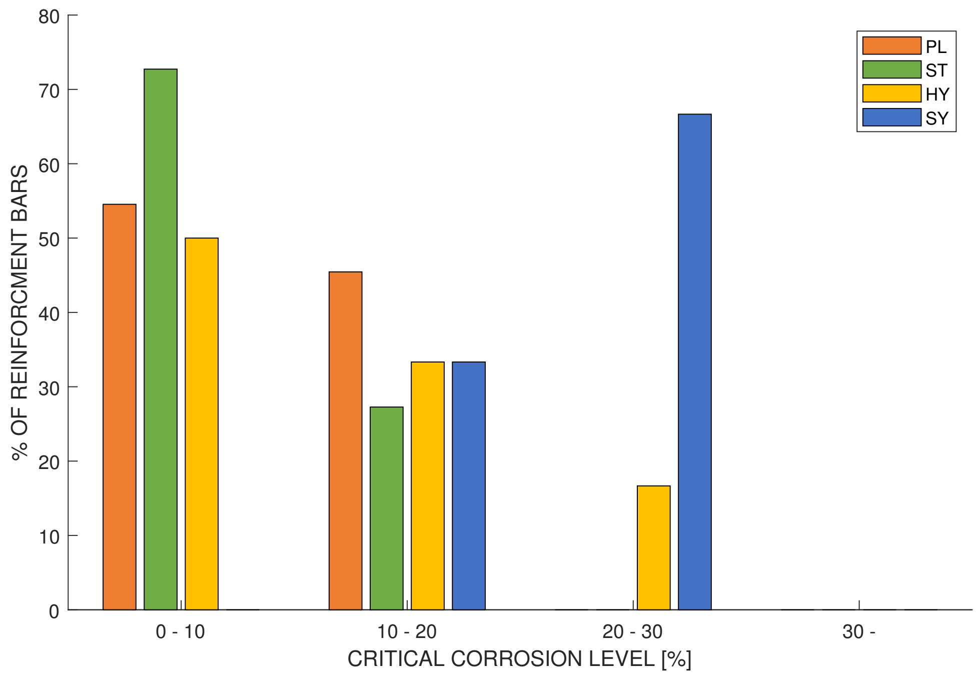

Figure B.47: Histograms of critical corrosion level for the bars in the beams with a target crack width of 0.1 mm.

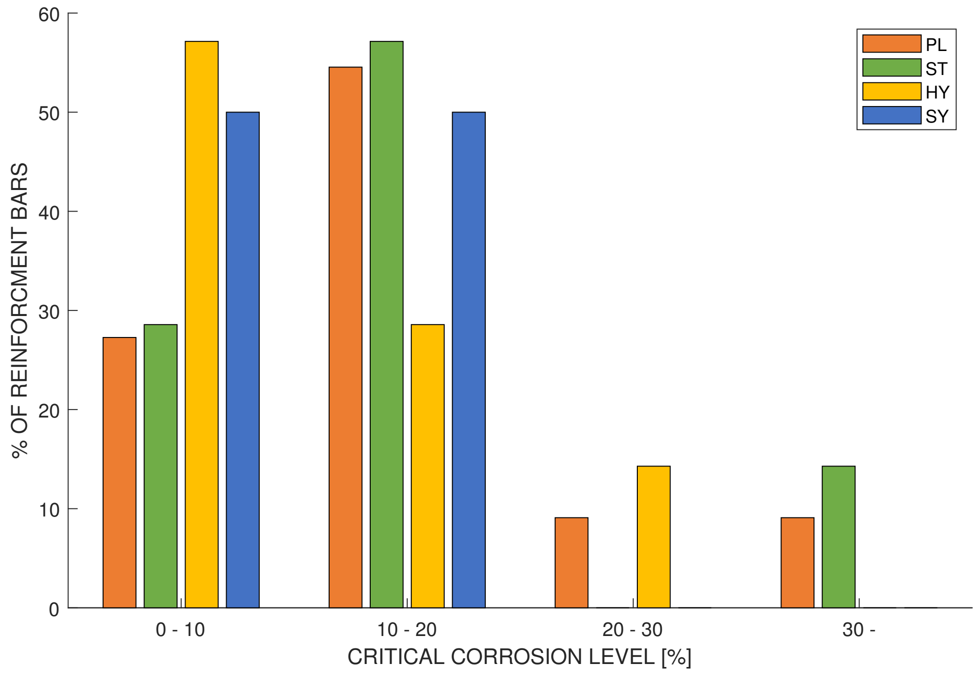

Figure B.48: Histograms of critical corrosion level for the bars in the beams with a target crack width of 0.4 mm.

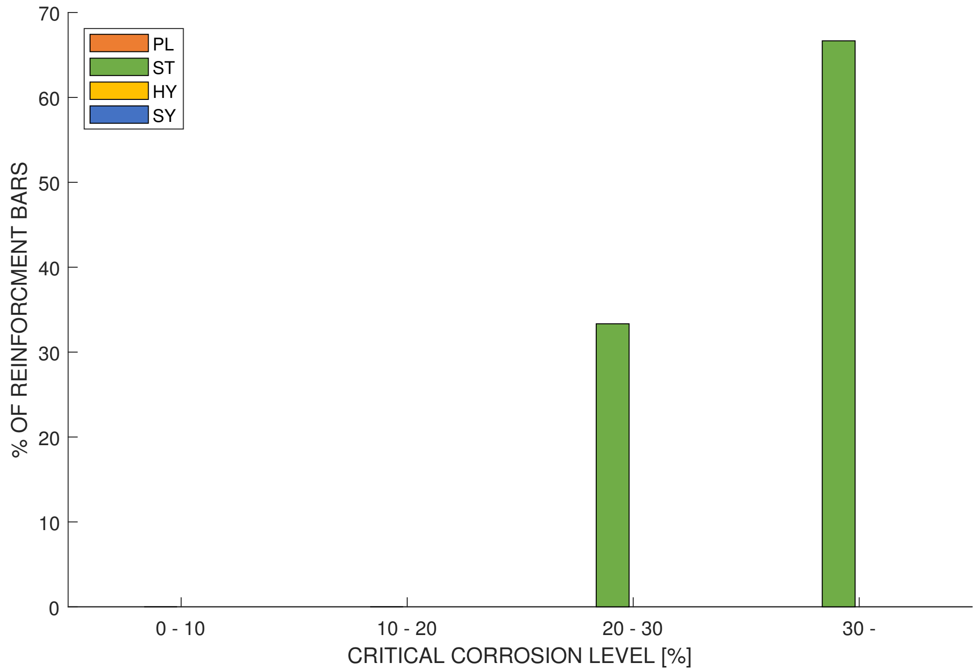

Figure B.49: Histogram of critical corrosion levels for the bars in the beam loaded to a maximum crack width of 0.8 mm. It should be noted that this only represent one beam that was loaded to 0.8mm by mistake.

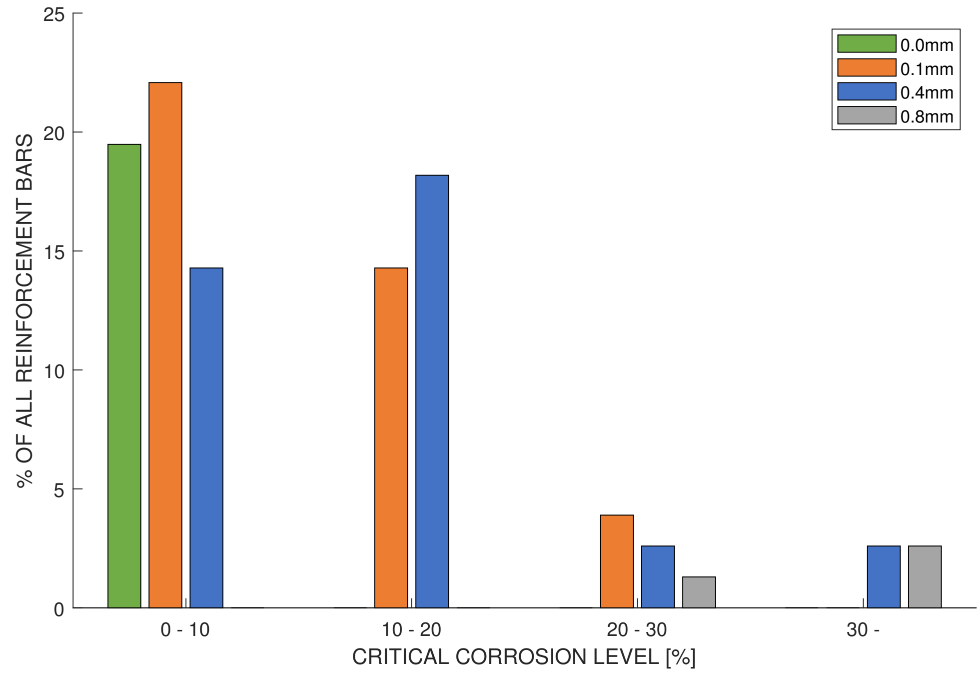

Figure B.50: Histograms of critical corrosion level for all bars, independent on fibre type

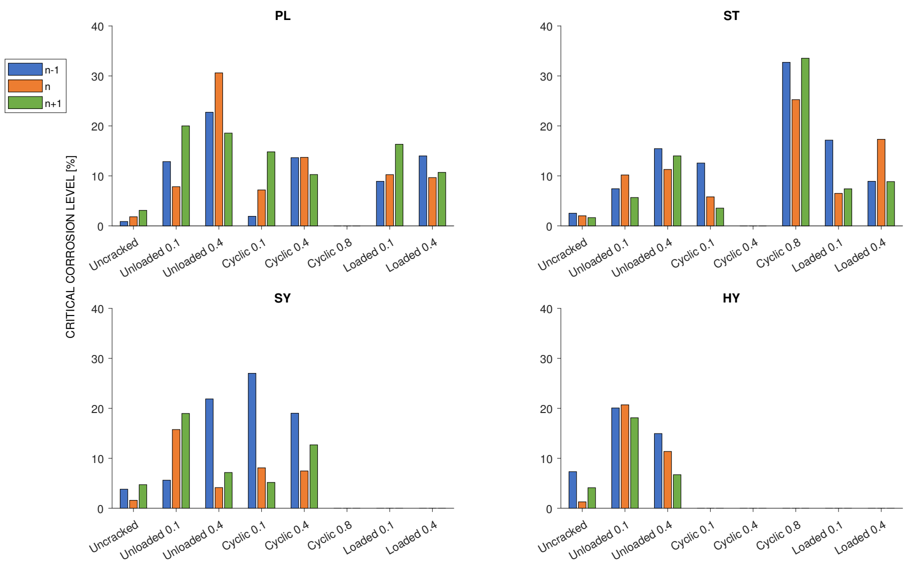

Figure B.51: Histograms of critical corrosion level for all bars in each beam.

B.8 Maximum pit vs. critical corrosion level

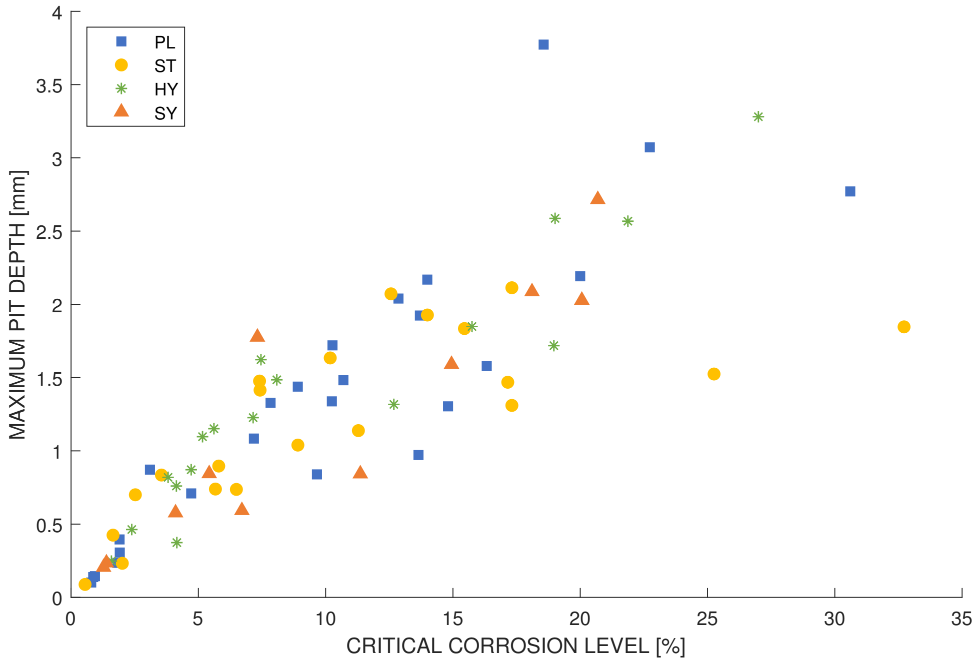

Figure B.52: Maximum pit vs. Critical corrosion level

B.9 Maximal longitudinal crack width vs. corrosion level

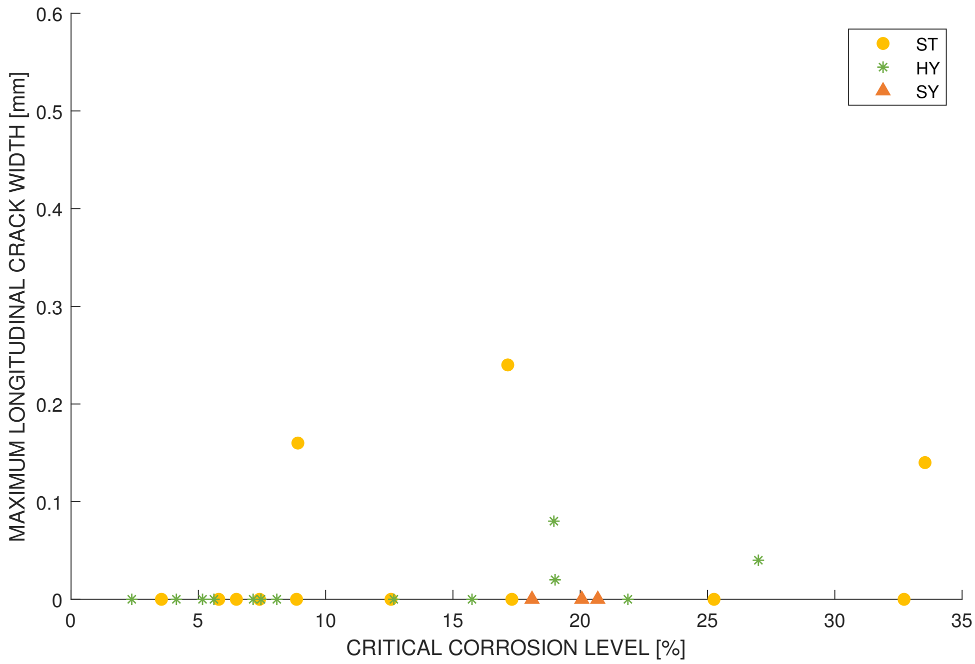

Figure B.53: Maximal longitudinal crack width vs. corrosion level

B.10 Maximal transverse crack width near the critical section

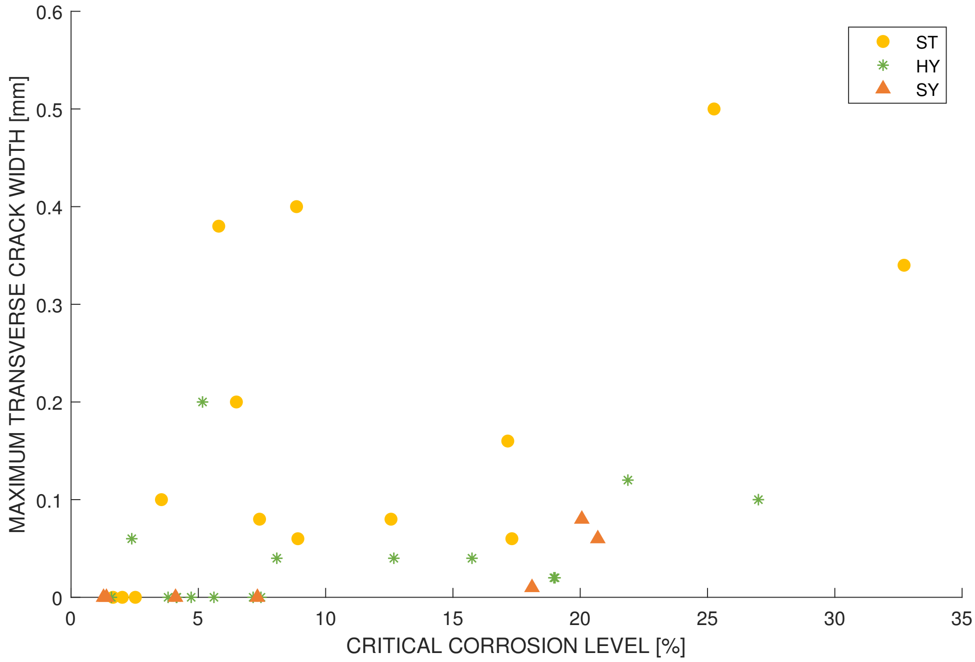

Figure B.54: Maximal transverse crack width near the critical section

B.11 Maximal transverse crack width in the whole beam

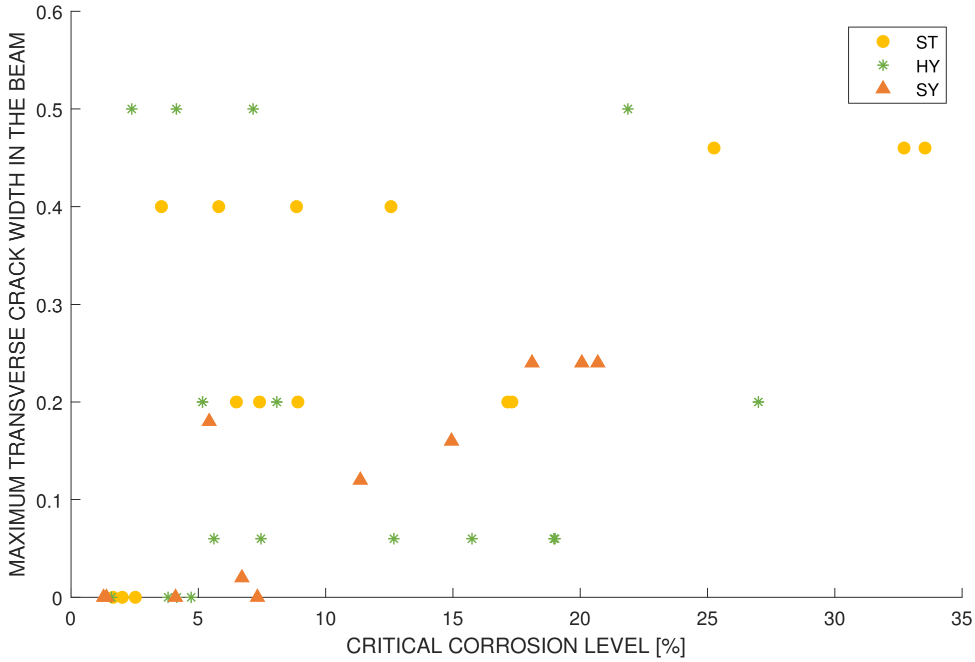

Figure B.55: Maximal transverse crack width in the whole beam

B.12 Transverse and longitudinal crack widths vs. corrosion level

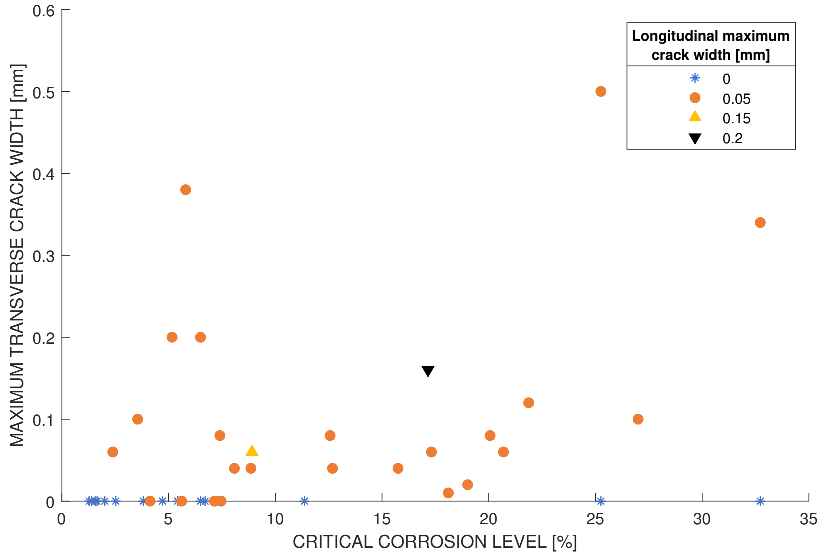

Figure B.56: Transverse and longitudinal crack width vs. corrosion level. All beams are presented

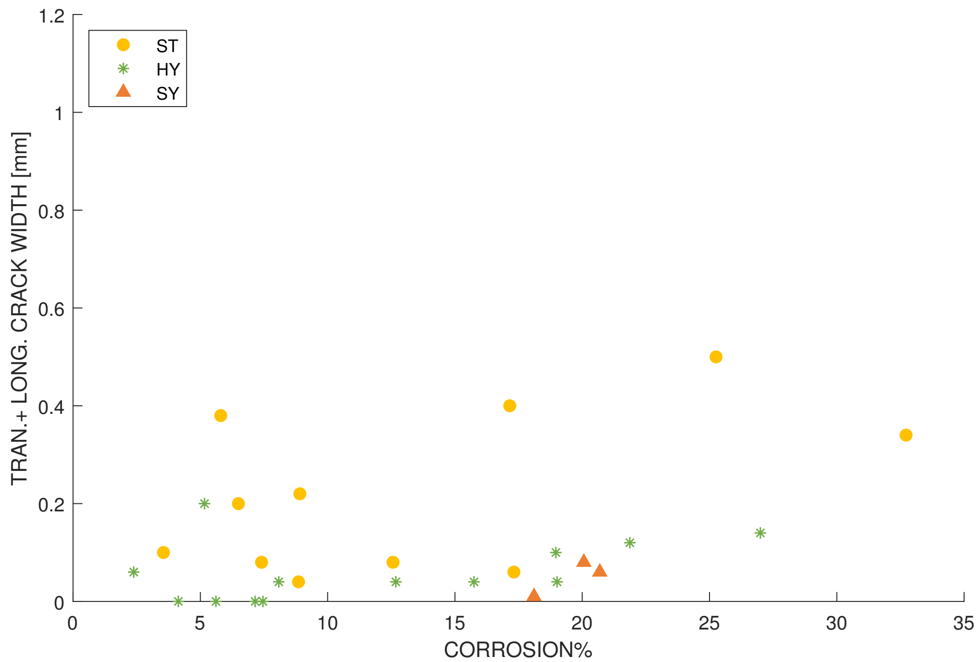

Figure B.57: Sum of longitudinal crack widths and transverse crack widths vs. corrosion